ABSTRACT

A MATHEMATICAL AND COMPUTATIONAL EXPLORATION OF THE EFFECT OF THE A-CURRENT IN DETERMINING THE ACTIVITY PHASE OF FOLLOWER NEURONS

by
Yu Zhang

Bursting oscillations are prevalent in neurons of central pattern generators (CPGs) that produce rhythmic motor activity, and the activity phase plays an important role in determining the normal or dysfunctional network output. The activity phase is the delay time—with respect to some reference time in each cycle and normalized by the oscillation cycle period—of the onset of action potentials by a neuron. This dissertation investigates how the A-current, in conjunction with other intrinsic properties, sets the activity phase of a neuron driven by inhibition.

This dissertation is divided into two major components. In the first component, methods of dynamical systems are applied to explore the transient properties of the activity phase of the follower neuron, which is modeled using a simplified three-variable model based on the Morris-Lecar equations. Based on the analysis of the effect of the A-current in determining the phase, recursive equations are derived to calculate the activity phase of the follower neuron, following a single inhibitory input as well as its steady state phase in response to a rhythmic input. The modeling findings are compared with experimental data from follower PY neurons in the pyloric CPG of the crab *C. borealis*. In these experiments, the Dynamic Clamp technique is used to produce artificial intrinsic and synaptic currents in the follower PY neurons. It is found that the activity phase can be determined by the period and duty cycle of the pacemaker, and the recursive equations

provide faithful predictions of the activity phase when the cycle period of the pacemaker is varied under different protocols.

In the second component of the dissertation, a five-compartment model is built based on the morphology of the PY neuron to produce a realistic representation of the biological PY neurons in order to investigate how the distribution of the A-current affects the activity phase. This model involves a set of 53 coupled nonlinear ordinary differential equations which are numerically integrated using a 4^{th} order Runge-Kutta method. A Genetic Algorithm is applied to recursively optimize the possible parameters for all the intrinsic currents in each compartment. The results show that different distributions of the A-current lead to different bursting behaviors even if the total A-current conductance is kept constant.

These results show that the activity phase of the follower neurons can be affected significantly by the strength and the distribution of the A-current, together with other intrinsic and synaptic properties. The activity phase can be predicted by the results of a low-dimensional model, and the possible distribution of the intrinsic currents can be computed by developing more realistic models based on the shape of biological neurons.

A MATHEMATICAL AND COMPUTATIONAL EXPLORATION OF THE EFFECT OF THE A-CURRENT IN DETERMINING THE ACTIVITY PHASE OF FOLLOWER NEURONS

by
Yu Zhang

A Dissertation
Submitted to the Faculty of
New Jersey Institute of Technology and
Rutgers, the State University of New Jersey - Newark
in Partial Fulfillment of the Requirements for the Degree of
Doctor of Philosophy in Mathematical Sciences

Department of Mathematical Sciences, NJIT
Department of Mathematics and Computer Science, Rutgers - Newark

August 2008

APPROVAL PAGE

A MATHEMATICAL AND COMPUTATIONAL EXPLORATION OF THE EFFECT OF THE A-CURRENT IN DETERMINING THE ACTIVITY PHASE OF FOLLOWER NEURONS

Yu Zhang

6/17/08

Dr. Farzan Nadim, Dissertation Advisor — Date
Professor, Department of Mathematical Sciences, NJIT and
Department of Biological Sciences, Rutgers University - Newark

6-17-08

Dr. Amitabha Bose, Committee Member — Date
Professor, Department of Mathematical Sciences, NJIT

6/17/08

Dr. Jorge Golowasch, Committee Member — Date
Associate Professor, Department of Mathematical Sciences, NJIT and
Department of Biological Sciences, Rutgers University - Newark

6/17/08

Dr. Victor Matveev, Committee Member — Date
Assistant Professor, Department of Mathematical Sciences, NJIT

6/17/08

Dr. Andrew Hill, Committee Member — Date
Assistant Professor, Department of Biological Sciences, NJIT

BIOGRAPHICAL SKETCH

Author: Yu Zhang

Degree: Doctor of Philosophy

Date: August 2008

Education:

- Doctor of Philosophy in Mathematical Sciences,
  New Jersey Institute of Technology, Newark, NJ, 2008

- Master of Science in Applied Mathematics,
  New Jersey Institute of Technology, Newark, NJ, 2006

- Bachelor of Science in Computational Mathematics
  Beijing University of Technology, Beijing, China, 2001

Selected Presentations and Publications:

Zhang Y., Bose A. and Nadim F.
"Geometric and Analytic Analysis of the Role of the A-Current on the Transient and Long-Term Behavior of a Neuron Receiving Inhibitory Input", the SIAM (Society for Industrial and Applied Mathematics) Conference on the Life Sciences, Montreal, Canada, August 2008

Zhang Y., Bose A. and Nadim F.
"Using Recursive and Genetic Algorithms to explore how intrinsic properties of neurons affect their activity phase following inhibitory input", the 34th Annual East Coast Nerve Net, Woods Hole, MA, April 2008

Zhang Y., Bose A. and Nadim F.
"Determining the Effect of the A-Current on the Activity Phase of a Follower Neuron in an Inhibitory Network", 8-P48
BMC Neuroscience 2007

Zhang Y., Bose A. and Nadim F.
"The Effect of the A-Current on the Activity Phase of Follower Neurons in an Inhibitory Network", the 16th Annual Meeting for Computational Neuroscience (CNS), Toronto, Canada, July 2007

This dissertation is dedicated to all of my family and friends who have given me kind support over the last four years.

ACKNOWLEDGMENT

The person I would like to thank the most is my advisor Dr. Farzan Nadim. During the four years of my PhD study, he was always helpful. As a scientist, he has sharp insight and extensive knowledge. By discussing issues with him, I often got valuable advice or useful knowledge. He is more a mentor than an advisor, since he helped me realize the beauty of mathematical biology, and helped me to become strong enough to defend my research in all kinds of presentations and conferences.

I would also like to thank Dr. Amitabha Bose and Dr. Jorge Golowasch, who provided a great deal of help during my PhD research. By talking with Dr. Bose, I was able to think deeply about the mathematical modeling. Dr. Golowasch helped me to understand important knowledge of biology and the techniques of experiments. Also, I would like to thank Dr. Victor Matveev and Dr. Andrew Hill, who gave me very good suggestions to improve my dissertation. All five gentlemen I mentioned above are on my dissertation committee, and each of them was most helpful during my dissertation writing period.

Next, I would like to thank all of the members in the Nadim and Golowasch laboratories, especially Shunbing, who collaborated with me in doing most of the experiments in my research. Without his help in dissection the animals and recording the cells I could not finish any experiment. I also want to thank Lian, Nick, Vahid, Yili, Farzad, Hua-an and Michael who helped me in different ways during these four years. I am truly grateful for having a chance to work in such a great team.

I would also like to thank Dr. Adam Taylor and Dr. Anne-Elise Tobin at Brandeis University who discussed with me the application of the Genetic Algorithm. Their suggestions helped me to finish the coding in a very efficient way.

At last, I would like to thank all the staff at the Department of Mathematical Sciences at NJIT. Especially I want to thank Ms. Susan Sutton who was always helpful in everything I asked for. I also want to thank the Graduate Studies Office for their helpful guidance and support.

TABLE OF CONTENTS

TABLE OF CONTENTS
(Continued)

Chapter **Page**

TABLE OF CONTENTS
(Continued)

Chapter **Page**

LIST OF TABLES

LIST OF FIGURES

LIST OF FIGURES
(Continued)

LIST OF ABBREVIATIONS

CPG	Central Pattern Generator
STNS	Stomatogastric Nervous System
STG	Stomatogastric Ganglion
PY	Pyloric Constrictor Neuron
PD	Pyloric Dilator Neuron
LP	Lateral Pyloric Neuron
LB	Left Branch
MB	Middle Branch
RB	Right Branch
LK	Lower Knee
UK	Upper Knee
FP	Fixed Point
GA	Genetic Algorithm
IB	Intrinsic Bursting
PTX	Picrotoxin
TEA	Tetraethylammonium

CHAPTER 1

INTRODUCTION

1.1 Objectives

The general objective of this dissertation is to explore how the intrinsic and synaptic properties affect the activity phase of neurons following inhibitory inputs. In order to approach this objective, mathematical and computational research is implemented in three major steps involving applying the knowledge of dynamical systems, mathematical and computational modeling and computer science. Biological experiments involving Dynamic Clamp (DC) were conducted by the author and the biologists at the STG laboratory of Rutgers University.

In the first step, the role of the A-current in determining the activity phase of the follower PY neurons has been observed by conducting several biological experiments, and a three-variable model for the follower neuron is developed in order to predict the activity phase of the follower neurons. The phase space and projection phase planes are studied and two possible cases are classified based on the structure of the nullclines in one phase plane. A series of recursive equations are derived for calculating the steady state value of the bursting phase of the follower PY neurons. The accuracy of the prediction is shown by comparing the analytic solutions with the experimental data.

In the second step, a complete mathematical analysis of the interaction between the A-current and the other intrinsic and synaptic properties is studied. Based on the possible shape and relative position of the nullclines, eight cases are studied systematically. In each case, the fate of the trajectories (and therefore the activity of the membrane potential) can

be predicted by comparing the values of different time constants. The relationship between the temporal properties of the pacemaker neurons, the synaptic properties and the behavior of the follower neurons is revealed.

In the third step, a high dimensional model is developed based on the biological shape of the PY neurons in the crustacean pyloric network. The model includes five compartments and eleven types of intrinsic currents. A Genetic Algorithm implemented in MATLAB and NETWORK helps to compute the possible distributions and kinetics of all the intrinsic currents among all the compartments. This model also generates the spiking property similar to the real PY neurons.

Following the three main steps above, more analysis and computation are implemented to explore other factors which may also play a role in shifting the activity phase of the follower neuron PY. The role of the *h*-current is analyzed by phase plane analysis. The coupling between PY and LP, another follower neuron in the pyloric network, is also studied analytically and numerically.

1.2 Significance

1.2.1 Bursting Neurons

The nervous system is one of the most important organ systems in a multicellular animal's body. It receives signals from the muscles and organs inside the body and sensory inputs from the environment. After integrating the signals, the nervous system responds to the stimuli by converting them into some form(s) of action, such as movement, release of hormones, changes in heart rate and so on.

Rhythmic activity is ubiquitous in the nervous system, and bursting, as an important slow oscillation, has been found among neurons and other cells of both vertebrate and invertebrate animals. Bursting is a special membrane potential behavior of neurons. Different from tonic spiking, bursting shows discrete groups of spikes separated by a quiescent state. Bursting oscillations occur in many neurons and other cell types and underlie rhythmic activity in many networks of the central nervous system. In the mammalian thalamocortical system, for example, bursting occurs in the thalamocortical neurons during EEG-synchronized sleep (McCormick and Bal, 1997). In the isolated cortical slabs about 40% of cells, twice as many as in intact cortex, show an intrinsic bursting behavior (Timofeev et al., 2000). Similarly the visual cortical IB neurons are also classified as intrinsically bursting (Nowak et al., 2003). Other examples include the circadian rhythmicity which results from the interaction of the circadian pacemaker, comprising of the neurons of the suprachiasmatic nucleus and other neurons such as the photoreceptors (Moore, 1999).

Bursting oscillations are particularly prevalent in neurons of central pattern generators (CPGs) that produce rhythmic motor activity. These types of neurons include, for instance, the respiratory neurons in the pre-Botzinger complex of the brain stem that exhibit pacemaker bursting activity (Johnson et al., 1994). The activity of oscillatory networks of neurons is determined by the oscillation frequency as well as the activity phase of the component neurons within each cycle. In many oscillatory networks, the relative bursting phase among neurons plays an important role in determining the normal or dysfunctional output of the network. In CPGs, for instance, the relative phase of neurons or groups of neurons determines the order of muscle contractions and therefore the motor

behavior (Marder and Bucher, 2007). It has also been shown that the motor system dysfunction associated with Parkinson's disease is critically dependent on the phase relationships between basal ganglia nuclei which are affected by the loss of dopamine (Walters et al., 2007). The phase difference between neurons is often maintained over a wide range of frequency (Marder and Calabrese, 1996; Marder et al., 2005), and it has been shown that the A-current, a transient outward potassium current, plays an important role in determining the activity phase of neurons in many neuronal networks (Selverston, 2005).

1.2.2 The A-Current

As a transient potassium current, the A-current is present in most neuronal types and contributes to spike timing. Similar to some other intrinsic currents, the A-current is voltage-dependent: it is activated transiently when the membrane potential is depolarized, and then decays due to inactivation.

The A-current is an essential factor in determining the spike frequency-current response of neurons, as was first shown in the seminal paper of Connor and Stevens (Connor and Stevens, 1971). In the CA3 pyramidal cells in the hippocampus, the activation of the A-current underlies the propagation failure of action potentials in axons (Debanne et al., 1997). The A-current has been shown to be important in determining the post-inhibitory rebound bursting phase of neurons and its effect on determining this phase is subject to the neuromodulation of the current by dopamine (Harris-Warrick et al., 1995a).

The A-current has been shown to exist in various types of neurons (Huguenard et al., 1991; Herrington and Lingle, 1994; Wustenberg et al., 2004) and is known to be important in setting the timing of action potentials(Gerber and Jakobsson, 1993),

especially following inhibitory input (Harris-Warrick et al., 1995a), contributing to the generation of a coordinated motor pattern (Hess and El Manira, 2001), and acting as a bursting trigger in the absence of a slow variable (Tabak et al., 2007; Toporikova et al., 2007). In a network of bursting neurons, the A-current often acts to delay the onset of the burst, thus setting the activity phase of different neurons within the network (Harris-Warrick et al., 1995a). In a previous study, the role of the A-current in setting the activity phase of a follower neuron that received a periodic inhibitory synaptic input has been examined in a model with simplified kinetics. It has been demonstrated that if the inhibitory input shows short-term depression, the A-current can act synergistically with the depression parameters to produce phase maintenance of the follower neuron when the frequency of the periodic input is varied (Bose et al., 2004).

1.2.3 The Advantages of Invertebrate Nervous Systems

The complexity of the mammalian nervous system limits scientists' research activities. Because of the huge number of neurons and the complex connections between them, it is hard to distinguish a certain neuron from the network. Also, the multiple patterns of activity of the mammalian neuronal networks makes it difficult to analyze the properties of networks based on current experimental techniques, and it is thus hard to predict its possible behavior using mathematical and computational modeling. Fortunately, since CPGs and similar bursting behaviors also exist in invertebrate animals which have less complex nervous systems, neuroscientists are able to investigate their rhythmic activities in more convenient ways (Marder and Calabrese, 1996; Nusbaum and Beenhakker, 2002). In this research the neuronal networks in the crustacean stomatogastric ganglion system are used as the prototypes of the modeling neurons. The connectivity diagrams among neurons

can be established, and the functions of the intrinsic properties of each single neuron and the synaptic dynamics in generating and modulating oscillations can be studied experimentally and mathematically.

1.2.4 Summary

This dissertation includes detailed research for understanding how the A-current, together with other intrinsic and synaptic properties, modulates the bursting phase of follower neurons under the condition of different periods and duty cycles. A highlight of this research can be generally described as using the knowledge of mathematics and computing science to analyze and predict some widespread but not well-studied biological phenomena, such as bursting and phase shift. Developing appropriate mathematical and computational models helps scientists to understand the kinetics of the biological nervous networks, and choosing a simple nervous system allows biologists to conduct relevant experiments to verify the modeling results.

1.3 Background

1.3.1 The Crustacean Stomatogastric Nervous System

The Stomatogastric Nervous System (STNS) of lobsters and crabs is valuable for neuroscientists because of its clear rhythmic behavior and its small neuronal network (Marder and Calabrese, 1996). The main function of STNS is to digest food in the stomach of the crustacean animals. STNS produces two primary activity rhythms of motor output: the gastric mill rhythm which contributes to the chewing process, and the pyloric rhythm

which contributes to the process of filtering chewed food. The research in this dissertation is focused on the neuronal behavior in the pyloric network of crab *Cancer borealis*.

Figure 1.1 shows the STNS plot and the pyloric network of the crab. In the pyloric network, the CPG is an interneuron named anterior burster (AB) which typically oscillates with a frequency of about 1 Hz (Marder and Calabrese, 1996). As a pacemaker neuron, AB maintains its oscillation activity when synaptically isolated from the remainder of the network and, moreover, makes other neurons in the pyloric network oscillate in the same rhythm by synaptic connections.

Figure 1.1(b) shows the structure of the pyloric network. There are two kinds of synapses in nervous systems: electrical synapses (which are also called gap junctions) and chemical synapses. An electrical synapse is a conductive link formed at a narrow gap between two adjacent neurons which allows ions and even medium sized molecules, like signaling molecules, to flow transiently from one cell to the next (Hormuzdi et al., 2004). Therefore an electrical synapse between two cells promotes the synchronization of their membrane potentials. There are two pyloric dilator neurons (PD) electrically coupled with AB which oscillate in phase with AB, and they are also considered as pacemaker neurons in the pyloric network.

A chemical synapse has a much longer delay than an electrical synapse (Llinas et al., 1982). The lateral pyloric neuron (LP) and pyloric dilator neurons (PY) receive inhibitory chemical synaptic signals from the pacemaker, and in return, LP inhibits PDs through a feedback chemical synapse as well. LP and PY inhibit each other through chemical synapses, and there is also a rectifying gap junction from LP to PY. In this

dissertation the study is focused on the network consisting of these four types of neurons, and the effect of the inferior cardiac (IC) and ventricular dilator (VD) neurons is ignored.

LP and PY, known as near-oscillators or follower neurons, spike tonically when isolated from the pacemaker AB and PD (Golowasch et al., 1999). However, they are able to burst in response to inhibitory synapses from pacemaker neurons. Figure 1.1(c) shows a recording of the AB, PD, LP and PY neurons. The pacemaker neurons AB and PD oscillate in phase, and the LP and PY neurons burst during the inactive state of the pacemaker neurons. It also shows a phase difference between the LP and PY bursts: LP bursts earlier than PY during each cycle. There are three to five PY neurons in each pyloric network and these neurons can have fairly distinct activity phases.

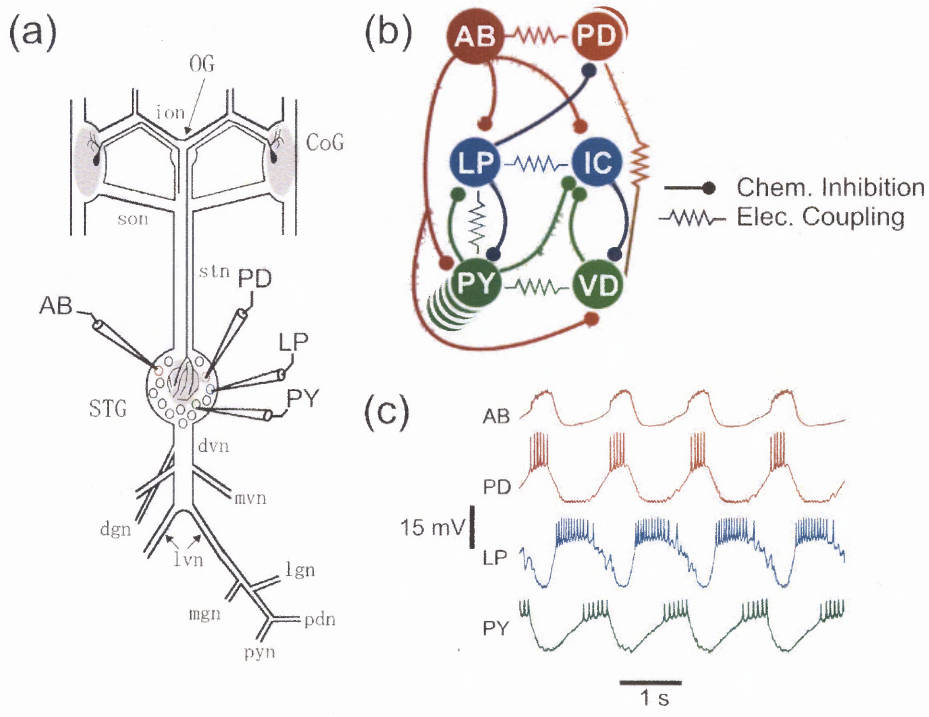

Figure 1.1 The Pyloric Network of the Stomatogastric Ganglion (STG) System of Crab *Cancer borealis*. (a) The simplified plot of the stomatogastric nervous system (STNS). Neurons in both pyloric and gastric mill networks are located in the STG. **(b)** The structure of the pyloric network. AB, PD, LP, IC, PY, VD are the six types of neurons in the pyloric network. There are complex electrical and chemical synapses among these neurons. **(c)** The tri-phasic oscillation in the pyloric network: The pacemaker neurons AB and PD oscillate in phase. The follower neurons LP and PY burst during the quiescent duration of the pacemaker, and LP bursts in a more advanced phase than PY.

Source: F. Nadim, unpublished.

1.3.2 Neuromodulation and Synaptic Blockers

During the neuromodulation process, a neuromodulator is a substance released by a neuron at a synapse and transfers signals to adjacent or distant neuron(s). Neuromodulators exist in both vertebrate and invertebrate animals, and they change the intrinsic properties of individual neurons and/or the strength of the synapses between them (Pearson, 1993; Marder and Calabrese, 1996; Nusbaum and Beenhakker, 2002).

Neuromodulation plays an important role in modulating the activities of the pyloric network. For example, Dopamine (DA) reduces the maximum conductance of the A-current in LP and PY and increases the voltage threshold for activation and inactivation of the A-current and the h-current at the same time (Harris-Warrick et al., 1995a).

Synaptic blockers are chemicals which can be used to block or attenuate certain synapse(s). For instance, Picrotoxin (PTX) blocks all glutamatergic synapses in the pyloric network (Marder and Paupardin-Tritsch, 1978; Bidaut, 1980), including those from the pacemaker neuron AB. Tetraethylammonium (TEA) or atropine blocks the cholinergic inhibitory synapses including the synapses from PD to LP and PY(Marder and Eisen, 1984). One application in this research is that PTX is applied to block the inhibitory synapses from the pacemaker neuron AB to the follower neurons LP and PY. (The synapses from PD to LP and PY are very weak in STG of *Cancer Borealis*, therefore their existence is ignored during the experimental work (Rabbah and Nadim, 2007).) Dynamic Clamp is then applied to make an artificial pacemaker neuron whose period and duty cycle can be changed easily.

1.3.3 Dynamic Clamp

Dynamic Clamp is a new technique which provides an interface between the computer and biological cells. It allows scientists to inject artificial current(s) developed at the computer into the biological cells (Prinz et al., 2004). The artificial currents are described by mathematical equations, and they can represent both intrinsic and synaptic currents. The Dynamic Clamp method has been applied in various fields including cardiac

electrophysiology (Wilders, 2006), lumbar motoneurones (Brizzi et al., 2004) and Cerebellar Purkinje Cells (Jaeger and Bower, 1999).

In this research, the Dynamic Clamp is applied in the follower neurons PY in a series of experiments. The aim is to detect how the intrinsic properties, such as the A-current, affect the activity phase of PY, and how to predict the shift of the activity phase when the period and duty cycle of the pacemaker neurons vary. The Dynamic Clamp experiments were performed in the Nadim lab (unpublished data) on *Cancer borealis* PY neurons in two-electrode current clamp mode as described in (Rabbah et al., 2005). The Dynamic Clamp software used here has been developed in the Nadim laboratory and is available for free download at (http://stg.rutgers.edu/software/index.htm).

1.3.4 Dynamical Systems and Singular Perturbation

The techniques of mathematical and computational modeling are applied in this dissertation for exploring the effect of the A-current interacting with other intrinsic and synaptic properties on the activity phase of the follower neurons, and for predicting the membrane potential behavior of the biological neurons. Knowledge of dynamical systems and the theorems of geometric singular perturbation are used to analyze the systems of the non-linear ordinary differential equations (ODEs).

The mathematical theory of dynamical systems is based on the qualitative theory of ordinary differential equations which was first formulated by Poincaré (Poincaré, 1905; Poincaré, 1907). Originally a dynamical system was considered as an isolated mechanical system described by Newtonian differential equations. At present the concept of a

dynamical system applies to any time-dependent process (Chueshov, 2002). With the usage of dynamical systems, problems in various fields including physics, chemistry, biology and economics can be analyzed qualitatively.

Phase space analysis is one of the most important tools for understanding the dynamical systems. It is especially useful for analyzing problems which cannot be solved analytically since it provides geometric views for the transient and steady state behaviors of the dynamical systems (Perko, 2001). For example, in a dynamical system with two ordinary differential equations, a two-dimensional phase plane can be used to visualize the steady state values (or the nullcline) of each dependent variable, the flow vector field which shows the direction of the movement and the flow of the trajectory in the phase plane. Periodic solutions, specifically stable ones known as limit cycles, are widespread in problems of neuroscience. It has been shown that many kinds of periodic solutions can be studied using phase plane analysis (Morris and Lecar, 1981; Bell and Craciun, 2005; Hodge et al., 2006).

Many dynamical systems descriptions of biological problems are singularly perturbed due to the different time scales involved in the biological processes. Different from a regular perturbation problem, a singular perturbation problem includes a small positive parameter (ε) which results in a solution that evolves in two scales (Verhulst, 2005). Usually the solution of a singularly perturbed system can be approximated by replacing the small parameter ε by zero, in the original or rescaled equations, and then solving a group of lower-dimensional systems.

It has been proved that under certain conditions, a two-variable singularly perturbed system can have the solution of a unique stable limit cycle which lies $O(\varepsilon)$ close

to the singular solution (Mishchenko and Rosov, 1980). This theory has been widely applied in mathematical modeling for understanding the spiking and bursting properties in various neural networks. For example, the spiking property in some small neural networks was studied by using the techniques of dynamical systems and the theorems about limit cycles (Ermentrout and Kopell, 1998). Other examples show that the maintenance of the bursting phases was explored based on the singular perturbation and the limit cycle theories (Bose et al., 2004; Mouser et al., 2008).

The mathematical models used in this dissertation are based on a two-dimensional singularly perturbed model which can be tuned to have a limit cycle solution by setting the parameters appropriately (Mishchenko and Rosov, 1980). Other time-dependent variables are added into the model in order to describe the dynamics of the A-current and other intrinsic properties; therefore, in the current models, the number of dependent variables is more than two. Under this circumstance the dynamics in the phase space can be analyzed by considering the dynamics of the trajectory in a family of "phase planes" determined by the periodic property. By replacing the small perturbation parameter by zero or rescaling the time variable, lower dimensional systems can be obtained and used for solving for the analytic solutions.

1.3.5 Genetic Algorithms

Genetic Algorithm (GA) is a computing technique inspired by genetic biology. It simulates the natural evolution processes which follow the principle of "survival of the fittest" first laid down by Charles Darwin. From the mathematical point of view, GA is a probabilistic search algorithm; and from the engineering point of view, it is an adaptive iterative optimization process. When GA is implemented as a computer simulation, each individual

in a population can be translated into a chromosome, traditionally represented as a binary string (other encodings are also possible, such as float strings etc.). Individuals in the first generation are generated randomly within their ranges. The fitness value for each individual is then calculated by an evaluation function. The iteration is ended if any individual satisfies the terminating condition; otherwise a new population is generated. Based on the fitness values, some individuals are selected stochastically for a series of operations (such as mutation and crossover) and then added back to the population. Individuals in the new population are then evaluated by the evaluation function. The same procedure is repeated until the terminating condition is satisfied. Unlike other optimization methods such as the steepest decent method, GA avoids reaching the local extreme solutions because of its global selection property.

Genetic Algorithms have been applied for solving various high-dimensional problems. For instance, GAs can be used to find the most effective stimulus in large parameter spaces for sensory neurons in the cochlear nucleus and inferior colliculus of anaesthetised guinea pigs in a relatively short period of time (Bleeck et al., 2003). Another example is that GA is applied to determine the conductance density distributions for a computational model in order to simulate endogenous bursting behavior of the leech heart interneurons (Tobin et al., 2006). In this dissertation GA is applied in a similar way in the second example.

In this research, a Genetic Algorithm is implemented in MATLAB in order to build a five-compartment computational model to simulate the biological PY neuron. There are more than fifty equations in this model, and the dimension of the parameter space is between 10 and 100 during different stages of computation. During the execution of the

evaluation function, a program written in NETWORK is called for solving the ODEs system.

CHAPTER 2

PREDICTION OF THE ACTIVITY PHASE

The research in this chapter is focused on simulating the follower neurons PY which receive inhibitory synaptic inputs from the pacemaker neurons AB and PD. Since AB and PD neurons oscillate in phase, in the rest of the dissertation I will use the membrane potential traces of PD to represent the pacemaker neurons.

2.1 Introduction

Bursting oscillations occur in many neurons and other cell types and underlie rhythmic activity in many networks of the central nervous system. In the mammalian thalamocortical system, for example, bursting occurs in the thalamocortical neurons during EEG-synchronized sleep (McCormick and Bal, 1997). Other examples include the circadian rhythmicity which results from the interaction of the circadian pacemaker, comprised of the neurons of the suprachiasmatic nucleus and other neurons such as the photoreceptors (Moore, 1999). Bursting oscillations are particularly prevalent in neurons of central pattern generators (CPGs) that produce rhythmic motor activity. These types of neurons include, for instance, the respiratory neurons in the pre-Botzinger complex of the brain stem that exhibit pacemaker bursting activity (Johnson et al., 1994).

The activity of oscillatory networks of neurons is determined by the oscillation frequency as well as the activity phase of the component neurons within each cycle. In

many oscillatory networks, the relative bursting phase among neurons plays an important role in determining the normal or dysfunctional output of the network. In CPGs, for instance, the relative phase of neurons or groups of neurons determines the order of muscle contractions and therefore the motor behavior (Marder and Bucher, 2007). It has also been shown that the motor system dysfunction associated with Parkinson's disease, is critically dependent on how the phase relationships between basal ganglia nuclei are affected by the loss of dopamine (Walters et al., 2007). The phase difference between neurons is often maintained over a wide range of frequencies (Marder and Calabrese, 1996; Marder et al., 2005).

The A-current is a transient outward potassium current that is present in most neuronal types and contributes to spike timing. The A-current is an essential factor in determining the frequency-current response of neurons, as was first shown in the seminal paper of Connor and Stevens (Connor and Stevens, 1971). In the CA3 pyramidal cells in the hippocampus, the activation of the A-current underlies the propagation failure of action potentials in axons (Debanne et al., 1997). The A-current has been shown to be important in determining the post-inhibitory rebound bursting phase of neurons and its effect on determining this phase is subject to the neuromodulation of the current by dopamine (Harris-Warrick et al., 1995a).

In order to investigate how the A-current interacts with other intrinsic and synaptic factors to affect the activity phase of a follower neuron, the research is focused on a simple inhibitory network consisting of a pacemaker neuron and a follower neuron. The prototype of the modeling includes two neurons, the pyloric dilator (PD) and the pyloric constrictor (PY), of the pyloric CPG in the stomatogastric nervous system of the crab *Cancer borealis*.

The PD neurons are members of the pyloric pacemaker ensemble and produce very regular bursting activity with a period of around 1 sec. The follower PY neurons are also members of the pyloric system which oscillate due to the synaptic inhibition they receive from the pacemaker neurons.

The activity phase of pyloric follower neurons such as PY has been partially attributed to the presence and extent of the A-currents in these neurons (Harris-Warrick et al., 1995a; MacLean et al., 2005). In the current study, the dynamic clamp technique has been used to verify the role of the A-current in setting the activity phase of follower PY neurons. Based on these results, a 3-variable model has been developed to analyze how the interaction between the A-current and other intrinsic properties of the follower neuron determine the post-inhibition activity phase of this neuron. This model, which is based on the model of Bose et al. (2004), focuses on the bursting envelope of the follower neuron and the spiking properties are ignored.

The techniques of phase space analysis and separation of time scales are applied to determine the factors that determine the fate of the follower neuron trajectory following inhibition in a single cycle of oscillation. These results are then used to derive a set of equations that describe the steady state phase of the follower neuron in response to a repetitive periodic input. These equations depend on a set of model parameters, including the active and inactive durations of the pacemaker neurons. Finally, the phase of the follower neuron as predicted by these equations is compared with the phase of the biological PY neurons when the network cycle period is varied using different protocols.

2.2 Post-Inhibition Phase of an Oscillatory Neuron and the Role of the A-Current

This study is motivated by the observation that different neurons in a CPG network are active at different phases of each cycle of oscillations. These distinct phases often command the contraction phases of distinct muscles which, in a coordinated fashion, produce meaningful movements. CPG network neurons are typically subject to inhibitory inputs and produce activity upon rebound from this inhibition. An example of this type of activity is shown for the PY neurons in Figure 2.1(a). There are three to five PY neurons in the pyloric CPG and these neurons can have fairly distinct activity phases. As seen in Figure 2.1(a), PY1 has a more advanced phase than PY2, while PY3 does not spike at all. It has been shown that the activity phase of the PY neuron is affected by the strength of the A-current (Harris-Warrick et al., 1995a). The study in this chapter is based on the hypothesis that the strength and kinetics of the A-current in individual PY neurons can determine their distinct activity phases.

In order to quantitatively demonstrate how the A-current affects the activity phase, an artificial A-current is injected into a single PY neuron using the dynamic clamp technique and measured the shift in the PY neuron activity phase while varying the maximum conductance (g_A) of the A-current. Figure 2.1(b) shows the experimental results. In Case i, g_A is equal to zero and therefore the trace shows the membrane potential of the PY neuron without any additional input. In Cases ii-iv g_A was increased gradually, and the activity of the PY neuron is shifted to a later phase. When the maximum conductance was very large (Case iv), there were no action potentials and the active phase of the PY neuron was effectively suppressed. This case was similar to the ongoing activity of the PY3 neuron in Figure 2.1(a).

In the following sections, we will use a simplified neuronal model to analytically explore the role of the A-current in determining the activity phase of CPG neurons such as the PY neuron. These analytical results will then be used to predict this phase for the biological neuron as a function of the frequency and duty cycle of the oscillatory inhibition it receives.

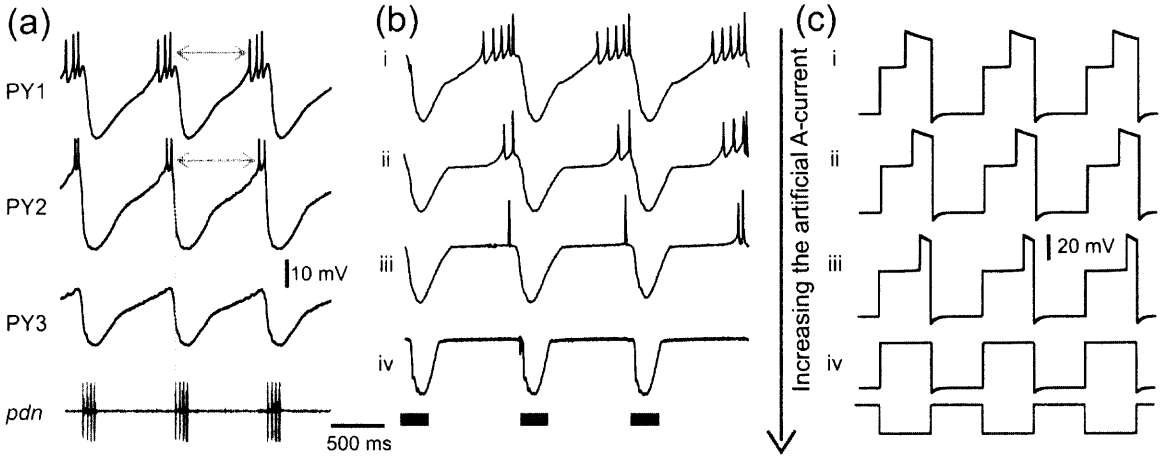

Figure 2.1 The Effect of the A-Current on the Activity Phase of Biological and Model PY Neurons. (a) Simultaneous recording of three biological PY neurons in the crab STG. All PY neurons receive periodic inhibitory synaptic input from the pyloric pacemaker neurons. The activity of the pacemaker neurons can be seen in the extracellular nerve recording (*pdn*, bottom trace). Note that the PY neurons burst with different time delays (arrows) with respect to onset of the pacemaker input (vertical dotted line). PY2 has a more delayed phase than PY1, while PY3 does not spike at all. **(b)** An artificial A-current was injected into a PY neuron, using the dynamic clamp technique, and its strength (g_A, the maximum conductance) was increased from top to bottom (in nS: i: 0, ii: 50, iii: 100, iv: 200), resulting in an increase in the delay to the active state. When the maximum conductance was too large (iv), the PY neuron was not able to reach the active state and there were no action potentials. Note that even without the dynamic clamp A-current, there was a delay to the active state of the PY neuron presumably due to its intrinsic biological A-current. **(c)** The effect of the A-current shown in panel b can be mimicked by simulating the three-variable model with different values of g_A. Note that this model represents only the envelope of slow oscillations and the spikes seen in the biological neuron are smoothed over. Model parameters: (in ms) $T_{in} = T_{act} = 500$, $\tau_{hl} = 495$, $\tau_{hm} = 810$, $\tau_{hh} = 1000$, $\tau_{wl} = 40$, $\tau_{wm} = 100$, $\tau_{wh} = 800$; (in mV) $E_L = -60$, $E_{Ca} = 120$, $v_m = -1.2$, $k_m = -18$, $E_K = -84$, $v_w = 15$, $k_w = -5$, $v_n = -6$, $k_n = -0.5$, $v_h = -10$, $k_h = 0.1$, $E_{inh} = -80$; (in nS) $g_L = 2$, $g_{Ca} = 4$, $g_K = 8$, $g_A = 3.5$(i), 3.7(ii), 4(iii), 5(iv), $g_{inh} = 2$; (in pA) $I_{ext} = 75$.

2.3 Models

2.3.1 General Equations

The model in this chapter is based on the model of Bose et al. (2004) which includes three variables to determine the bursting envelope: two variables (v and w) are from the Morris-Lecar (ML) model representing the membrane potential of the follower neuron and the activation variable of the potassium current, and one variable h describing the A-current inactivation. This model represents only the envelope of the oscillatory activity in the PY neurons; the spikes shown in Figures 1(a) and 1(b) are smoothed over as they do not play an important role in determining the effect of the A-current. The equations for the model are given as

$$\begin{aligned} \varepsilon \frac{dv}{dt} &= f(v,w) - g_A n_\infty(v) h (v - E_A) - I_{inh} \\ \frac{dw}{dt} &= \frac{w_\infty(v) - w}{\tau_w(v)} \\ \frac{dh}{dt} &= \frac{h_\infty(v) - h}{\tau_h(v)} \end{aligned} \tag{2.1}$$

where

$$f(v,w) = I_{ext} - g_L(v - E_L) - g_{Ca} m_\infty(v)(v - E_{Ca}) - g_K w (v - E_K) \tag{2.2}$$

represents the ML terms, and $w_\infty(v)$, $n_\infty(v)$ and $h_\infty(v)$ are sigmoidal functions respectively representing the steady state values of the activation variable for the potassium current, the activation and inactivation variables for the A-current. Each sigmoidal function has the form:

$$x_\infty(v) = \frac{1}{1 + \exp(\frac{v - v_x}{k_x})} \tag{2.3}$$

Here k_x is negative for activation variables and positive for deactivation variables. The sigmoid is considered to be steep when the parameter $k_x \sim O(\varepsilon_1)$ where $0 < \varepsilon_1 << 1$. In the current model k_n and k_h are set to be small ($\sim O(\varepsilon_1)$), but k_w, which determines the shape of the w-nullcline, can be small or large. The time constants $\tau_w(v)$ and $\tau_h(v)$ determine the speed with which the variables w and h change in different voltage regions.

The synaptic current has the following expression:

$$I_{inh} = g_{inh} s_\infty(v_0)(v - E_{inh}) \tag{2.4}$$

$s_\infty(v_0)$ was set as a steep sigmoid in order to simplify the synaptic mechanics.

Figure 2.1 (c) shows the voltage traces simulated by the model for different values of g_A. As in the model of Bose et al., the activity of the pacemaker neuron is simplified by defining the membrane potential v_0 of the PD neuron as a square wave oscillating periodically between -50 mV and 0 mV with active duration T_{act} and inactive duration T_{in} (Figure 2.1(c), bottom trace). As seen in Figure 2.1c, the model neuron membrane potential oscillations consist of three voltage ranges (low, medium and high) and transitions between these three states. The low voltage state corresponds to the inhibition from the pacemaker; the high voltage state represents the spiking or active state and the medium voltage state represents the post-inhibition state before spiking occurs. As with the biological neuron (Figure 2.1(b)), when the value of g_A is increased from top to bottom, the duration spent in the high voltage state decreases (Figure 2.1(c), Cases i-iii) and thus the active phase is more and more delayed. For large enough g_A the active phase is suppressed (Case iv).

2.3.2 The Role of the A-Current and the Inhibition in the *v-w* and *w-h* Phase Planes

The trajectory of the follower neuron in its three-variable phase space can be analyzed by considering the dynamics of the trajectory on two distinct two-dimensional manifolds: the *v-w* plane and the *w-h* plane (described further below). The dynamics of the trajectory in the *v-w* plane are described using a family of "phase planes" parameterized by the slow variable *h* which represents the inactivation of the A-current.

Without the A-current term, the ML model is described by a cubic *v*-nullcline and a sigmoidal *w*-nullcline in the *v-w* phase plane (Rinzel and Ermentrout, 1998). When a trajectory lies near the left branch the neuron is said to be silent; when it is near the right branch the neuron is called active. The left and right branches of the *v*-nullcline correspond, respectively, to the low- and high-voltage states as described in Figure 2.1(c). In the ML model, if a fixed point lies on the sections of the *v*-nullcline that have negative slope (i.e. the left or right branch) it is stable and if it is in the section with the positive slope (between the minimum and maximum) it is unstable (Rinzel and Ermentrout, 1998). With the parameters used in Figure 2.1(c), in the absence of an A-current, the *v*- and *w*-nullclines intersect on the right branch at a stable fixed point (FP_2 in Figure 2.2(a)), which implies that without inhibition, the model neuron is always active. This corresponds to the fact that the PY neurons are active (spike tonically) when they do not receive inhibition from the pacemaker (Rabbah and Nadim, 2005).

In the presence of the A-current term, however, there is an additional "middle branch" on the *v*-nullcline that has negative slope and therefore the nullcline shape is quintic (Figure 2.2(a)). Due to the negative slope of this branch, any fixed point that lies on it would also be stable. The notations LB, MB and RB will be used to denote the left

branch, middle branch and right branch, respectively (Figure 2.2(a)). The assumption that the steady state inactivation curve of the A-current is steep (k_n is small) implies that MB is almost vertical. In fact, for the remainder of this manuscript it is assumed that MB is vertical ($\varepsilon_1 = 0$). The consequences of relaxing this assumption have been examined in a separate study (Zhang and Nadim, 2008). The lower knee, the upper knee and the fixed point (when present; FP in Figure 2.2(a)) on MB are named as LK, UK and FP. When h decreases (i.e. the A-current inactivates), LB is unchanged, but MB shrinks (LK moves up), and RB moves up as well (Figure 2.2(a)).

The inhibition from the pacemaker neuron causes the v-nullcline to move down vertically for a distance depending on the strength of the inhibitory synapse (Figure 2.2(b)), as seen by the influence of the negative term I_{inh} in Equation (1). For large enough inhibition, this shift always results in a stable fixed point (FP_1) on the left branch (called LB^1 for the inhibited nullcline; Figure 2.2(b)). In this study, it has been assumed that the onset and decay of inhibition is fast and therefore the inhibition is only important during the active state (T_{act}) of the pacemaker.

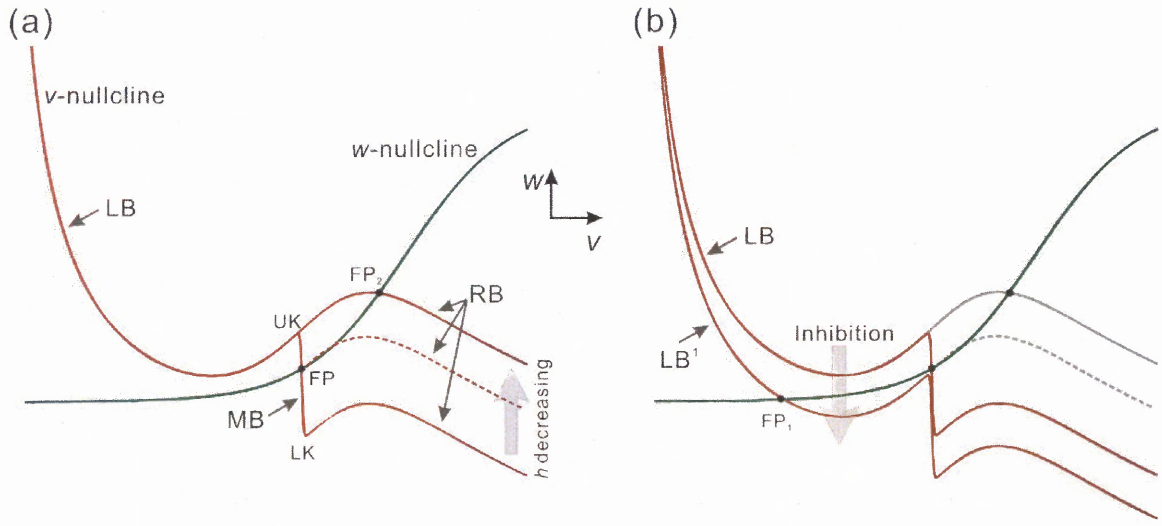

Figure 2.2 The Changes of the Nullclines Caused by the A-Current and the Inhibition in the *v*-*w* Phase Plane. (a) The presence of the A-current term causes an additional middle branch on the *v*-nullcline that has negative slope and therefore the nullcline shape is quintic. LB, MB and RB represent the left, middle and right branches of the *v*-nullcline respectively. UK and LK denote the upper and lower knee of MB. As the inactivation fraction *h* decreases, MB shrinks from LK. The dashed nullcline represents an intermediate value of *h*. **(b)** The inhibition from the pacemaker neuron causes the *v*-nullcline to move down vertically for a distance depending on the strength of the inhibitory synapse. FP, FP_1 and FP_2 represent fixed points in the *v*-*w* phase plane.

In the *v*-*w* phase plane, the steepness and midpoint of the *w*-nullcline determine the existence of a stable fixed point on MB. If there is an intersection on MB (Figure 2.3(a)), then the fixed point exists and is locally stable. If the *w*-nullcline sits above MB, there will be no fixed point on MB. However, in this case the flow on MB is still attracted by the *w*-nullcline and, although there is no fixed point on MB, for each point on MB there is a "pseudo-fixed point" on the *w*-nullcline above MB (Figure 2.3(c)). The pseudo-fixed point can be formally defined for any point (*v*, *w*) located on the middle branch as the point (*v*, *w'*) with the same *v*-coordinate on the *w*-nullcline. Any fixed point or pseudo fixed point is labeled by FP.

The *w*-*h* phase plane is used to analyze the dynamics of the trajectory following the release from inhibition, when the A-current is large enough to prevent an immediate jump

to the active state. In this case, the trajectory lands on MB (corresponding to the middle-voltage state in Figure 2.1(c)). Although MB is a one-dimensional curve in the *v*-*w* phase plane, the dynamics of the trajectory are in fact determined primarily by both slow variables. Thus, it is simpler to analyze the fate of the trajectory on MB by examining its evolution in the *w*-*h* phase plane.

Figures 2.3(b) and 2.3(d) show the curves representing LK UK and FP in the *w*-*h* phase plane, corresponding, respectively, to the two cases shown in Figures 2.3(a) and 2.3(c). The curves LK, UK and FP represent the lower and upper knees of MB and the fixed point as seen in the *v*-*w* phase plane. The shadowed areas represent the possible ranges of the trajectories. UK and FP are vertical lines as their positions in the *w*-direction are not changed. LK is a curve with negative slopes since the *h* value deceases as the *w* value is increasing when the trajectory is moving on MB. Consistent with the locations of FP and UK shown in the *v*-*w* phase plane (Figures 2.3(a) and 2.3(c)), in Figure 2.3(b), FP is on the left of UK while, in Figure 2.3(d), FP is on the right of UK. The black arrow in each of these two figures shows the flow direction in the *w*-*h* phase plane.

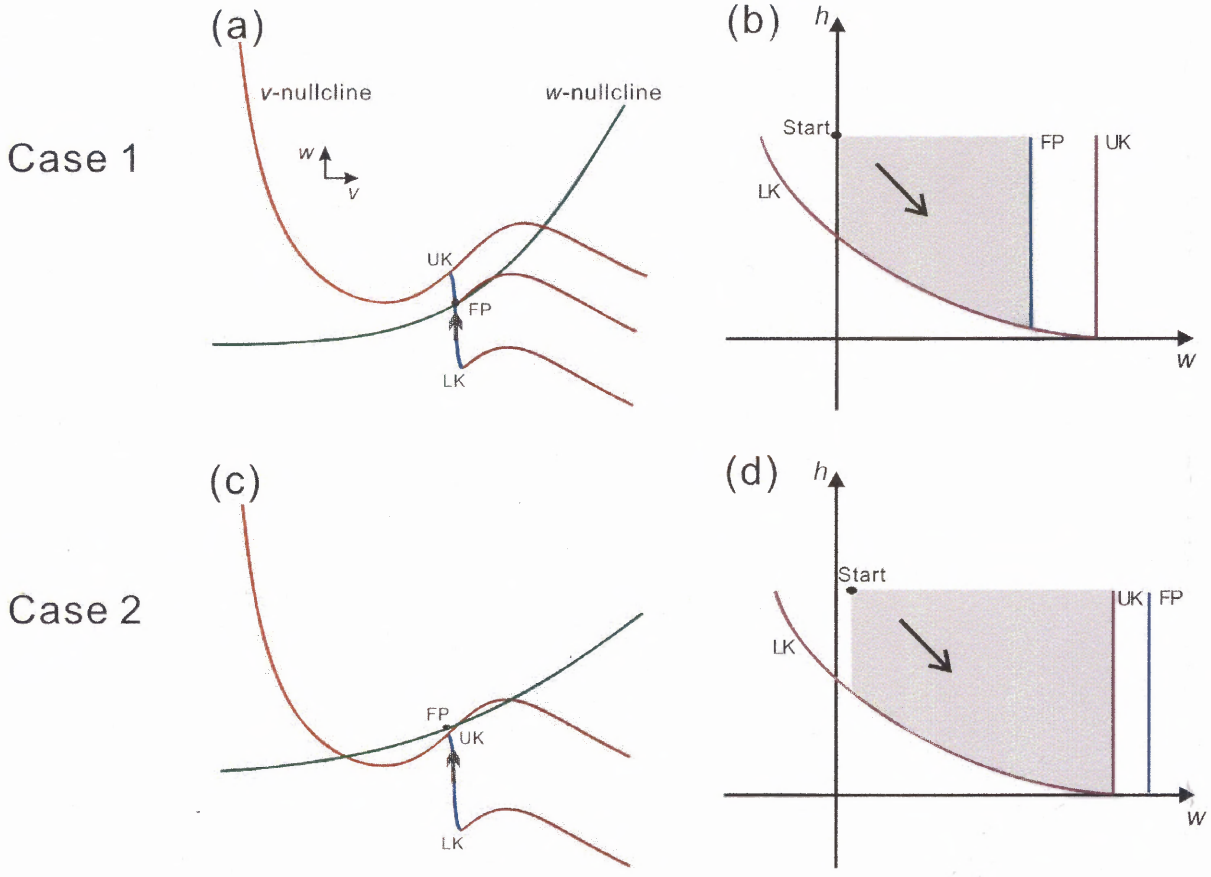

Figure 2.3 The Parameters of the A-Current, in Conjunction with Other Intrinsic Model Parameters, Can Determine the Fate of the Follower Neuron Trajectory. Two qualitatively distinct cases are shown in the phase space based on the shape and relative position of the nullclines which are in turn determined by the relative positions of $w_\infty(v)$ and MB (blue segment of the v-nullcline). Panels a and c show these two cases in the v-w phase plane; panels b and d show the same cases in the w-h phase plane respectively. In the w-h phase plane (b and d), the curves LK, FP and UK correspond to the lower knee LK, the upper knee UK and the fixed point FP in the v-w phase plane. The point "Start" denotes the entrance of the trajectory into the w-h phase plane and the grey area represents the potential paths of the trajectory. Case 1 (a & b; fixed point on MB): **(a)** In the v-w phase plane, the two nullclines intersect at FP on the middle branch (MB). **(b)** In the w-h phase plane, the trajectory is blocked by FP and can never reach UK. Case 2 (c & d; no fixed point on MB): **(c)** In the v-w phase plane, there is no intersection on the middle branch of the v-nullcline. **(d)** In the w-h phase plane, FP is to the right of UK and therefore the trajectory may reach UK.

2.3.3 The Singular Perturbation Assumption and the Reduced Equations

The membrane potential of the follower neuron can be mapped to a trajectory on the *v*-*w* phase plane. For ε small enough (see Equations (2.1)), the system is singularly perturbed (Mishchenko and Rosov, 1980). As a consequence, in some regions of phase space, *v* changes very quickly while *w* and *h* remain nearly constant. In other regions, the behavior of *v* can be slaved to that of *w* and *h*. Equations to describe either can be obtained by setting $\varepsilon = 0$ in Equations (2.1) or a time-rescaled version of Equations (2.1). These two sets of equations are respectively referred to as the slow and the fast equations and can be obtained as follows.

The slow equations are found by setting $\varepsilon = 0$ in Equations (2.1):

$$\begin{aligned} 0 &= f(v,w) - g_A n_\infty(v) h (v - E_A) - I_{inh} \\ \frac{dw}{dt} &= \frac{w_\infty(v) - w}{\tau_w(v)} \\ \frac{dh}{dt} &= \frac{h_\infty(v) - h}{\tau_h(v)} \end{aligned} \tag{2.5}$$

Note that the first equation in (2.5) describes the *v*-nullcline, thus indicating that the slow equations describe the dynamics of the trajectory on this nullcline.

The fast equations are obtained by rescaling $t = \varepsilon\xi$ in Equations (2.1) and then setting $\varepsilon = 0$:

$$\begin{aligned} \frac{dv}{d\xi} &= f(v,w) - g_A n_\infty(v) h (v - E_A) - I_{inh} \\ \frac{dw}{d\xi} &= 0 \\ \frac{dh}{d\xi} &= 0 \end{aligned} \tag{2.6}$$

These equations control the trajectory during the jumps between the branches of the v-nullcline. Note that the last two equations in (2.6) imply that the values of w and h do not vary during these jumps.

Each cycle of the trajectory is pieced together using solutions of Equation (2.5) to determine the movement on the branches of the v-nullcline and of Equation (2.6) to determine the jumps between these branches. For instance, during the inhibition by the pacemaker neurons, the trajectory moves toward FP_1 on LB^1 during T_{act}, and it stays near FP_1 due to its stability (Figure 2.4(a)). When the inhibition ends, the v-nullcline is raised (as described in Figure 2.2(b)). FP_1 no longer exists therefore the trajectory can jump to MB. In fact the trajectory is able to jump when it reaches the knee on any branch. For example, when the trajectory encounters the lower knee of MB, it jumps to RB. These jumps correspond to saddle-node bifurcation in the fast equations (Equation (2.6)) (Rinzel and Ermentrout, 1998). The existence of a trajectory to the full system (Equations (2.1)) that is close to the "pieced-together" trajectory obeying the lower-dimensional slow and fast Equations (2.5) and (2.6) follows from the results of geometric singular perturbation theory as described by Mishchenko and Rosov (1980).

The trajectories of interest are restricted to three branches of the v-nullcline: the left branch LB^1 in the presence of inhibition and the middle and right branches (MB and RB) in its absence, and the jumps between these branches. The slow equations for the trajectory moving on LB^1, MB and RB are given as:

On LB^1:

$$
\begin{aligned}
0 &= f(v,w) - g_A n_\infty(v) h(v - E_A) - g_{inh}(v - E_{inh}) \\
\frac{dw}{dt} &= \frac{-w}{\tau_{wl}} \\
\frac{dh}{dt} &= \frac{1-h}{\tau_{hl}}
\end{aligned}
\tag{2.7}
$$

On MB:

$$
\begin{aligned}
0 &= f(v,w) - g_A n_\infty(v) h(v - E_A) \\
\frac{dw}{dt} &= \frac{w_{FP} - w}{\tau_{wm}} \\
\frac{dh}{dt} &= \frac{-h}{\tau_{hm}}
\end{aligned}
\tag{2.8}
$$

On RB:

$$
\begin{aligned}
0 &= f(v,w) - g_A n_\infty(v) h(v - E_A) \\
\frac{dw}{dt} &= \frac{w_\infty(v) - w}{\tau_{wh}} \\
\frac{dh}{dt} &= \frac{-h}{\tau_{hh}}
\end{aligned}
\tag{2.9}
$$

The simplifying assumption that $h_\infty(v)$ is steep (k_h is small) implies that $h_\infty(v) = 1$ on LB[1] and $h_\infty(v) = 0$ on MB and RB. The time constants for w and h on the left branches (LB and LB[1]), the middle branch (MB) and the right branch (RB) are set as τ_{wl} and τ_{hl}, τ_{wm} and τ_{hm}, and τ_{wh} and τ_{hh} respectively. All time constants are assumed to be of the same order of magnitude as T_{act} (O(T_{act})) unless otherwise specified in the Results. In cases where two time constants are assumed to be of different orders of magnitude (i.e. $\tau_1 << \tau_2$), the larger one (τ_2 in this case) is assumed to be O(T_{act}).

2.4 Results

As described above, a numerical simulation of the model (Equations (2.1)) with different parameter sets can reproduce the variety of phase delays observed in the biological PY neurons. The goal in this study is to determine which parameters result in the distinct values of the activity phase delay in the model neuron following inhibition, and to derive the relationships among parameters that would allow this activity phase to be predicted as a function of the activity of the pacemaker neuron. At the beginning the behavior of the trajectory in a single cycle is described and then this information is used to derive the activity phase in response to a periodic input. Because the activity phase of the neuron following inhibition is determined by the time it spends on the middle branch MB, the research focus is how the trajectory lands on MB, the factors that determine its fate on MB and where it goes after leaving MB.

2.4.1 The Fate of the Trajectory on MB

Suppose at the beginning the trajectory is at FP_2 (Figure 2.4(a)). Assume at $t = 0$ the follower neuron is inhibited and the trajectory lands on LB^1. For the duration of inhibition (T_{act}), the trajectory moves downwards along LB^1 towards the stable fixed point FP_1 (Figure 2.4(a)). An assumption is that τ_{wl} is small enough on LB^1 such that, during the inhibited state, the trajectory reaches a small neighborhood of FP_1. At the same time, the inactivation variable h of the A-current increases with time constant τ_{hl}. The growth of h does not affect the shape of LB^1, but does result in a larger MB^1. In fact, the size of MB^1 is related to how long the follower neuron stays in the inactive state. At the end of the inhibition, the trajectory in the v-w plane is released from a neighborhood the fixed point

FP_1 and jumps horizontally to MB. Once the trajectory lands on MB, h begins to decay with the time constant τ_{hm} which causes MB to shrink from the lower knee LK. At the same time, the trajectory moves at the rate τ_{wm} towards the fixed point FP.

Figures 2.4(a) and 2.4(c) show two possible cases – Case 1 and Case 2 – depending on the shape and relative position of the v and w nullclines in the v-w phase plane. In Case 1 the w-nullcline crosses the v-nullcline on the middle branch and UK is always higher than FP in the w direction, while in Case 2 UK is lower than FP as the w-nullcline is above the middle branch of the v-nullcline. The trajectory cannot reach UK in Case 1 therefore it can only jump to the right if LK moves fast enough during T_{in}. In Case 2, however, FP is above the middle branch, which allows the trajectory to jump left if it moves fast enough to reach UK during T_{in}. Although these two possibilities are not exhaustive, they indicate how the structure of the nullclines can determine the fate of the trajectory on MB.

Figures 2.4(b) and 2.4(d) show the possible trajectories of Case 1 and Case 2, respectively, in the w-h phase plane. The curves LK, UK and FP are as defined in Figure 2.3. The difference between Cases 1 and 2 is that, in the w-h phase plane, the FP curve lies to the left of the UK curve in the former case but to its right in the latter (Figures 2.4(b) and 2.4(d)). Thus, from the relative positions of the LK, UK and FP curves, it immediately follows that, in Case 1, the trajectory can only leave MB by jumping from LK to RB (because FP blocks the access to UK), whereas in Case 2, a trajectory could leave MB either by reaching LK and jumping to RB or by reaching UK and jumping to LB.

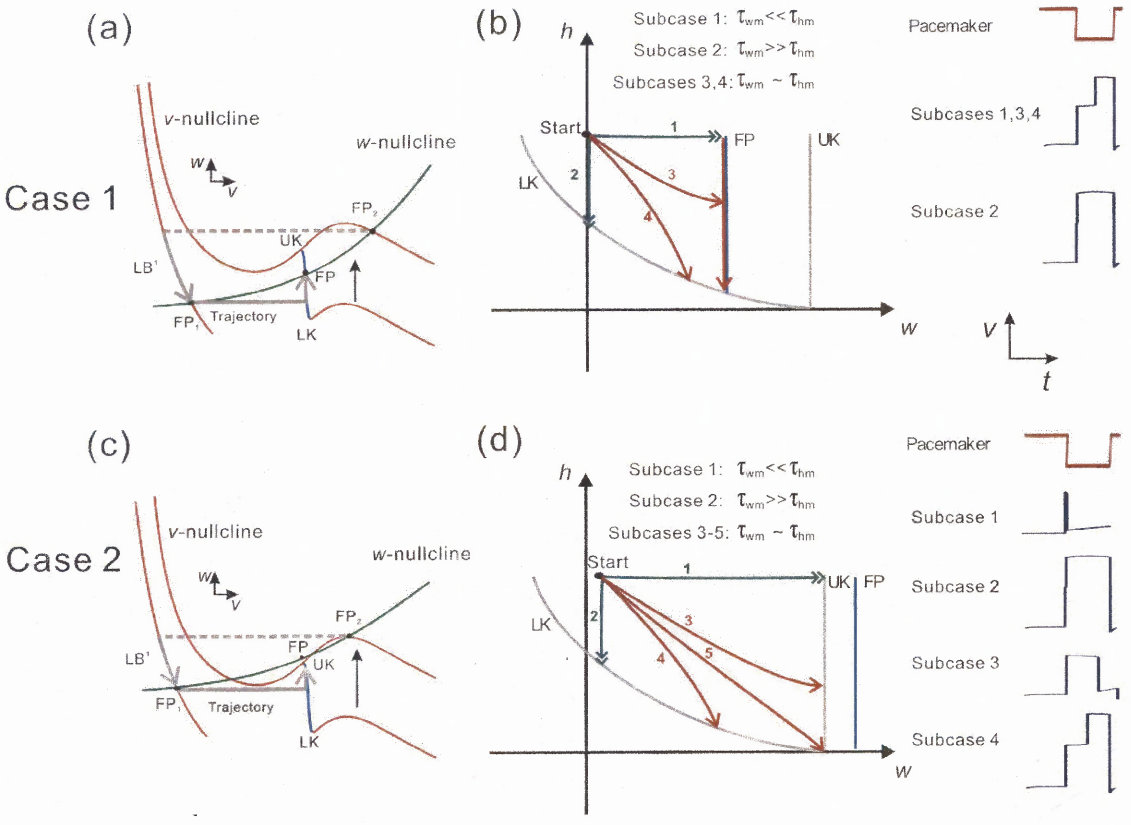

Figure 2.4 The Dynamics of Cases 1 (a & b) and 2 (c & d) in the *v*-*w* and *w*-*h* Phase Planes. **(a)** In Case 1, the trajectory jumps to the left branch (LB^1) from FP_2 at the onset of inhibition and then moves along LB^1 to FP_1 during T_{in}. When the inhibition ends, the trajectory jumps to the middle branch MB and moves toward FP. At the same time, MB shrinks from LK due to the decay of h. **(b)** In the *w*-*h* phase plane, four subcases are possible based on the relative size of the two time constants τ_{wm} and τ_{hm}. Note, however, that the only way the trajectory can leave this phase plane is by reaching LK. **(c)** In Case 2 the shape of the *w*-nullcline causes $w_{FP} > w_{UK}$ on MB. After landing on MB, the trajectory moves toward FP, and LK rises simultaneously as the MB shrinks. **(d)** Five subcases can be achieved in the *w*-*h* phase plane based on the relative size of τ_{wm} and τ_{hm}. In this case, trajectories 1 and 3 leave the phase plane by reaching UK whereas trajectories 2 and 4 leave from LK. The fate of trajectory 5 is unclear since it reaches the intersection of LK and UK. Insets on the right of panels b and d show the time traces of the pacemaker and the follower neuron in each subcase.

2.4.1.1 Case 1 The trajectory arrives on MB through a horizontal jump (in the *v*-*w* plane) and therefore the initial w value on MB is the same as the last value on LB^1. The movement of the trajectory in the *w*-*h* phase plane is determined by the time constants τ_{wm} and τ_{hm}. According to these time constants, several subcases can be defined that represent

all possible trajectories on MB. Each subcase is shown as an arrowed curve on the *w*-*h* manifold (Figure 2.4(b)). In Case 1, for instance, there are four subcases: Subcase 1 satisfies the condition $\tau_{wm} << \tau_{hm}$ which causes a fast motion in the *w* direction, therefore the trajectory rapidly moves to FP immediately after landing on MB, and it follows the FP curve vertically down until it reaches the LK curve. Subcase 2 satisfies the condition $\tau_{wm} >> \tau_{hm}$, which makes the trajectory move rapidly in the *h* direction until it reaches the LK curve. In Subcase 3 and 4, τ_{wm} and τ_{hm} are of the same order and therefore there is no rapid movement in either the *w* or the *h* direction. The trajectory either reaches FP first and then moves vertically down to LK (Subcase 3) or moves directly to LK without encountering FP (Subcase 4). Note that in all four subcases, the trajectory eventually reaches LK and jumps to RB. Subcases 1 and 3 are distinguished from 2 and 4 by the fact that the fixed point is playing a role in determining the movement of the trajectory. Bose et al. (2004) examined only Subcase 1 as defined here.) Note also that Subcases 1, 3 and 4, but not 2, result in a measurable delay to activity of the follower neuron (insets in Figure 2.4(b)).

2.4.1.2 Case 2 A similar method is applied to analyze Case 2. In this case, because the w-nullcline is relatively shallow, it does not intersect MB in the v-w plane. In Subcase 1 the trajectory moves quickly in the w-direction and reaches UK almost immediately after landing on MB, which leads to a left jump back to LB. Subcase 2 is the same as that in Case 1, in which the trajectory reaches LK fast and then jumps to RB. Subcase 3 and 4 show the cases when τ_{wm} and τ_{hm} are of the same order. The trajectory reaches UK and jumps left in the former and it reaches LK and jumps right in the latter. Subcase 5 shows a rare possibility that the trajectory reaches UK and LK at the same time when MB shrinks to a point or when $h = 0$. In this case the fate of the trajectory remains ambiguous.

Note that in Case 1, although the delay to activity in Subcases 1, 3 and 4 can be quite similar, Subcase 1 is inherently distinct from the other two. In this subcase, the delay to the active phase is caused only by the presence of the fixed point FP and the delay caused by the time spent in MB would completely disappear if the FP disappeared (e.g. if g_{Ca} is increased in Equations(2.1)), in which case the behavior of the follower neuron would be identical to that of Subcase 1 of Case 2 (Figure 2.4(d)).

2.4.1.3 Simulation of the Biological Neurons The geometric setup described in Figure 2.4 now is used to demonstrate the distinct behaviors of the biological PY neurons. In order to simulate the biological PY neurons, only the subcases in Case 1 need to be considered, since the membrane potential of PY never moves to the inactive state without receiving inhibition. Therefore in the *v*-*w* phase plane, the trajectory can only jump to the right or stay on MB (till the next cycle of inhibition) after landing on it. Figures 2.5(a) and 2.5(b) show these two possibilities. In Figure 2.5(a), the left panel shows the model solution which represents the activity of PY1 in Figure 2.1(a) and Case i in Figure 2.1(b); the middle panel shows the trajectory of the solution in the *v*-*w* phase plane; and the right panel shows the trajectory in the *w*-*h* phase plane describing the activity on MB. In this case the trajectory moves faster in the *h* direction than in the *w* direction (as in Subcase 4 of Figure 2.4(b)) and therefore it reaches LK directly and then jumps to the right.

Figure 2.5(b) shows a simulation with a stronger A-current corresponding to PY3 in Figure 2.1(a) and Case iv in Figure 2.1(b). The three panels show the same information as in Figure 2.5(a). It is clear (especially in the right panel) that in this case, the trajectory does not move fast in the *h* direction: it reaches FP first and then moves along it. It fails to reach LK during T_{in}, thus it cannot jump to the right. The trajectory remains near FP on MB

until the next cycle of inhibition arrives (see PY trace in Figure 2.5(b)). The inhibition moves the *v*-nullcline down and the trajectory jumps to the left.

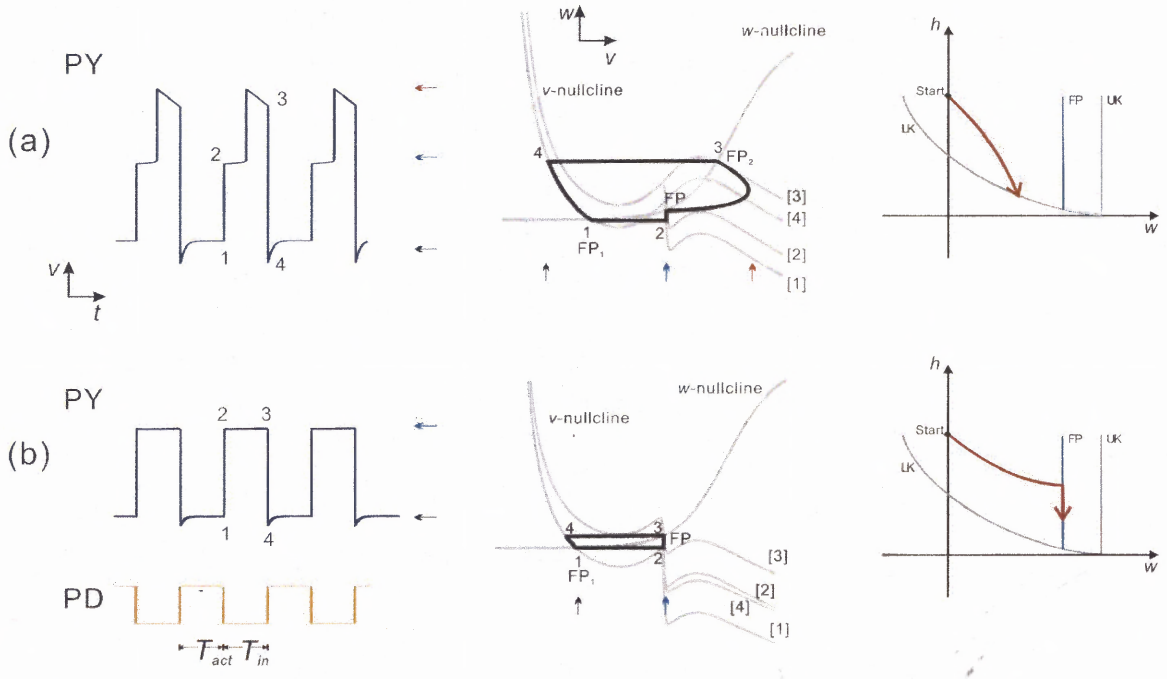

Figure 2.5 The Periodic Solutions in Case 1 When the A-Current is Moderate (a) or Strong (b). (a) Left panel: a modest A-current causes a phase delay to the active state. **Middle panel**: the periodic solutions in the *v*-*w* phase plane. **Right panel**: The trajectory in the *w*-*h* phase plane, which shows the dynamics on the middle branch. The trajectory reaches the curve of the lower knee (LK) during T_{in}, therefore the membrane potential reaches the active state after a phase delay. **(b) Left panel**: the follower neuron cannot reach the active state when the A-current is strong. **Middle panel**: the periodic solutions in the *v*-*w* phase plane. The trajectory jumps back to the left branch when the inhibition starts. **Right panel**: The trajectory reaches the curve of the fixed point (FP), and then it moves downward along FP. It does not reach LK during T_{in}, therefore the membrane potential does not reach the active state. The arrows in the left and middle panels denote the inactive (black), active (red) and intermediate (blue) states. The labels [1-4] in the middle panels denote the *v*-nullcline corresponding to the times denoted by the same label in the left panel.

2.4.2 Periodic Solutions

The analysis in the *w*-*h* manifold provides a clear view of the possible fates of the trajectory on the middle branch in a single cycle. However, the determination of this fate does not guarantee knowledge of the long-term behavior of the follower neuron. This is because the values of *w* or *h* may vary from cycle to cycle and may also depend on the history of these variables in previous cycles. It is possible that these variables converge to a stationary value (dynamic equilibrium) after a number of cycles. In order to determine the long-term behavior of the follower neuron, it is necessary to track the values of *w* and *h* over multiple cycles. In the following sections analytic expressions for each variable as a function of the pacemaker and other network parameters are derived. These expressions are derived for a representative case discussed above.

At first the accumulation of the inactivation variable *h* in Case 1 is examined, which provides a vertical MB and a stable fixed point FP on it (Figures 2.3(a) and 2.4(a)). For simplicity, it is assumed that the movement in the *w* direction on MB is fast compared to the movement in the *h* direction (Subcase 1 or 3 in Figure 2.4(b)) and that τ_{wl}, τ_{wh} and τ_{hh} are set properly to guarantee the trajectory lands on MB only from LB^1 in every cycle. Under these two conditions there is no need to consider the variability of the *w* value in each cycle. Suppose at $t = 0$ the pacemaker becomes active, and therefore the follower neuron moves to its inactive state due to inhibition. Suppose the trajectory starts in the *v*-*w* plane on the left branch with $h(0) = 0$. During $0 < t < T_{act}$, the trajectory moves downwards and obeys Equation (2.7); therefore at $t = T_{act}$:

$$h(T_{act}) = 1 - \exp(-\frac{T_{act}}{\tau_{hl}}) \tag{2.10}$$

Following $t = T_{act}$, the follower neuron is released from inhibition, which is reflected in the v-w phase plane as a jump from LB^1 to MB. When the trajectory lands on the middle branch, it moves to FP and the lower knee LK begins to rise with time constant τ_{hm}. (The assumptions above require that the trajectory does not reach LK before it reaches FP.) The time t_m spent on the middle branch is determined by the equation

$$f(v_\theta, w_{FP}) - g_A h(T_{act}) \exp(-\frac{t_m}{\tau_{hm}})(v_\theta - E_K) = 0 \tag{2.11}$$

Here v_θ is the v value of the middle branch and t_m represents the time the trajectory spends on the middle branch, which can be calculated explicitly (see also (Bose et al., 2004)) as

$$t_m = \tau_{hm} \ln \frac{g_A h(T_{act})(v_\theta - E_K)}{f(v_\theta, w_{FP})} \tag{2.12}$$

If the trajectory is able to jump to the right branch during $(T_{act}, P-\varepsilon_\alpha)$ where $P \equiv T_{act}+T_{in}$, then at $t = P$:

$$h(P) = (1 - \exp(-\frac{T_{act}}{\tau_{hl}})) \exp(-\frac{t_m}{\tau_{hm}} - \frac{T_{in} - t_m}{\tau_{hh}}) \tag{2.13}$$

Here ε_α represents the time the trajectory takes to exceed the w value of the upper knee of MB^1, w_{UK1}, in the w direction while it is moving along RB. ε_α equals to zero if $w_{FP} \geq w_{UK1}$; when $w_{FP} < w_{UK1}$, if the trajectory jumps from MB to RB at a moment in $(P-\varepsilon_\alpha, P)$, then when the inhibition starts at $t = P$, the trajectory will return to MB^1 instead of LB^1. ε_α can be calculated by the following equation:

$$\varepsilon_\alpha = \max(0, \tau_{wh} \ln \frac{w_{FP} - w_{FP2}}{w_{UK1} - w_{FP2}}) \tag{2.14}$$

In order to avoid the trajectory landing on MB^1, τ_{wh} and τ_{hh} are set to be small thereby forcing ε_α to also be small. Under this condition the interval $(P-\varepsilon_\alpha, P)$ can be ignored for simplicity.

If the trajectory is unable to jump to the right branch during (T_{act}, $P-\varepsilon_a$), then at t = P:

$$h(P) = (1-\exp(-\frac{T_{act}}{\tau_{hl}}))\exp(-\frac{T_{in}}{\tau_{hm}}) \tag{2.15}$$

Based on the above steps it is concluded that the following recursive equations describing the values of h in cycle n (h^n) at the moments that the inhibition from the pacemaker is removed at $t = (n\text{-}1)P + T_{act}$:

$$h^n \equiv h(np+T_{act}) = 1+[h((n-1)p+T_{act})\exp(-\frac{T_{in}}{\tau_{hh}}+(\frac{1}{\tau_{hh}}-\frac{1}{\tau_{hm}})t_m{}^n)-1]\exp(-\frac{T_{act}}{\tau_{hl}}) \quad \text{(a)}$$

$$t_m{}^n = \max\{0,\tau_{hm}\ln\frac{g_A h((n-1)p+T_{act})(v_\theta-E_K)}{f(v_\theta,w_{FP})}\} \quad \text{(b)} \tag{2.16}$$

where $t_m{}^n$ denotes the time spent on the middle branch in the n^{th} cycle. Note that if the time spent on the left branch is too short, h would not become large enough (MB does not grow enough) in that cycle and the log term in Equation (2.16)b can be negative. In this case, the trajectory would not land on the middle branch and $t_m{}^n$ is defined to be 0. The activity phase φ in each cycle can be calculated by

$$\phi^n = \frac{T_{act}+t_m{}^n}{P} \tag{2.17}$$

They converge to the steady state values h^* and $t_m{}^*$ which satisfy

$$h^* = 1-\exp(-\frac{T_{act}}{\tau_{hl}})+\exp(-\frac{T_{in}}{\tau_{hh}}-\frac{T_{act}}{\tau_{hl}})(\frac{g_A(v_\theta-E_K)}{f(v_\theta,w_{FP})})^{(\frac{\tau_{hm}}{\tau_{hh}}-1)}(h^*)^{\frac{\tau_{hm}}{\tau_{hh}}} \quad \text{(a)}$$

$$t_m{}^* = \max\{0,\tau_{hm}\ln\frac{g_A h^*(v_\theta-E_K)}{f(v_\theta,w_{FP})}\} \quad \text{(b)} \tag{2.18}$$

In these equations, h^* denotes the steady state value of h (inactivation of the A-current) at the end of the inhibition from the pacemaker in each cycle and $t_m{}^*$ is the

steady state value of the time spent on the middle branch. Therefore the steady state activity phase is

$$\phi^* = \frac{T_{act} + t_m^*}{P} \tag{2.19}$$

Equations (2.16)-(2.19) show that h, t_m and φ can be represented as functions of T_{in} and T_{act}, and therefore the cycle period (P) and the duty cycle (T_{act}/P) of the pacemaker neurons play an important role in determining the activity phase of the follower neuron.

A natural question that arises from these calculations is whether these simplified Equations (2.16)-(2.19) can be used to predict the activity phase of the biological PY neurons. This question is addressed by using an experimental protocol to measure the activity phase of the biological PY neurons as a function of the cycle period of the pacemaker neurons. This experiment was performed by using two PY neurons. In order to control the cycle period, the biological synapses from the pacemaker neurons to the PY neurons were blocked (Rabbah and Nadim, 2005) and the dynamic clamp technique was applied to produce an artificial synaptic input (from a model pacemaker neuron) to the PY neurons. This allowed scientists to change the values of T_{in} and T_{act} (and therefore the cycle period) in a controlled manner. Three different protocols were applied for changing the cycle period.

In the first protocol, the cycle period was changed by varying T_{in} but keeping T_{act} fixed. Figure 2.6(a) shows the membrane potentials of the two PY neurons when T_{act} = 500 ms and T_{in} = 300, 500, 1300 ms. Figure 2.6(b) shows the comparison of steady state phases as predicted by Equations (2.16)-(2.19) and the activity phase of the biological PY neurons. It is clear that the activity phase decreases with T_{in}. In the second protocol, the cycle period was changed by varying both T_{in} and T_{act} while keeping the duty cycle

constant. In the third protocol, the cycle period was changed by keeping T_{in} fixed and varying T_{act}. The results of the model and experiments for these two protocols are shown, respectively, in Figures 2.6(c) and 2.6(d). As seen in Figures 2.6(b)-(d), the model provides a good qualitative prediction of the activity phase of the PY neurons for all three protocols. For the first two protocols and a large range of periods in the third protocol, there is also very good quantitative agreement between the model and the experiments. Note that in many central pattern generators, including the pyloric network, variations of cycle period are similar to the protocol shown in Figure 2.6(c), where the duty-cycle of the pacemaker neurons remains constant (Abbott et al., 1991; Bucher et al., 2005). Despite the fact that the recursive equations were derived using several simplifying assumptions Figure 2.6 indicates that they can faithfully predict the activity phase of the biological neurons.

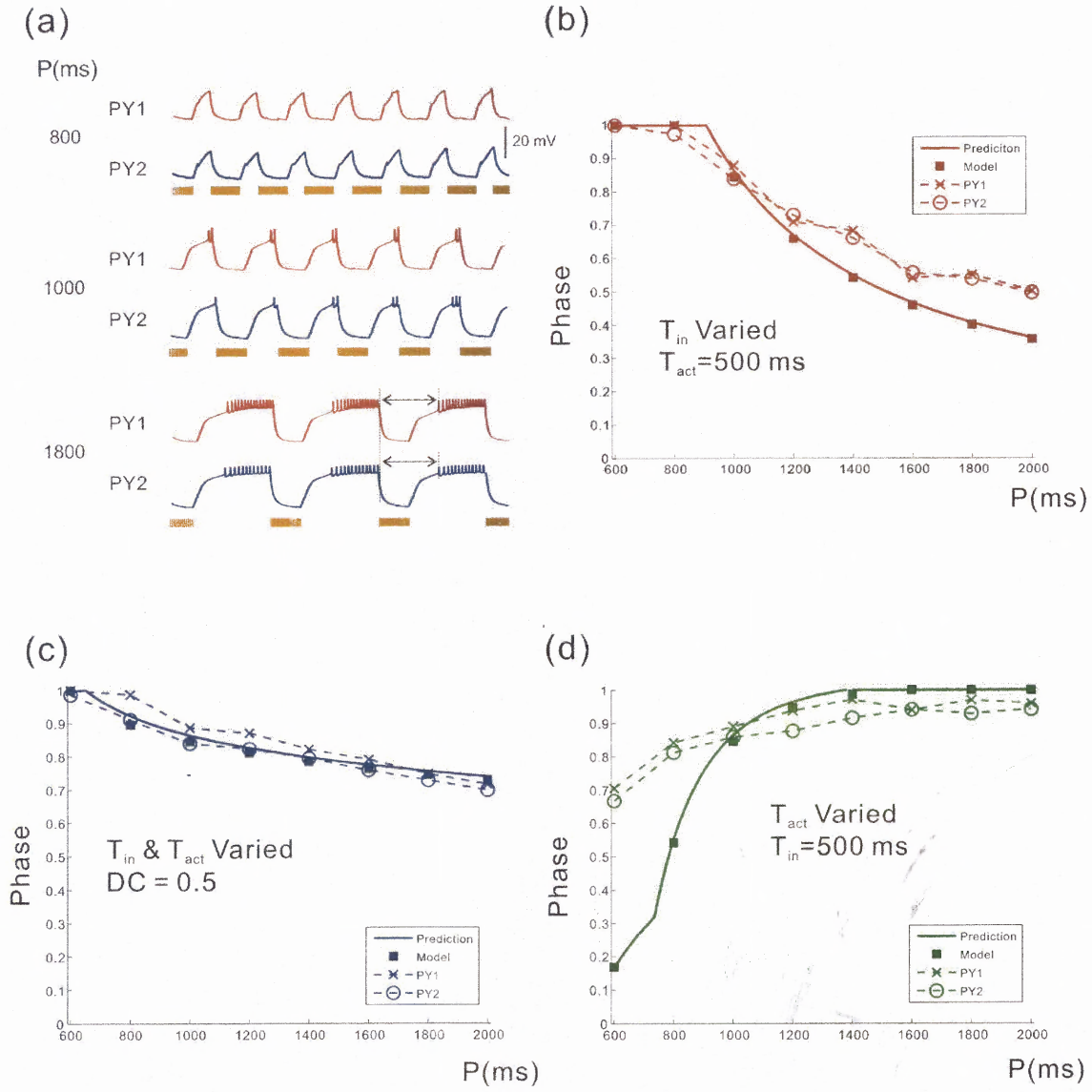

Figure 2.6 The Recursive Equations Predict the Activity Phase of the Model Neuron and the Biological PY Neurons in a Reasonable Accuracy. (a) The time traces of two biological PY neurons when P is varied by varying T_{in} (T_{act} is fixed). The solid bars denote the active duration of the pacemaker input. The phase-period plot when P is varied by varying T_{in} and keeping T_{act} fixed **(b)**; by varying T_{in} and T_{act} but keeping the duty cycle fixed **(c)**; by varying T_{act} and keeping T_{in} fixed **(d)**. In (b-d), the solid curve shows the phase calculated from Equations (16-19); the filled squares show the phase of the 3-variable model; the two dashed curves show the burst phase of the biological PY neurons.

2.5 Summary

The A-current exists in many types of neurons and plays an important role in determining the timing of the spiking or bursting activities (Gerber and Jakobsson, 1993; Harris-Warrick et al., 1995a). In a network of bursting neurons, the A-current often acts to delay the onset of the burst, thus setting the activity phase of different neurons within the network (Harris-Warrick et al., 1995a).

In a previous modeling study (Bose et al., 2004), it was examined as to how the A-current can interact with short-term synaptic depression to promote phase maintenance in a follower neuron when the frequency of the periodic input is varied. Because the focus of the study of Bose et al. was on synaptic depression, only a single set of parameters associated with the A-current were considered. In the current study, the focus of this work is to understand how the parameters associated with the A-current lead to different activity phases of a follower neuron. The study in this chapter was done in two stages. First, dynamical systems analysis was used to determine the fate of the trajectory of the follower neuron following inhibition in a single cycle. This information then was used to derive a set of equations that describe the steady state activity phase of this neuron in response to a periodic input. The activity phase predicted by these equations matched the activity phase of follower PY neurons in the crab pyloric network when cycle period was varied through different experimental protocols.

Although the analysis of the potential post-inhibition fates of the trajectory and the resulting time delays in this chapter is not exhaustive, it indicates how such analysis could be used effectively to determine the factors that control the activity time of a follower

neuron. A more detailed analysis requires examining all possible phase-plane structures that could arise due to the various model parameters and is shown in Chapter 3.

A three-variable model has been used to explore the factors that determine the activity time of a neuron with A-current following periodic inhibitory inputs, and to predict the activity phase of the biological follower neurons by solving the system analytically. The results indicate that, even with a very simple model neuron, the interaction of the A-current parameters and other intrinsic parameters can be quite complex and lead to distinct model behaviors. Although the role of additional factors such as synaptic dynamics and the interaction with other network neurons that can affect the role of the A-current in determining the activity phase remains to be explored, the basic geometric tools have been provided which could be used for such analysis in more complicated settings. The analysis demonstrates that depending on the parameter configurations - corresponding to different states of the biological neuron, different parameters could control the post-inhibition activity phase.

CHAPTER 3

A DETAILED PHASE SPACE ANALYSIS

3.1 Introduction

In Chapter 2, a three-variable model is built and utilized to predict the activity phase of the biological PY neurons. Phase plane analysis is applied to study how the intrinsic properties affect the membrane potential behavior, and a set of recursive equations are derived for calculating the activity phase in each cycle and the steady state value of the activity phase, which can be used to predict the activity phase of the biological PY neurons. There is an assumption for all of these works, which is that the middle branch MB is vertical, or the activation fraction of the A-current, $n_\infty(v)$, is a steep sigmoid.

When the middle branch is not vertical, or $n_\infty(v)$ is not steep, the dynamics of MB becomes more complicated, and the fate of the trajectory on MB becomes more difficult to predict. This chapter shows a complete classification of the possible cases based on the structure and dynamics of the nullclines in the *v*-*w* phase plane. The fate of the trajectory in each case is predicted by comparing the time constants of the slow variables and the motions of the nullclines. More recursive equations are derived for more general cases. In Chapter 2 only the slow variable *h* is considered accumulative during cycles. In this chapter the value of the other slow variable, *w*, is also considered and expressed by another set of recursive equations.

In addition, a set of recursive equations is also derived for calculating the two slow variables of the follower neuron when it receives a relatively weaker synaptic inhibition.

Under this circumstance, the activity phase of the follower neuron with a moderate A-current does not differ from the normal inhibition cases, but with a strong A-current, the activity phase is fairly different, and some unintuitive results can be seen.

3.2 Models

The equations for the model used in this chapter are basically the same as those in Chapter 2. However, there are two differences:

1. The activation fraction of the A-current, $n_\infty(v)$, can be a non-steep sigmoidal function. In other words, the value of k_n in Equation (2.3) in Chapter 2 can be either small or large.

2. When the synaptic inhibition is relatively weak, the trajectory may stay on the middle branch during the active duration of the pacemaker. Therefore it is necessary to show the slow equation on the inhibited middle branch, MB^1:

$$\begin{aligned} 0 &= f(v,w) - g_A n_\infty(v) h(v - E_A) - g_{inh}(v - E_{inh}) \\ \frac{dw}{dt} &= \frac{w_\infty(v) - w}{\tau_{wm}} \\ \frac{dh}{dt} &= \frac{-h}{\tau_{hm}} \end{aligned} \tag{3.1}$$

The other properties of the model keep the same as that in Chapter 2.

3.3 The Fate of the Trajectory on the Middle Branch

As in Chapter 2, the transient behavior of the trajectory on the middle branch is explored at first. Assume at $t = 0$ the follower neuron begins to receive inhibition (as shown in Figure 2.4), and the trajectory jumps from FP_2 and lands on LB^1 in the v-w phase plane. During the

duration of inhibition (T_{act}), the trajectory moves downwards along LB^1 towards the neighborhood of the stable fixed point FP_1 (w decreases), and the value of h increases which causes an extension of the middle branch MB. After the inhibition, the trajectory is released for jumping to MB and starts to move up along MB towards FP. At the same time, MB begins to shrink from the lower knee LK due to the h decaying. For the non-vertical case, the slope of MB also changes. In general there are three possible situations that can arise once the trajectory reaches MB:

Fate 1. The trajectory encounters LK and then jumps to the right branch.

Fate 2. The trajectory encounters UK and then jumps to the left branch.

Fate 3. The trajectory is not able to reach either LK or UK during T_{in}; therefore it cannot leave the middle branch in this cycle.

The fate of the trajectory can be affected by a number of factors, including the time constants of the w and h variables, the shape of the v and w nullclines, and T_{in} and T_{act}, the inactive and active duration of the pacemaker. The two cases – Case 1 and Case 2 in Chapter 2 (Figure 2.4), for instance, are determined by the shape and relative position of the two nullclines under the condition that MB is vertical. In Case 1, only Fate 1 and 3 are feasible. In case 2, all three fates can occur, given that the other conditions are set appropriately. Moreover, since in both cases the middle branch is vertical, the slope of the middle branch does not change during the shrinking process. When $n_\infty(v)$ is not steep, MB is not vertical anymore and its slope changes as h is decaying. Based on this significant difference, all possible cases are classified into two categories:

Category 1. the cases where $n_\infty(v)$ is steep (the two cases in Chapter 2).

Category 2. the cases where $n_\infty(v)$ is not steep.

In all cases it is assumed that τ_{wl} is small enough on LB^1 such that when silent, the trajectory reaches the neighborhood of FP_1. For simplicity it is also assumed that when the trajectory lands on MB it has a w value equal to that of FP_1 which, as can be seen, is less than the w value of FP.

Understanding the shrinking of MB in the v-w phase plane is difficult. This is why the w-h phase plane is considered, where the curves of LKs, UKs and FPs can be properly visualized, and the motion of the trajectory on MB can be shown as curves as well.

3.3.1 Category 1

This category includes the two cases (Case 1 and Case 2) in Chapter 2. In both cases the function $n_\infty(v)$ is a steep sigmoid and therefore, in the v-w phase plane, the v-nullcline has a close to vertical middle branch. For simplicity, it is assumed that this branch is in fact vertical ($\varepsilon_1 = 0$). For consistency, these two cases are renamed to Case 1.1 and Case 1.2 in this chapter.

In Case 1.1 the w-nullcline intersects MB at FP as shown in Figure 2.4(a), while in Case 1.2 the w-nullcline is above MB, therefore there is no fixed point on MB (Figure 2.4(c)). Instead there is a pseudo-fixed point on the w-nullcline as defined in the Model section of Chapter 2. By investigating the dynamics in the w-h phase plane, the fate of the trajectory can be tracked. In fact, in both cases the set of LK for different values of h

defines a curve in this manifold, and the values of UK and FP are represented by two vertical lines, due to the steep $n_\infty(v)$. The difference between Cases 1.1 and 1.2 is that, in the *w-h* phase plane, the FP curve lies to the left of the UK curve in the former case but to the right of it in the latter (Figures 2.4(b) and 2.4(d)). Thus, from the relative positions of the LK, UK and FP curves, it immediately follows that in Case 1.1, the fate of a trajectory leaving MB can only be a jump from LK to RB (there is no access to UK), whereas in Case 1.2, a trajectory could leave MB either by reaching LK and jumping to RB or by reaching UK and jumping to LB.

A detailed study of these two cases can be found in Chapter 2.

3.3.2 Category 2

In all cases of Category 2, $n_\infty(v)$ is not steep which results in a non-vertical MB in the *v-w* phase plane. Under this condition, the slope of MB changes during the shrinking, which leads to a change of position for FP and UK. In addition to the typical cases that determine the fate of the trajectory on MB and that are similar to those described in Category 1, there are two additional non-intuitive possibilities in the geometry of the nullclines that arise as a result of a non-steep $n_\infty(v)$ and can be summarized as follows:

1. If LK moves faster than UK in the *w* direction, then it is possible that LK becomes equal or higher than UK in the *w* direction, or $w_{LK} > w_{UK}$, as MB is shrinking. Then the middle branch becomes unstable and the trajectory jumps to the left or right and this ambiguity cannot be removed. Figure 3.1(a) shows this structure.

2. The traces of FP and UK can cross each other during the shrinking of MB. In another words, FP can exceed UK in the *w* direction, even though it is lower than UK at the beginning. It is then possible for the trajectory to reach UK and jump to the left. This is shown in Figure 3.1(b).

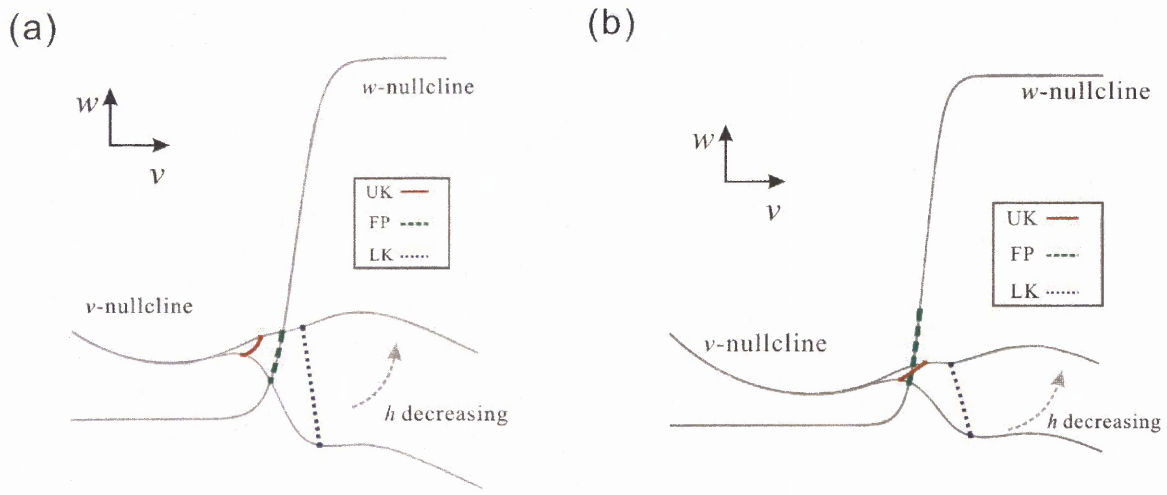

Figure 3.1 Two Geometric Possibilities in the *v*-*w* Phase Plane for the Cases in Category 2. (a) LK can exceed UK in the *w* direction due to a shallow $n_\infty(v)$. At the moment when MB becomes horizontal (or $w_{LK} = w_{UK}$), the fate of the trajectory becomes ambiguous. **(b)** In this case FP can exceed UK in the *w* direction as *h* decays, even though it starts lower than UK. This makes it possible for the trajectory to reach UK and then jump to the left.

Six cases can be defined in Category 2, and the analysis can be done in two phase planes as for the cases in Category 1. A significant difference (from Category 1) in the *w*-*h* phase plane is that in these cases FP and UK are not vertical lines anymore – they are curves with negative slope in the *w*-*h* phase plane.

Case 2.1 represents the case in which both LK and FP are always lower than UK in the *v*-*w* phase plane (Figure 3.2(a)). This condition can also be expressed by the inequality

$$w_{LK} \leq w_{FP} < w_{UK}$$

for any positive value of *h* when the trajectory is on MB. In this case the trajectory can never jump to the left because FP prevents it from reaching UK. Again the possible trajectories are divided into three groups by considering the relative scales of the two relevant time constants: $\tau_{wm} << \tau_{hm}$, $\tau_{wm} >> \tau_{hm}$ or $\tau_{wm} \sim \tau_{hm}$. As shown in Figure 3.2(b), when

$\tau_{wm} << \tau_{hm}$, the trajectory moves rapidly (in the w-h phase plane) to FP in the w direction and then tracks the FP curve down until it reaches LK (Subcase 1). In contrast, when $\tau_{wm} >> \tau_{hm}$, the trajectory moves vertically down in the h direction until it reaches LK (Subcase 2). When τ_{wm} and τ_{hm} are of the same order, the trajectory may reach FP first or reach LK directly (Subcases 3 and 4). There is a rare possibility that FP intersects LK and UK at a single point when $h = 0$. The fate of the trajectory will be unclear if it reaches this intersection point.

In Case 2.2, as in Case 2.1, FP is still below UK for any h ($w_{FP} < w_{UK}$), but LK can move above UK ($w_{LK} \geq w_{UK}$) due to a shallow $n_\infty(v)$ (see Figure 3.2(c)). As LK moves above UK the entire MB becomes unstable and therefore the trajectory needs to make a jump. However, the direction of the jump is ambiguous because both LB and RB are reachable. Figure 3.2(c) and (d), respectively show the geometry on the v-w phase plane and the possible trajectories on the w-h phase plane. Let w^* denote the w value at which $w_{LK} = w_{UK}$. When $w > w^*$, FP becomes unstable (dotted curve Figure 3.2(d)). Subcases 2 and 4 are similar to those in Case 2.1. Subcases 1 and 3 show that the trajectory moves to FP and stays there until $w_{LK} = w_{UK}$ if $\tau_{wm} << \tau_{hm}$ or $\tau_{wm} \sim \tau_{hm}$. Subcase 5 shows the case in which the trajectory reaches FP at exactly the time when $w_{LK} = w_{UK}$. In Subcases 1, 3 and 5 the fate of the trajectory is unclear; it could jump to RB or LB. Although this ambiguity in the fate of the trajectory is similar to that described in Subcase 5 of Case 1.2, there is an important difference between that situation (which is a rare case) and the subcases mentioned here (which are not rare). In the cases shown here, the curve FP funnels the trajectories (1, 3 and 5) towards the point where the LK and UK curves intersect, thus making the ambiguity in the trajectory fate inevitable. Figure 3.2(e) demonstrates a

numerical simulation of such a trajectory over several cycles, showing that the trajectory jumps to either UK (active state) or LK (inactive state) in different cycles.

The trajectories and the traces of LK, UK and FP on the middle branch are also displayed in the full 3D phase space (*v*-*w*-*h*) in Figure 3.2(f). The point at which the trajectory lands on MB on the *v*-*w* phase plane is mapped to a point on the plane $h = h_{start}$ in the *v*-*w*-*h* space. After the trajectory lands on the middle branch, it moves downwards between the curves LK and FP. It will reach either LK or FP depending on the time constants. Note that w^* here is a straight line parallel to the *v*-axis instead of a point on the *w*-*h* manifold. As the trajectory reaches w^*, the fixed point becomes unstable. Thus, the fate of the trajectory, once it reaches w^*, is now dependent on the fast equations: it will jump in the *v* direction through either LK (to RB) or UK (to LB). The direction of this jump depends on whether the trajectory hits the w^* line on the "LK side" or the "UK side" of FP. However, if the trajectory has been attracted to FP prior to reaching w^*, its fate at this point will be ambiguous, potentially leading to a chaotic behavior in the full trajectory of the follower neuron. This can be seen, for example, in the trajectory for Subcase 3 of Figure 3.2(d), as shown in Figure 3.2(e).

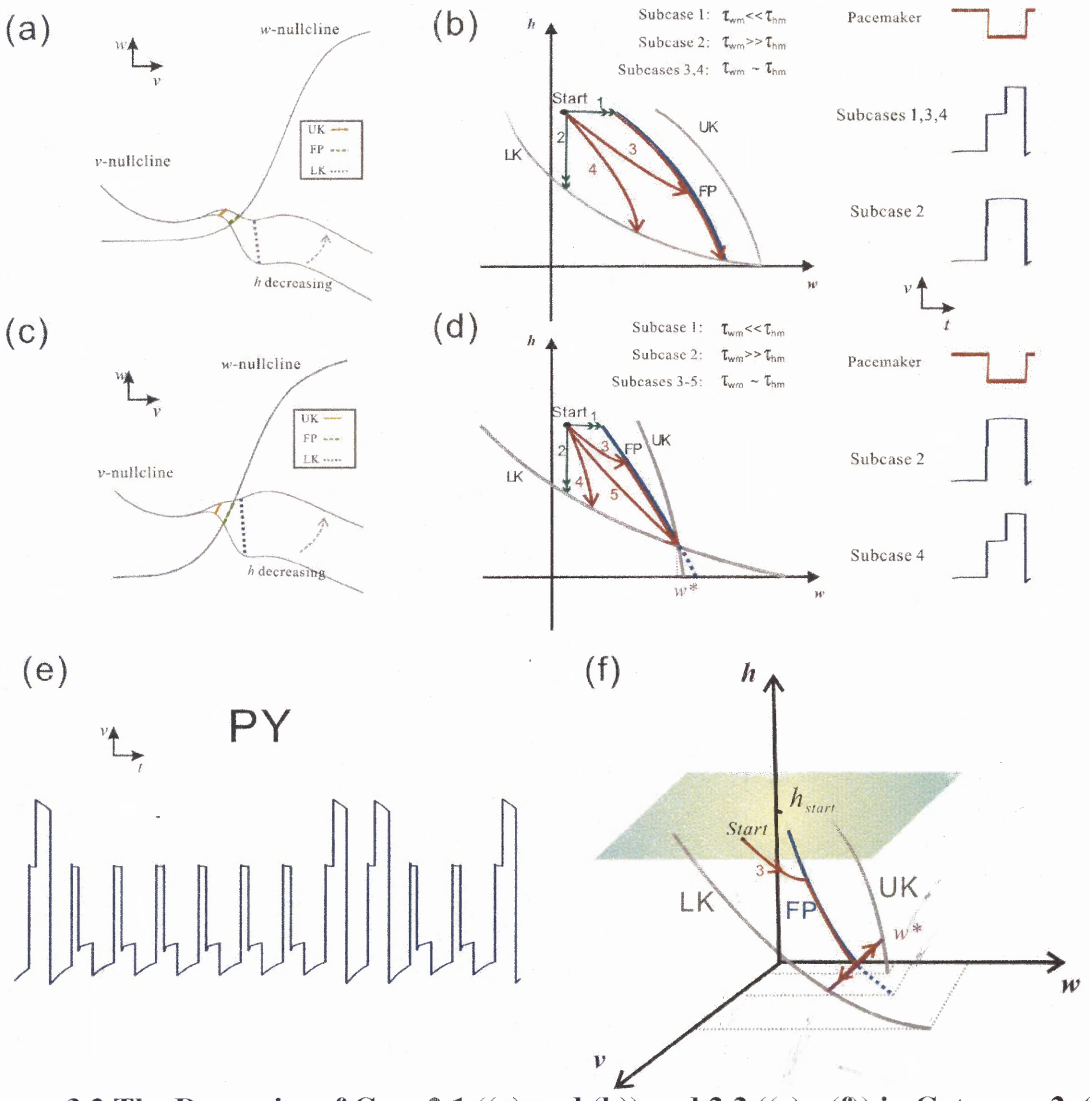

Figure 3.2 The Dynamics of Case 2.1 ((a) and (b)) and 2.2 ((c) - (f)) in Category 2. (a) In Case 2.1, since $w_{LK} \leq w_{FP} < w_{UK}$ in the v-w phase plane, the trajectory moves to FP with time constant τ_{wm} along MB. At the same time, MB shrinks from LK with time constant τ_{hm} and its slope changes due to a non-steep $n_\infty(v)$. **(b)** In the w-h phase plane, four subcases are possible based on the relative size of the two time constants τ_{wm} and τ_{hm}. The time traces for each subcase are shown on the right. **(c)** In Case 2.2, the condition $w_{LK} \leq w_{FP} < w_{UK}$ is satisfied, but w_{LK} can equal w_{UK} during the shrinking of MB due to a shallow $n_\infty(v)$, and then the trajectory can jump either to the left or to the right. **(d)** Five subcases can be achieved in the w-h phase plane based on the relative size of the two time constants τ_{wm} and τ_{hm}. The fate of the trajectories in Subcases 1, 3 and 5 is unclear since they reach the intersection of LK and UK at $w=w^*$. The time traces for Subcases 2 and 4 are shown on the right. **(e)** An example of numerical simulation for Subcases 1 or 3 over cycles, which demonstrates that in different cycles the trajectory (membrane potential) can jump to either RB (active state) or LB (inactive state). **(f)** The analysis of the trajectory for Case 2.2 (**(c)** and **(d)**) in the v-w-h space shows that the intersection of LK and UK (marked by w^* in **(d)**) is in fact a line in the full 3D space. The trajectory of Subcase 3 is shown to demonstrate its ambiguous fate (arrows toward LK or UK) when it reaches the line $w = w^*$.

Case 2.3 and Case 2.4 are the cases in which FP is always higher than UK on the *v*-*w* phase plane:

$$w_{LK} \leq w_{UK} < w_{FP}$$

The distinction between these two cases is that in Case 2.3 $n_\infty(v)$ is steeper than in Case 2.4, thus resulting in differences in the fate of some trajectories. Case 2.3 is summarized in Figures 3.3(a) and 3.3(b). In this case w_{UK} is always greater than w_{LK} until h is very close to 0. In Case 2.3 it is considered that $w_{UK} = w_{LK}$ when $h = 0$, i.e. when the length of MB becomes 0. Since the FP curve is to the right of the UK curve in the *w*-*h* phase plane, the trajectory can reach UK and then jump to the left if it moves fast enough in the *w* direction (τ_{wm} is small enough), as in Subcases 1 and 3 (Figure 3.3(b)). In contrast, if the trajectory moves fast enough in the *h* direction (τ_{hm} is small enough), it can reach UK and jump to the right, as in Subcases 2 and 4. As in Case 1.2 described above, if $\tau_{wm} \sim \tau_{hm}$, there could be a rare trajectory (Subcase 5) whose fate is unclear and may jump either left or right. This trajectory reaches UK and LK at the point where these two curves intersect. Even in the full 3D phase space, this intersection remains a single point representing the time when the knee points coalesce, thus making such a trajectory a rare occurrence.

The fate of the trajectories in Case 2.4 is similar to Case 2.3, and the difference is that $w_{UK} = w_{LK}$ when $h > 0$ and therefore w_{LK} can become greater than w_{UK} due to a shallow $n_\infty(v)$. Figure 3.3(c) and 3.3(d) show the two phase planes respectively. Again, the fate of trajectories on MB is determined by the relative time constants and in MB there is a trajectory (Subcase 5) that approaches the point where $w_{LK} = w_{UK}$ (denoted by w^*) and whose fate remains ambiguous. Note that, in the full 3D phase space, just as in Case 2.2 depicted in Figure 3.2(f), w^* is a line and therefore the trajectory shown in Subcase 5 in the

w-h phase plane represents a whole family of potential trajectories in the 3D space. Thus, Subcase 5 is not necessarily a rare occurrence and may yield a potentially chaotic trajectory of the follower neuron.

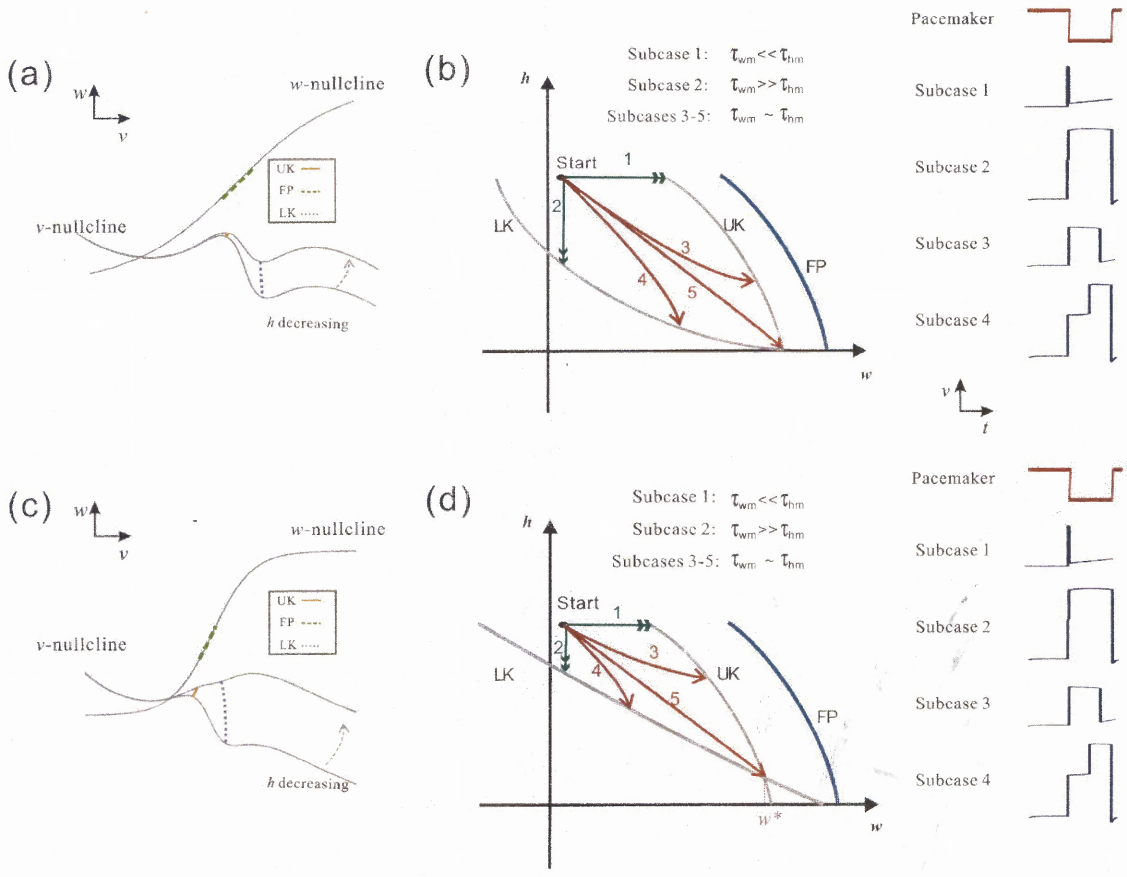

Figure 3.3 The Dynamics of Case 2.3((a) and (b)) and 2.4 ((c) and (d)). (a) In the *v-w* phase plane of Case 2.3, since $w_{LK} < w_{UK} < w_{FP}$, the trajectory moves to UK with time constant τ_{wm} along MB because of the attraction from FP. At the same time, MB shrinks from LK with time constant τ_{hm} and its slope changes due to a non-steep $n_\infty(v)$. **(b)** In the *w-h* phase plane, five subcases are possible based on the relative size of the two time constants τ_{wm} and τ_{hm}. The time traces for Subcases 1 - 4 are shown on the right. The fate of Subcase 5 (a rare case) is unclear since it reaches the intersection of LK and UK. **(c)** In Case 2.4, the condition $w_{LK} < w_{UK} < w_{FP}$ is satisfied, but w_{LK} can equal w_{UK} during the shrink of MB due to a shallow $n_\infty(v)$, and then the trajectory can either jump to the left or to the right. **(d)** Five subcases can be achieved in the *w-h* phase plane based on the relative size of the two time constants τ_{wm} and τ_{hm}. The fate of Subcases 5 is unclear since it reaches the intersection of LK and UK at $w=w^*$. This is not a rare case as it represents a family of trajectories in the *v-w-h* phase space (similar to Case 2.2 shown in Figure 3.2(c)-(f)).

Cases 2.5 and 2.6 involve the most complex phase plane geometries on MB. In these cases, LK is always below FP ($w_{LK} \leq w_{FP}$) in the *v*-*w* phase plane but, as *h* decreases, the trace of FP crosses that of UK (Figure 3.4(a) and 3.4(c)). In the *w*-*h* phase plane, the curve FP intersects UK as shown in Figure 3.4(b) and 3.4(d). Therefore, it is possible for the trajectory to reach UK and jump to the left even if FP is initially lower than UK. The difference between the two cases is similar to the difference between Cases 2.3 and 2.4 described above (Figure 3.3) and the fates of the trajectories can be similarly determined.

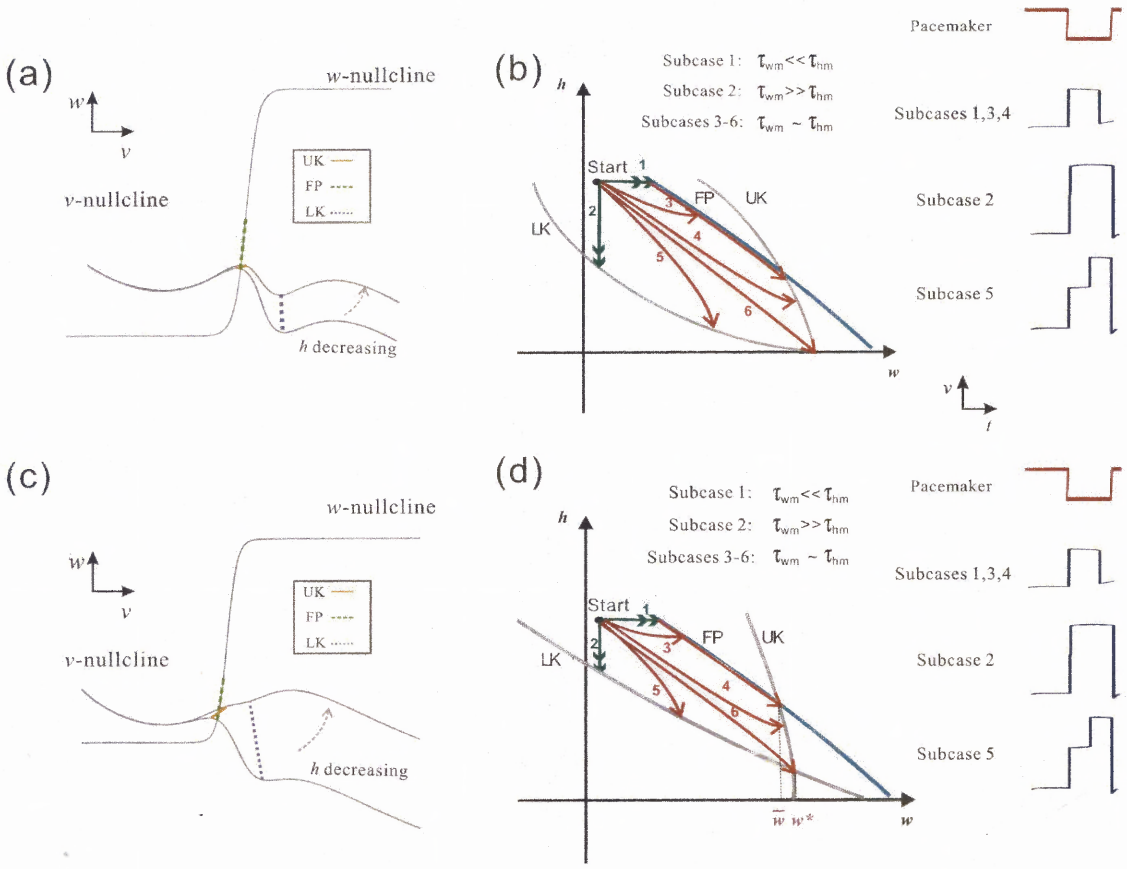

Figure 3.4 The Dynamics of Case 2.5((a) and (b)) and 2.6 ((c) and (d)). (a) In the *v-w* phase plane of Case 2.5, $w_{LK} < w_{UK}$ is satisfied but w_{FP} exceeds w_{UK} during the shrink of MB, which allows the trajectory to reach UK and jumps to the left. **(b)** In the *w-h* phase plane, six subcases are possible based on the relative size of the two time constants τ_{wm} and τ_{hm}. The time traces for Subcases 1 - 5 are shown on the right. The fate of Subcase 6 (a rare case) is unclear since it reaches the intersection of LK and UK. **(c)** In Case 2.6, w_{FP} can exceed w_{UK} during the shrink of MB, and w_{LK} can equal w_{UK} due to a shallow $n_\infty(v)$. **(d)** Six subcases can be achieved in the *w-h* phase plane based on the relative size of the two time constants τ_{wm} and τ_{hm}. The fate of Subcases 6 is unclear since it reaches the intersection of LK and UK at $w=w^*$. This is not a rare case as it represents a family of trajectories in the *v-w-h* phase space (similar to Case 2.2 shown in Figure 3.2(c)-(f)). Note that, $\overline{w}$, the point that FP crosses UK must be $< w^*$; otherwise this case will be qualitatively similar to Case 2.2.

3.4 Periodic Solutions

In Chapter 2 a set of recursive equations are derived for the slow variable h, under the condition that the value of w does not affect the value of h over cycles. The steady state value of the activity phase of the follower neuron based on those equations (Equation (2.16)-(2.19)) are then computed. The results provide a faithful prediction for the activity phase of the biological PY neurons when the cycle period of the pacemaker is varied under three different protocols.

In this section, both the periodic accumulation of h and that of w are considered. Recursive equations for w are derived in a similar way as for h in Chapter 2. With a linear assumption between the two variables, the values of both h and w in each cycle can be computed. These equations describe the relationship between the two slow variables, and provide a more general approach to predict the activity phase of the biological neurons.

3.4.1 The Accumulation of *h* and *w*

In Chapter 2, it is demonstrated that keeping track of the value of h over multiple cycles may be important for determining the long-term behavior of the trajectory of the follower neuron (Equation (2.16)). There are cases, however, where the time spent on the middle branch (t_m) will also be dependent on the time constant of w on MB. For instance, if the trajectory encounters LK before it reaches FP on MB, as Subcase 4 in Figure 2.4(b), then t_m is determined by the time constant of w instead of that of h. In such cases, it may be important to keep track of the value of w over multiple cycles in order to determine the long-term fate of the trajectory.

Similarly to the work which has been done for h in Chapter 2, the recursive equations for w in cycle n (w_n) at the instant the trajectory lands on MB can be derived as follow:

$$w_n = [w_{FP2} + (w_{FP} - w_{FP2} + (w_{n-1} - w_{FP})\exp(-\frac{t_m^{\,n}}{\tau_{wm}}))\exp(-\frac{T_{in} - t_m^{\,n}}{\tau_{wh}})]\exp(-\frac{T_{acl}}{\tau_{wl}}) \quad (3.2)$$

where $t_m^{\,n}$ satisfies

$$f(v_\theta, w_{FP} + (w^{n-1} - w_{FP})\exp(-\frac{t_m^{\,n}}{\tau_{wm}})) - g_A h^{n-1}\exp(-\frac{t_m^{\,n}}{\tau_{hm}})(v_\theta - E_K) = 0 \quad (3.3)$$

and w^n represent the value of w at $t = nP + T_{act}$.

These equations are derived based on the assumption that $w_{FP1} = 0$. The same method can be applied for deriving the equations for $w_{FP1} > 0$. This iteration yields a two dimensional map as both w^n and h^n need to be computed which makes the analysis of the map difficult. This difficulty can be alleviated by using a simplifying assumption. By approximating the LK curve using its linear Taylor-series expansion, it is possible to reduce Equation (3.3) to a one-dimensional map (a similar approximation is described by Bose et al. (2004)). With such a linear approximation yields the equation $C_1 w + C_2 h = 1$ (C_1, C_2 are constants which can be computed from the equations for the nullclines) for LK. In this case, $t_m^{\,n}$ satisfies the following equation:

$$C_1(w_{FP} + (w^{n-1} - w_{FP})\exp(-\frac{t_m^{\,n}}{\tau_{wm}})) + C_2 h^{n-1}\exp(-\frac{t_m^{\,n}}{\tau_{hm}}) = 1 \quad (3.4)$$

From Equation (3.4) h^{n-1} can be calculated and substituted into Equation (3.3), thereby yielding a recursive relationship involving only w^n.

3.4.2 The Effect of the Weak Inhibition

When the inhibitory synapse from the pacemaker to the follower neuron is relatively weak, the behavior of the activity phase over cycles can be fairly different from the strong inhibition situation. As mentioned in Chapter 2, the follower neuron with a large amount of A-current may not be able to reach the active state during T_{in}, the inactive duration of the pacemaker neurons. Instead it stays in an intermediate state. When the inhibition begins, the membrane potential of the follower neuron moves to the inactive state until the inhibition is over (Figure 3.5(a), left panel). When the inhibitory synapse from the pacemaker is relatively weaker, the membrane potential is still not be able to reach the active state during T_{in}. However, when the inhibition starts, the membrane potential may still stay in the intermediate state instead of jumping back to the inactive state (Figure 3.5(b), left panel).

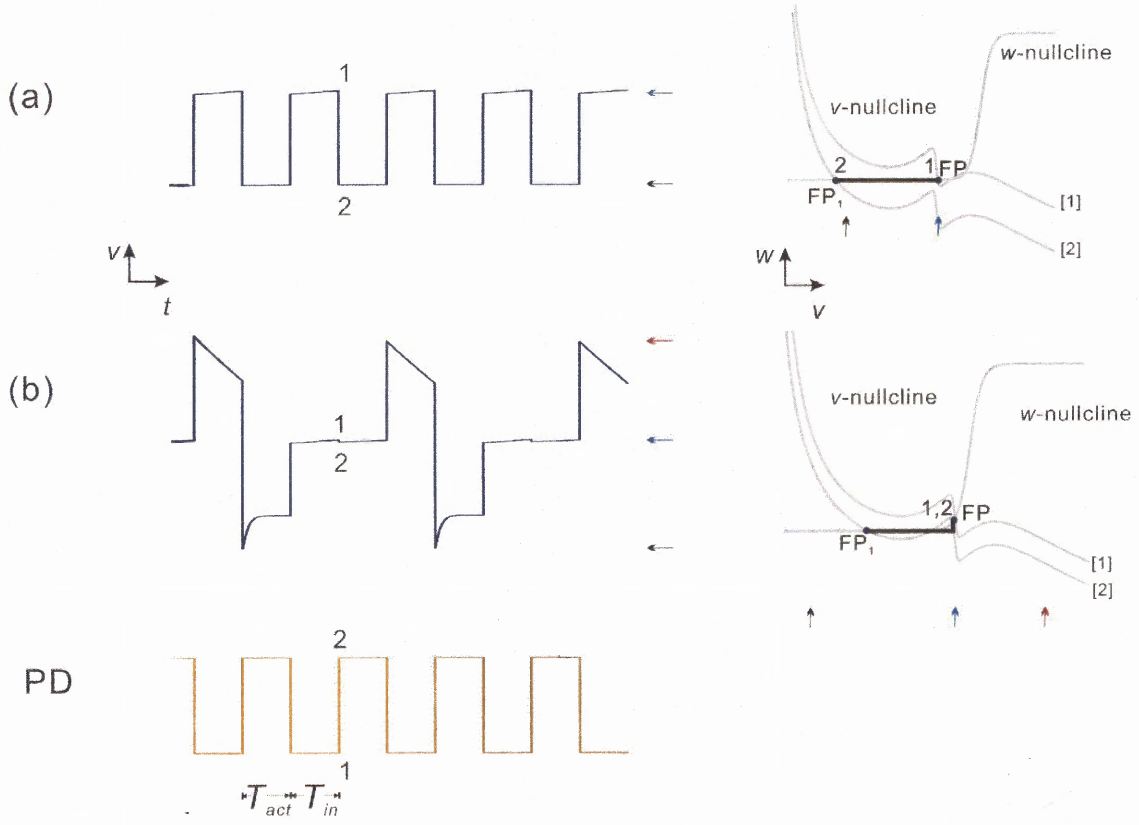

Figure 3.5 Comparison of the Strong Inhibition (a) and the Weak Inhibition (b) Cases under the Condition that There is a Strong A-Current in the Follower Neuron. **(a)** The membrane potential (left panel) and the v-w phase plane (right panel) for the PY neuron under a strong inhibition. **Left panel:** with a strong inhibition, the membrane potential moves back to the inactive state (from 1 to 2) when T_{act} begins. **Right panel:** the trajectory (from 1 to 2) and the corresponding nullclines in the v-w phase plane. When the inhibition starts, the v-nullcline moves down from [1] to [2], and therefore the trajectory jumps from FP to FP_1. **(b)** The membrane potential (left panel) and the v-w phase plane (right panel) for the PY neuron under a weak inhibition. **Left panel:** with a relatively weak inhibition, the membrane potential stays at the intermedia state during T_{act}. **Right panel:** the trajectory can stay at the middle branch under the inhibition. The v-nullcline does not move down enough and the fixed point FP still exists, which attracts the trajectory to stay.

3.4.2.1 The Accumulation of *h* The same method in Chapter 2 is used to derive recursive equations for h for the weak inhibition case (See Equations (2.10)-(2.16)). The only difference is that if the trajectory is unable to jump to the right branch during (T_{act}, $P-\varepsilon_\alpha$), then at $t = P$

$$h(P) = (1 - \exp(-\frac{T_{act}}{\tau_{hl}}))\exp(-\frac{T_{in}}{\tau_{hm}}) \tag{3.5}$$

It is concluded that the following recursive equations describing the values of h in cycle n (h^n) at the moments that the inhibition from the pacemaker is removed at $t = (n\text{-}1)P + T_{act}$:

$$h^n \equiv h(np + T_{act}) = \begin{cases} 1 + [h((n-1)p + T_{act})\exp(-\frac{T_{in}}{\tau_{hh}} + (\frac{1}{\tau_{hh}} - \frac{1}{\tau_{hm}})t_m^{\,n}) - 1]\exp(-\frac{T_{act}}{\tau_{hl}}) & \text{if } t_m^{\,n} < T_{in} \quad \text{(a)} \\ h((n\text{-}1)p + T_{act})\exp(-\frac{p}{\tau_{hm}}) & \text{if } t_m^{\,n} > T_{in} \quad \text{(b)} \end{cases} \tag{3.6}$$

$$t_m^{\,n} = \tau_{hm} \ln \frac{g_A h((n-1)p + T_{act})(v_\theta - E_K)}{f(v_\theta, w_{FP})} \quad \text{(c)}$$

where $t_m^{\,n}$ denotes the time spent on the middle branch in the n^{th} cycle.

If $t_m^{\,n} < T_{in}$ for all n, then h_n follows Equation (a) in (3.6) in each iteration, and it converges to a steady state h^* which satisfies the equations shown in Chapter 2 (Equations (2.16)-(2.19)). However, when $t_m^{\,n} > T_{in}$ for some n, the trajectory is not able to jump to the right branch during T_{in}, and therefore h_n may not converge to h^*. Figure 3.6 shows a trajectory and nullclines for this case. In the case shown, g_A is sufficiently large (or, alternatively, τ_{hm} sufficiently large). To follow the trajectory in this case the $g_K w$-$g_A h$ phase plane where the maximal conductances are explicitly incorporated along each axis is considered (Figure 3.6(d)). For large values of g_A, the starting position at $t = T_{act}$ as given by $g_A h(T_{act}) = g_A(1 - e^{\frac{-T_{act}}{\tau_{hl}}})$ will be large. Thus, it will take longer for the trajectory to decay to LK. Moreover, if the trajectory cannot reach LK in one cycle, the inhibition from the pacemaker moves LK to the left in the $g_K w$-$g_A h$ phase plane for a time duration equal to T_{act} (labeled LK^1 in Figure 3.6(d)). Thus during this time the follower neuron is unlikely to reach LK^1. Once the inhibition is removed, the trajectory again moves toward LK and the

process repeats. Thus for large g_A the pacemaker may go through several cycles while the follower neuron remains on MB. These are N-to-1 solutions, two of which are shown in Figure 3.7(a_2) and 3.7(a_3). Equations (3.6) are also solved in order to show how in these cases, h^n converges to a period 2 or 3 point, respectively (left panel of Figure 3.7), consistent with the modeling simulations (right panel of Figure 3.7).

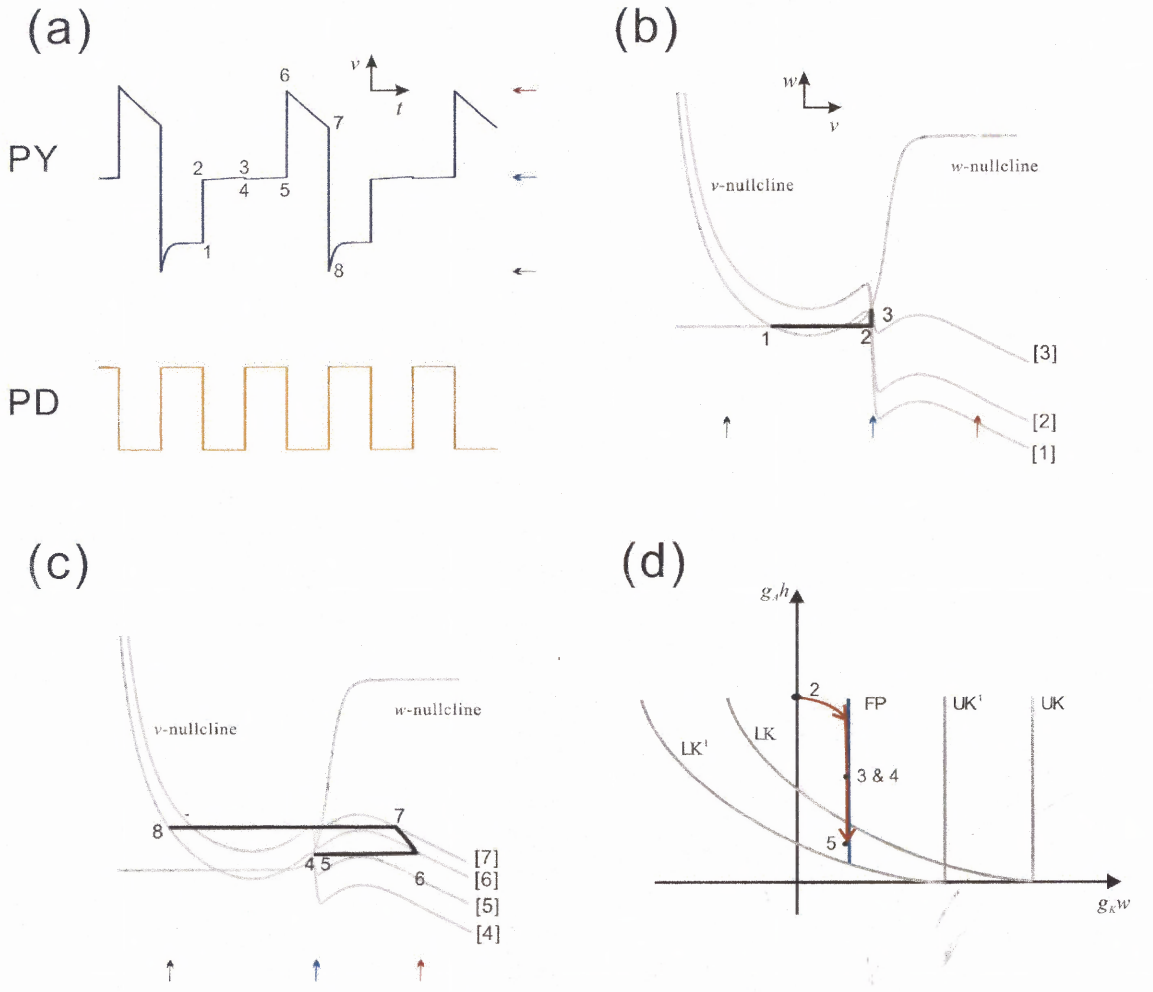

Figure 3.6 The 2-to-1 Oscillation of the Follower Neuron Due to a Strong A-Current. **(a)** The two time traces show the 2-to-1 solution of the follower neuron PY and the pacemaker PD respectively. Points 1-8 represent the eight critical positions in a (doubled) cycle. **(b)-(c)** show the dynamics in the *v*-*w* phase plane. [1]-[8] represent the relative *v*-nullclines when the trajectory reaches the correspondingly numbered critical point. **(b)** After the inhibition, the trajectory jumps from 1 to 2 due to the transient rise of the *v*-nullcline. Then it moves to 3 and stays there during T_{in}, and simultaneously the middle branch shrinks from LK. **(c)** The trajectory stays on MB^1 during the next cycle of T_{act} (4 and 5), and jumps to the right (6) following the inhibition. The trajectory then moves upwards to position 7, and jumps to the left branch (8) when the cycle inhibition begins. **(d)** The dynamics on the middle branch as seen in the *w*-*h* phase plane. The inhibition causes LK and UK to shift to LK^1 and UK^1 at the onset of T_{act}. The trajectory reaches 3 as LK shifts to LK^1 and keeps moving to 5 at the end of T_{act}. Because the point 5 is below LK, the shift back from LK^1 to LK at the end of T_{act} immediately releases the trajectory from the middle branch.

Figure 3.7(a_1), (a_2) and (a_3) show results for three discrete values of g_A. An interesting question arises as to whether these types of periodic states are the only ones that arise as g_A is smoothly increased. Figure 3.7(b) shows an example of a different type of periodic solution when the value of g_A is set to be in between those in cases (a_1) and (a_2). In this case the follower neuron stays on MB for an entire cycle of the pacemaker, but only on alternate cycles. This 3-to-1 solution is different from the 3-to-1 solution shown in Figure 3.7(a_3), as can be seen in the right panel. In fact one can distinguish different N-to-1 periodic solutions of the membrane potential by observing the analytic solutions of h^n. For instance, an "up-down-down" pattern in the h_n trace indicates that the solution is 3-to-1 periodic as in Figure 3.7(a_3) (right panel), while an "up-up-down" pattern implies a 3-to-1 periodic solution as in Figure 3.7(b) (right panel).

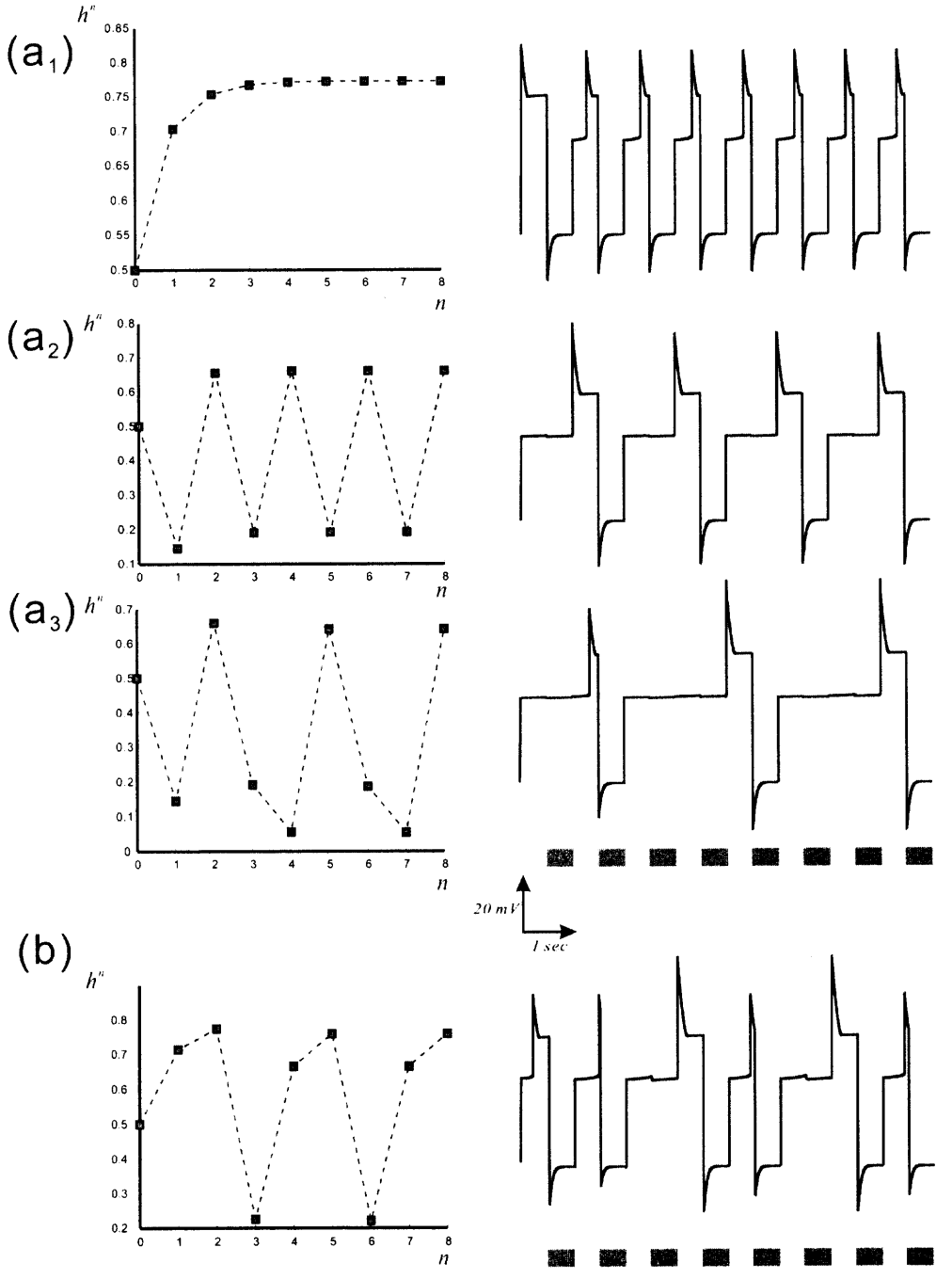

Figure 3.7 The Analytic Solutions of h_n (Left Panel) and the Numerical Simulation of the Membrane Potential of PY (Right Panel). The boxes in the right panel represent the active duration of the pacemaker or T_{act}. **(a_1)-(a_3)** h_n and the membrane potential shown for three values of g_A (4 , 8 and 20 nS, respectively). The periodic solution changes from 1-to-1 to 2-to-1 and then 3-to-1. **(b)** An unusual solution when g_A = 5 *nS* (between the values in (a_1) and (a_2)). In this case, the solution is also 3-to-1, but different from the solution in Case (a_3). The parameters used in the recursive computation have the following values: (in ms) $T_{in} = T_{act} = 500$, $\tau_{hl} = 495$, $\tau_{hm} = 810$, $\tau_{hh} = 500$; (in mV) $v_\theta = -6$, $E_L = -60$, $E_{Ca} = 120$, $v_{Ca} = -1.2$, $k_{Ca} = -18$, $E_K = -84$; (in nS) $g_L = 2$, $g_{Ca} = 4$, $g_K = 8$; (in pA) $I_{ext} = 75$; $w_{FP} = 0$.

3.4.2.2 The Accumulation of *w* Similar to the work which has been done for w in the previous section, the recursive equations for w for the weak inhibition case can also be derived as follow:

$$w^n = \begin{cases} [w_{FP2} + (w_{FP} - w_{FP2} + (w^{n-1} - w_{FP})\exp(-\frac{t_m^{\,n}}{\tau_{wm}}))\exp(-\frac{T_{in} - t_m^{\,n}}{\tau_{wh}})]\exp(-\frac{T_{act}}{\tau_{wl}}) & \text{if } t_m^{\,n} < T_{in} \text{ (a)} \\ w_{FP} + (w_{n-1} - w_{FP})\exp(-\frac{p}{\tau_{wm}}) & \text{if } t_m^{\,n} > T_{in} \text{ (b)} \end{cases} \quad (3.7)$$

where $t_m^{\,n}$ satisfies

$$f(v_\theta, w_{FP} + (w^{n-1} - w_{FP})\exp(-\frac{t_m^{\,n}}{\tau_{wm}})) - g_A h^{n-1}\exp(-\frac{t_m^{\,n}}{\tau_{hm}})(v_\theta - E_K) = 0 \quad (3.8)$$

Again these equations are derived based on the assumption that $w_{FP1} = 0$ and the same method can be applied to derive the equations for $w_{FP1} > 0$.

Similar to the work in Section 3.3.1, this iteration yields a two dimensional map as both w^n and h^n need to be computed which makes the analysis of the map difficult. This difficulty can be alleviated by using a simplifying assumption. By approximating the LK curve using its linear Taylor-series expansion, it is possible to reduce Equation (3.8) to a one-dimentional map (a similar approximation is described by Bose et al. (2004)). With such a linear approximation it yields the equation $C_3w + C_4h = 1$ (C_3, C_4 are constants which can be computed from the equations for the nullclines) for LK. In this case, $t_m^{\,n}$ satisfies the following equation:

$$C_3(w_{FP} + (w^{n-1} - w_{FP})\exp(-\frac{t_m^{\,n}}{\tau_{wm}})) + C_4 h^{n-1}\exp(-\frac{t_m^{\,n}}{\tau_{hm}}) = 1 \quad (3.9)$$

In Equation (3.9) h^{n-1} can be calculated and substituted into Equation (3.6), thereby yielding a recursive relationship involving only w^n.

3.5 Summary

Chapter 2 shows the methods of analyzing the transient activity of a follower neuron with A-current using the knowledge of dynamical systems analysis and of predicting the steady state value of the activity phase of biological PY neurons with the help of recursive equations. In this chapter a systematic and complete mathematical analysis is achieved to explore the factors that determine the activity time of a neuron with A-current following periodic inhibitory inputs. The results indicate that, even with a simple model neuron, the interaction of the A-current parameters and other intrinsic parameters can be quite complex and lead to distinct and sometimes unintuitive model behaviors (when the A-current is strong but the inhibitory synapse is relatively weak). Although the roles of additional factors such as synaptic dynamics and the interaction with other network neurons that can affect the role of the A-current in determining the activity phase remain to be explored, the basic geometric tools have been provided which could be used for such analysis in more complicated settings. Recursive equations are derived for both slow variables h and w, which can be used to predict the activity phase of the follower neuron as in Chapter 2 but more accurately. With a linear assumption on the middle branch between the two variables, a one-dimensional mapping in each cycle can be simply obtained.

In general, after release from inhibition, the trajectory of the follower neuron leaves the inactive state (left branch) and lands on a two-dimensional manifold (the w-h phase plane) between the inactive and active states. Note that the w-h phase plane represents the set of middle branches (MB) in the v-w phase plane. What determines the fate of the trajectory on the w-h phase plane, i.e. whether it becomes active or returns to its inactive state, is the relative sizes of the time constants of the slow variables w and h. For example,

in Cases 1.2, 2.3 and 2.4 the steady state curve of w, shown as the w-nullcline in the v-w phase plane, is above the middle branch of the v-nullcline (Figures 2.4(c), 3.3(a) and 3.3(c)). Under this condition the trajectory can either encounter LK and jump to the right or encounter UK and jump to the left, if the pacemaker remains inactive (T_{in} is long enough). The fate of the trajectory can be determined by analyzing the dynamics on the w-h phase plane as a function of the relationship between the values of the two time constants (Figures 2.4(d), 3.3(b) and 3.3(d)). Note that, in a more complex model, this slow manifold may have higher dimensions as determined by other slow intrinsic variables of the follower neuron.

The analysis of the fate of the trajectory in the w-h phase plane indicates that, in some cases, the behavior of the model neuron following inhibition can be quite unintuitive and even ambiguous. These ambiguous cases are marked by the intersection between the LK and UK curves on the w-h phase plane, indicating the possibility of a trajectory reaching such an intersection point in which case its fate is unclear. Such intersections occur either when the A-current is completely inactivated ($h = 0$) or when the A-current is not inactivated entirely ($h > 0$). In the former case the trajectories that reach such an intersection point, as in Subcase 5 in Cases 1.2 and 2.3 (Figures 2.4(d) and 3.3(b)) or Subcase 6 in Case 2.5 (Figure 3.4(b)), would be extremely rare. Yet, if the intersection between LK and UK occurs for a non-zero value of h as in the latter case, such an intersection is represented by a line (w^* in Figure 3.2(f)) parameterized by the fast variable v in the full v-w-h phase space. Such intersections appear in cases where the steady state inactivation curve $n_\infty(v)$ of the A-current is shallow. A trajectory that reaches this intersection point in the w-h phase plane (e.g. Subcases 1, 3, 5 in Case 2.2, Subcase 5 in

Case 2.4, and Subcase 6 in Case 2.6; Figures 3.2(d), 3.3(d) and 3.4(d)) represents the projection of a family of trajectories in the full phase space and is not necessarily a rare occurrence. As an example, the trajectory representing Subcase 3 in Figure 3.2(d) can be seen in the 3D phase space (Figure 3.2(f)) to move asymptotically along the curve FP to the line w^*. It can either land on the LK-side and jump towards LK to the active state or land on the UK-side and jump towards UK to the inactive state. The deterministic behavior of such a trajectory can be determined by the local dynamics near FP and where the trajectory lands on MB in each cycle. If the local dynamics near FP allow the trajectory to end on either side of FP when it reaches w^*, the long-term behavior over several cycles can be chaotic (see simulation shown in Figure 3.2(e)). Even if there is no chaotic behavior in such a case, the global dynamics of the actual biological system can be ambiguous from cycle to cycle due to small perturbations from noise.

The recursive equations for the cases in Category 1 have been derived which can be used to track the long-term behavior of the variables h and w, under the conditions of both strong and weak inhibitions. Similar to Chapter 2 it can be proved that under certain conditions there is a steady state value for h and/or w and therefore the membrane potential can yield periodic behavior. The periodic solution of the membrane potential can be predicted by observing the trace of h and w over cycles. The analytic solutions for the cases in Category 2 can be derived in a similar way. A significant difference is that in the recursive equations v_θ and w_{FP} are no longer constants since their values change in a range around MB as the slope of MB changes due to a non-steep $n_\infty(v)$. Therefore in order to find an expression for t_m^n in each cycle, there is a need to express v_θ and w_{FP} as functions of time or other variables as the trajectory is traveling on MB.

When the inhibitory synapse from the pacemaker to the follower neuron is relatively weak, the follower neuron can have some unintuitive behaviors due to the presence of a strong A-current. For example, a strong A-current may cause "*N*-to-1" oscillations (*N* is an integer > 1) or non-periodic behaviors. Figures 3.7(a_2) shows a case in which the oscillation period of the follower neuron is doubled (2-to-1 oscillation). In each cycle the strong A-current prevents the membrane potential from reaching the active state during T_{in} (between 2 and 3 in Figure 3.7(a)). Following that, the membrane potential stays in the middle state during T_{act} despite the inhibitory synaptic input (between 4 and 5 in Figure 3.7(a)) as explained in the *w*-*h* phase plane in Figure 3.7(d).

The analysis in this chapter shows that the effect of the A-current on the behavior of the follower neuron can be fairly complicated, even though there are only three variables in the model. Depending on the parameter configurations - corresponding to different states of the biological neuron, different parameters could control the post-inhibition activity phase. When the inhibitory synapses from the pacemaker are relatively weak, unintuitive behaviors may be obtained. The steady state activity phase of the follower neuron can be predicted by sets of recursive equations for both the strong inhibition and the weak inhibition cases. It will be helpful to verify the modeling prediction for the weak inhibition cases by conducting experiments with biological follower neurons in the future.

CHAPTER 4

A STUDY OF CURRENT DISTRIBUTIONS BASED ON A DETAILED COMPUTATIONAL MODEL

4.1 Introduction

In Chapters 2 and 3 a three-variable model is used to explore how the mechanism and strength of the A-current, together with other intrinsic and synaptic properties, affect the activity phase of the follower neuron receiving inhibitory inputs. The geometric analysis in the phase space and two sub-phase planes helps the transient behavior of the trajectory corresponding to the membrane potential to be understood, and several sets of recursive equations are derived analytically for computing the activity phase of the follower neuron in every cycle as well as its steady state value. Experiments involving Dynamic Clamp technique have been conducted to verify the analytic results. It shows that the steady state equations can be used to faithfully predict the activity phase of the biological PY neurons. It has also been shown that when the A-current is strong, the strength of the inhibitory synapse may significantly affect the membrane potential of the follower neuron.

However, there are other factors which may also play roles in determining the activity phase of the follower neurons and have not been investigated as yet. For example, in the three-variable model there are only four intrinsic currents: the leak current, the calcium current, the delayed potassium current and the A-current. However there are many more types of intrinsic currents in a biological PY neuron (Mamiya et al., 2003). Whether any or all of them can modulate the activity phase remains unknown. Moreover, the three-variable model only includes one compartment and does not perform the spiking

property, which may or may not have a relationship with the activity phase. Other questions include whether the activity phase of a follower neuron can be affected by its morphology, and whether the distribution of all the currents at different parts of the neuron can also affect the activity phase.

Realistic models, or models describing the shapes and detailed intrinsic properties of biological neurons, have been built and used for studying different types of neurons. For instance, a group of two-compartment computational models have been built to simulate the pacemaker neurons AB and PDs in the pyloric network of the crustacean STG system (Soto-Trevino et al., 2005). Another example includes two detailed models for the LP neuron in the crustacean STG system: first a one-compartment detailed model was built to simulate all the intrinsic properties of the LP neuron (Buchholtz et al., 1992; Golowasch and Marder, 1992), and later Taylor et al. (unpublished results) built a seven-compartment realistic model based on the biological shape of the LP neuron.

Inspired by these ideas, a five-compartment model neuron is developed for studying the PY neuron. By applying a Genetic Algorithm, the possible parameters and distributions of the ionic channels in each compartment can be computed.

4.2 Models

Like other neurons in the invertebrate or vertebrate animals, the morphology of the biological PY neuron consists of several parts: the soma, the axon, the dendritic tree and the connections between them. Figure 4.1(a) is a photo of a biological PY neuron, which shows that the soma (the round part) connects with the dendritic tree and the axon through some intermediate parts. A five-compartment model is built to simulate the biological PY

neuron: Compartments S, P, B, D and A represent the soma, the pri-axon, the branch, the dendritic tree and the axon parts of the biological PY neuron (Figure 4.1(b)).

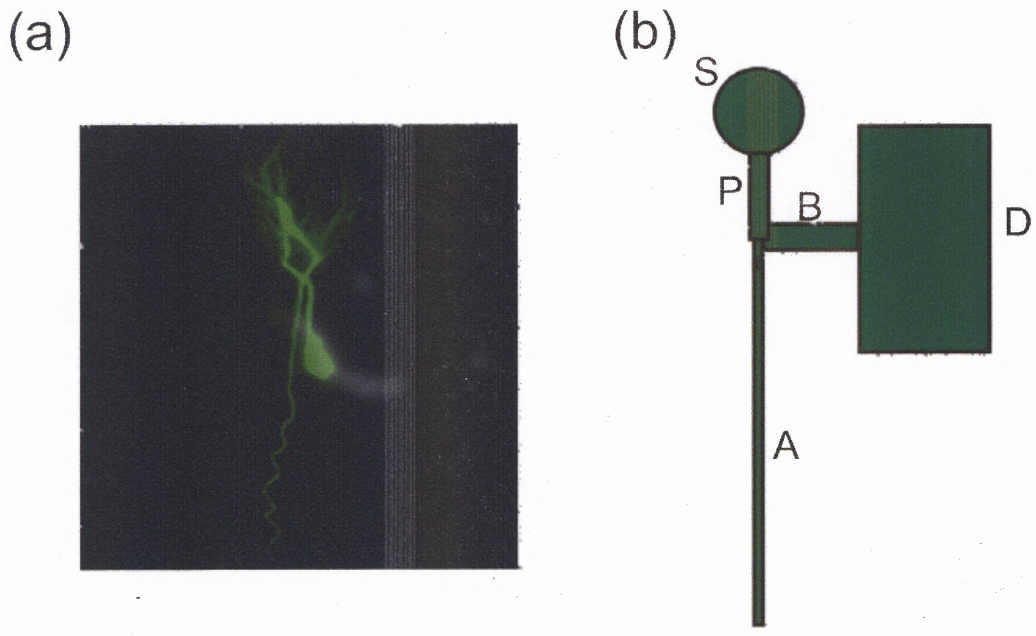

Figure 4.1 The Morphology of a Biological PY Neuron and a Corresponding Realistic Model. (a) The photo of a biological PY neuron in the pyloric network of the crustacean STG system. **(b)** The structure of the five-compartment model. S, P, B, D and A represent the soma, the pri-axon, the branch, the dendritic tree and the axon parts of the biological PY neuron.

For simplicity, Compartment S is set to be isopotential but other compartments are set to be cylindric based on the biological shape of the PY neuron. In each compartment, there are different types of ionic channels which allow different types of currents to transport across the membrane. Moreover, even for the same type of current, the amount and the distribution in each compartment can be fairly different.

There are totally nine types of intrinsic currents in the realistic model for PY: the delayed rectifier potassium current (I_{Kd}), the calcium-dependent potassium current (I_{KCa}), the transient A-current (I_A), the calcium current (I_{Ca}), the hyperpolarization activated current (I_h), the proctolin activated current (I_{proc}), the fast sodium current (I_{Na}), the low-threshold A-current (I_{Aa}) and the leak current (I_l). There is also a synaptic current (I_{syn}) which describes the inhibition from the pacemaker neurons. Each current has different equations and parameters based on their biological mechanisms. For each compartment k, the membrane potential is determined by

$$C_m \frac{dv}{dt} = I_{ext} - \sum_{j=1}^{J_k} I_j \tag{4.1}$$

The strength and distribution of each current varies in different compartments. Here a detailed description is provided for each current.

The delayed rectifier potassium current (I_{Kd})

This outward potassium current has a voltage-dependent delay before being activated, and it has no inactivation (Hodgkin and Huxley, 1952). The equation for this current is defined as

$$I_{Kd} = g_{Kd} w^4 (v - E_K) \tag{4.2}$$

where g_{Kd} represents the maximum conductance, w represents the activation fraction and E_K represents the reverse potential of the potassium current. The variable w is determined by the following equation:

$$\frac{dw}{dt} = \frac{w_\infty(v) - w}{\tau_w(v)} \tag{4.3}$$

where $w_\infty(v)$ corresponds to a sigmoidal function, and $\tau_w(v)$ is a function of v.

This current exists in all the compartments (S, P, B, D, A) in the model.

The calcium-dependent potassium current (I_{KCa})

The calcium-dependent potassium current has a relatively complex mechanism compared with other intrinsic currents, since its gating depends on the concentration of the calcium ions ($[Ca^{2+}]$) (Buchholtz et al., 1992). The equation for this current is defined as

$$I_{KCa} = g_{KCa} ab(v - E_K) \tag{4.4}$$

where g_{KCa} represents the maximum conductance, a and b represent the activation and inactivation fractions and E_K represents the reverse potential of the potassium current as in Equation (4.2). Different from the fractions for other intrinsic currents, a and b partially depend on the calcium concentration:

$$\begin{aligned} \frac{da}{dt} &= \frac{a_\infty(v,[Ca^{2+}]) - a}{\tau_a(v)} \\ \frac{db}{dt} &= \frac{b_\infty(v,[Ca^{2+}]) - b}{\tau_b(v)} \end{aligned} \tag{4.5}$$

The calcium concentration satisfies the following equations:

$$\begin{aligned} \frac{d[Ca^{2+}]}{dt} &= \frac{[Ca^{2+}]_\infty - [Ca^{2+}]}{\tau_{[Ca^{2+}]}} \\ [Ca^{2+}]_\infty &= -FI_{Ca} + C_0 \end{aligned} \tag{4.6}$$

where $\tau_{[Ca^{2+}]}$ is the Ca^{2+} buffering time constant, C_0 is the background intracellular Ca^{2+} concentration, and F describes the relationship between the calcium current and the intracellular Ca^{2+} concentration (Buchholtz et al., 1992; Soto-Trevino et al., 2005). The calcium-dependent potassium current exists at the S, P, B and D compartments.

The transient A-current (I_A)

The A-current is controlled by a voltage-dependent activation fraction (n) and a voltage-dependent inactivation fraction (h). The equation is defined as

$$I_A = g_A nh(v - E_K) \tag{4.7}$$

where g_A represents the maximum conductance, and n and h represent the activation and inactivation fractions following the equations:

$$\begin{aligned} \frac{dn}{dt} &= \frac{n_\infty(v) - n}{\tau_n(v)} \\ \frac{dh}{dt} &= \frac{h_\infty(v) - h}{\tau_h(v)} \end{aligned} \tag{4.8}$$

Here $n_\infty(v)$ and $h_\infty(v)$ are sigmoidal functions representing the steady state values of n and h. This transient A-current exists in the S, P, B and D compartments.

The calcium current (I_{Ca})

The experimental result shows that there are two components for the calcium current (Buchholtz et al., 1992). One component includes both an activation fraction (a_{Ca1}) and an inactivation fraction (b_{Ca1}), and the other component only includes a single activation fraction (a_{Ca2}). The equation for the calcium current is defined as

$$I_{Ca} = (g_{Ca1} a_{Ca1} b_{Ca1} + g_{Ca2} a_{Ca2})(v - E_{Ca}) \tag{4.9}$$

where a_{Ca1}, b_{Ca1} and a_{Ca2} satisfy the equations:

$$\begin{aligned} \frac{da_{Ca1}}{dt} &= \frac{a_{Ca1\infty}(v) - a_{Ca1}}{\tau_{a_{Ca1}}(v)} \\ \frac{db_{Ca1}}{dt} &= \frac{b_{Ca1\infty}(v) - b_{Ca1}}{\tau_{b_{Ca1}}(v)} \\ \frac{da_{Ca2}}{dt} &= \frac{a_{Ca2\infty}(v) - a_{Ca2}}{\tau_{a_{Ca2}}(v)} \end{aligned} \tag{4.10}$$

and the reverse potential E_{Ca} is partially dependent on the calcium concentration. Their relationship is determined by the Nernst equation (Buchholtz et al., 1992):

$$E_{Ca} = \frac{R \cdot T \cdot F}{z} \ln\left(\frac{[Ca^{2+}]_{out}}{[Ca^{2+}]}\right) \tag{4.11}$$

where $z = 2$, $[Ca^{2+}]_{out} = 13\ mM$ and $[Ca^{2+}]$ is the intrinsic calcium concentration calculated in mM from Equation (4.6).

The calcium current exists in the Compartments S, P, B and D.

The hyperpolarization activated current (I_h)

The *hyperpolarization* current, or h-current, is an inward current activated at low voltages, and is determined by a single activation fraction (Golowasch and Marder, 1992):

$$I_h = g_h r(v - E_h) \tag{4.12}$$

where g_h is the maximum conductance and E_h is the reverse potential of the h-current. The activation fraction r satisfies:

$$\frac{dr}{dt} = \frac{r_\infty(v) - r}{\tau_r(v)} \tag{4.13}$$

The h-current can be found in Compartment S, P, B and D.

The proctolin activated current (I_{proc})

This current is activated by various neuromodulators (Golowasch and Marder, 1992; Swensen and Marder, 2000) and located in Compartment S, P, B and D. It is defined by the following equation:

$$I_{proc} = g_{proc} a_{proc} (v - E_{proc}) \tag{4.14}$$

where g_{proc} and E_{proc} represent the maximum conductance and the reverse potential of the proctolin-activated current. The activation fraction a_{proc} satisfies

$$\frac{da_{proc}}{dt} = \frac{a_{proc\infty}(v) - a_{proc}}{\tau_{a_{proc}}(v)} \tag{4.15}$$

The fast sodium current (I_{Na})

The fast sodium current is a Hodgkin-Huxley like sodium current located in Compartment A (or the axon of the neuron) and it contributes to the spiking properties together with the potassium current (I_{Kd}). It is defined as the following equation:

$$I_{Na} = g_{Na} m_{Na}^{3} h_{Na} (v - E_{Na}) \tag{4.16}$$

where g_{Na} and E_{Na} are the maximum conductance and the reverse potential of the sodium current, and the activation and inactivation fractions m_{Na} and h_{Na} satisfy

$$\begin{aligned} \frac{dm_{Na}}{dt} &= \frac{m_{Na\infty}(v) - m_{Na}}{\tau_{m_{Na}}(v)} \\ \frac{dh_{Na}}{dt} &= \frac{h_{Na\infty}(v) - h_{Na}}{\tau_{h_{Na}}(v)} \end{aligned} \tag{4.17}$$

The low-threshold A-current (I_{Aa})

There is another type of A-current, I_{Aa}, located only in the axon or the A compartment (Meyrand et al., 1992). A significant difference is that the half-maximum potentials of $n_\infty(v)$ and $h_\infty(v)$ are much lower than the values for I_A. The equation for this current is defined as

$$I_{Aa} = g_{Aa} n_a^{3} h_a (v - E_K) \tag{4.18}$$

where g_{Aa} represents the maximum conductance, and n_a and h_a represent the activation and inactivation fractions, and satisfy

$$\frac{dn_a}{dt} = \frac{n_{a\infty}(v) - n_a}{\tau_{n_a}(v)}$$
$$\frac{dh_a}{dt} = \frac{h_{a\infty}(v) - h_a}{\tau_{h_a}(v)} \tag{4.19}$$

The leak current (I_l)

The leak current is located in every compartment and has no activation or inactivation fractions. It follows the equation

$$I_l = g_l(v - E_l) \tag{4.20}$$

where g_l and E_l represent the maximum conductance and the reverse potential of the leak current.

The synaptic current (I_{syn})

The inhibitory synapse is located in Compartment D or the dendritic tree of the PY neuron. The synaptic current has the following equation:

$$I_{syn} = g_{syn} s_\infty(v_0)(v - E_{syn}) \tag{4.21}$$

Where g_{syn} and E_{syn} represent the maximum conductance and the reverse potential of the inhibitory synapse, v_0 represents the presynaptic membrane potential and $s_\infty(v_0)$ represents the activation fraction.

The values for the parameters for each current can be found in Table 4.2.

4.3 Results

In order to solve this high-dimensional problem (53 ODEs and more than 100 parameters), a Genetic Algorithm (GA) is applied for the computation. The initial population is set as a group of arbitrary solutions, and the evaluation function is defined differently during different stages of the computation.

4.3.1 The Application of the Genetic Algorithm (GA)

Genetic Algorithms have been applied for solving various high-dimensional and global optimization problems. For examples, GAs have been used to predict the secondary structure of the RNA sequences (van Batenburg et al., 1995), to predict the procedures of protein folding and ligand docking (Willett, 1995), to find the most effective stimulus in large parameter spaces for sensory neurons in the cochlear nucleus and inferior colliculus (Bleeck et al., 2003) and to determine the conductance density distributions for a computational model in order to simulate endogenous bursting behavior of the leech heart interneurons (Tobin et al., 2006).

The steps of the GA used in this work are shown in Table 4.1. The solution domain is a large parameter space which includes parameters for currents in each compartment. A set of parameters is considered as an individual in the GA program. At the beginning a group of individuals are chosen as the initial generation. An evaluation function is then executed to calculate a fitness value for each individual. If any individual has a fitness value qualifying the terminating condition, the computation is ended and the optimal individual is exported. If there is no satisfactory fitness value, then the iteration continues and a certain number of individuals are selected stochastically as the parents of the next generation. The fitness values determine the probability for each individual to be chosen.

Each selected individual is chosen for one of the two operations: mutation and crossover. In order to implement these operations, each individual is translated into a binary string representing a chromosome. A mutation operation modifies an arbitrary bit in the string with certain probability, and a crossover operation exchanges parts of two strings. After these operations the strings are translated back into the individuals (sets of parameters) and a new generation is produced. The evaluation function is then executed for calculating the fitness value of each individual in the new generation, and the same procedure is implemented again. The iteration is ended either when an optimal individual is found (which is considered as the terminating condition shown in Table 4.1), or when the maximum number of generations is reached.

The GA program was implemented in MATLAB and NETWORK, a homemade software from the STG lab at Rutgers University. In order to reach a group of desirable solutions, there is a need to set appropriate numbers for the generations and the individuals in each generation in the program. If the numbers are too small, the best solution may not be reached at the end; if the numbers are too large, the computation time may be unnecessarily long. The evaluation function is used to evaluate the fitness value of each individual in each generation which partially determined if an individual can survive in the next generation or not. Therefore, it is critical and needs to be accurate and optimized.

Table 4.1 Schematic Illustration for the Genetic Algorithm

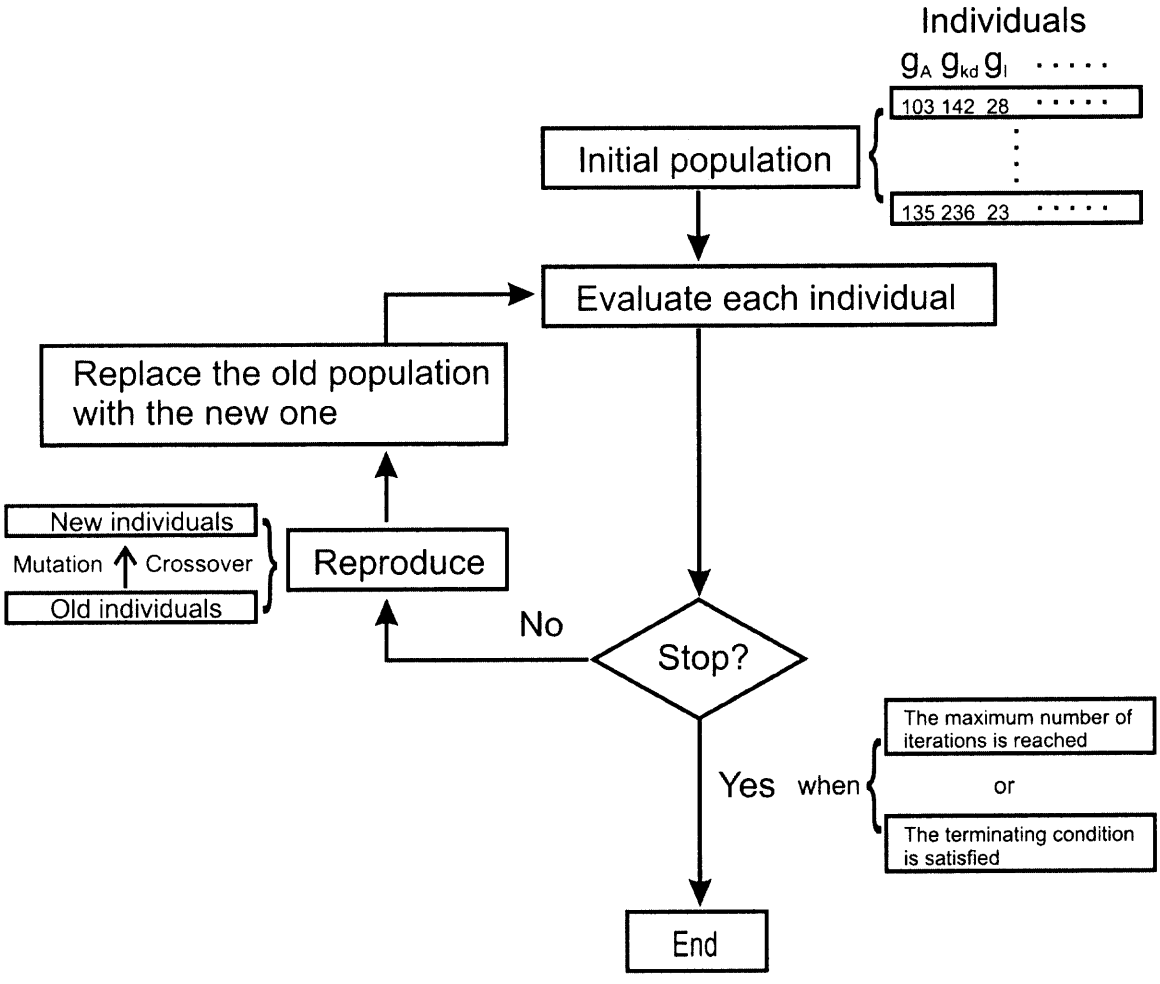

There are two stages involved in the computation. In the first stage, GA was used to obtain solutions with a reasonable number of spikes during each burst without the effect of the A-current. The parameter space is over 50 dimensions which include most of the intrinsic parameters. The evaluation function is set as a function of the average number of spikes in each burst. The individuals (or sets of parameters) generating spikes in the desired range obtain higher scores from the evaluation function. In the second stage, the A-current is assigned to the model neuron and GA is applied for evaluating the reasonable effect of

the A-current on the phase delay. For example, when the activation fraction of the A-current is set to be a steep sigmoid, the individuals that have middle states closer to the half-maximum voltage value can obtain greater scores from the evaluation function. Therefore they are more likely to survive in the next generation.

The GA program has been run more than a hundred times and six good solutions are obtained after the two stages computation. Table 4.2 and Table 4.3 show a representative set of parameters and steady state functions computed by GA which lead to a solution close to the biological PY neuron. Figure 4.2 shows the membrane potentials in Compartment S based on these set of parameters and functions. In Figure 4.2(a) there is no A-current in the model PY neuron, therefore the membrane potential has no delay caused by the A-current before each burst. In Figure 4.2(b) a moderate A-current is assigned to each compartment evenly based on their surface areas, and it causes a phase delay before each burst. When the A-current is fairly strong, the delay is prolonged and the membrane potential may not be able to spike (Figure 4.2(c)). All the three figures show that the three-variable model provides a close simulation to the biological PY neurons.

Table 4.2 Parameters for the Currents in Each Compartment

Currents		S	P	B	D	A
I_{Kd}	g_{Kd} (μS)	636.2	127.2	86.5	1979.2	1500
	E_{Kd} (mV)	-80	-80	-80	-80	-80
I_{KCa}	g_{KCa} (μS)	141.4	70.1	40	100	\
	E_{KCa} (mV)	-80	-80	-80	-80	\
I_A	g_A (μS)	300	210	144	300	\
	E_A (mV)	-80	-80	-80	-80	\
I_{Ca}	g_{Ca1} (μS)	42.4	32.8	10.3	330.8	\
	g_{Ca2} (μS)	52.2	39.6	17	293.4	\
I_h	g_h (μS)	157	24.7	23.5	260.7	\
	E_h (mV)	-25	-25	-25	-25	\
I_{proc}	g_{proc} (μS)	180	56.5	38.5	879.6	\
	E_{proc} (mV)	-10	-10	-10	-10	\
I_{Na}	g_{Na} (μS)	\	\	\	\	2000
	E_{Na} (mV)	\	\	\	\	85
I_{Aa}	g_{Aa} (μS)	\	\	\	\	500
	E_{Aa} (mV)	\	\	\	\	-80
I_l	g_l (μS)	17.7	3.5	2.4	55	20.2
	E_l (mV)	-72	-72	-72	-72	19
I_{syn}	g_{syn} (μS)	\	\	\	1200	\
	E_{syn} (mV)	\	\	\	-70	\
$[Ca^{2+}]$	$\tau_{[Ca^{2+}]} = 2.78\ ms$, $F = 0.83\ \mu$M/nA, $C_0 = 0.05\ \mu$M					

Table 4.3 Steady State Activation and Inactivation Functions of Each Current

Currents	Activation	Inactivation
I_{Kd}	$\frac{1}{1+\exp(-(v+24.5)/4.1)}$	\
I_{KCa}	$(\frac{[Ca]}{[Ca]+2.5})\frac{1}{(1+\exp(-(v+0.6[Ca])/23))}*$ $\frac{1}{(1+\exp(-(v+16+0.6[Ca])/5))}$	$\frac{0.7}{0.6+[Ca]}$
I_A	$\frac{1}{1+\exp(-(v+50)/0.5)}$	$\frac{1}{1+\exp((v+51)/0.1)}$
I_{Ca1}	$\frac{1}{1+\exp(-(v+11)/7)}$	$\frac{1}{1+\exp((v+50)/8)}$
I_{Ca2}	$\frac{1}{1+\exp(-(v-22)/7)}$	\
I_h	$\frac{1}{1+\exp((v+84.3)/6.4)}$	\
I_{proc}	$\frac{1}{1+\exp(-(v+49)/5)}$	\
I_{Na}	$\frac{1}{1+\exp(-(v+22.3)/4)}$	$\frac{1}{1+\exp((v+23.4)/3.8)}$
I_{Aa}	$\frac{1}{1+\exp(-(v+75.8)/16)}$	$\frac{1}{1+\exp((v+76.1)/8.3)}$

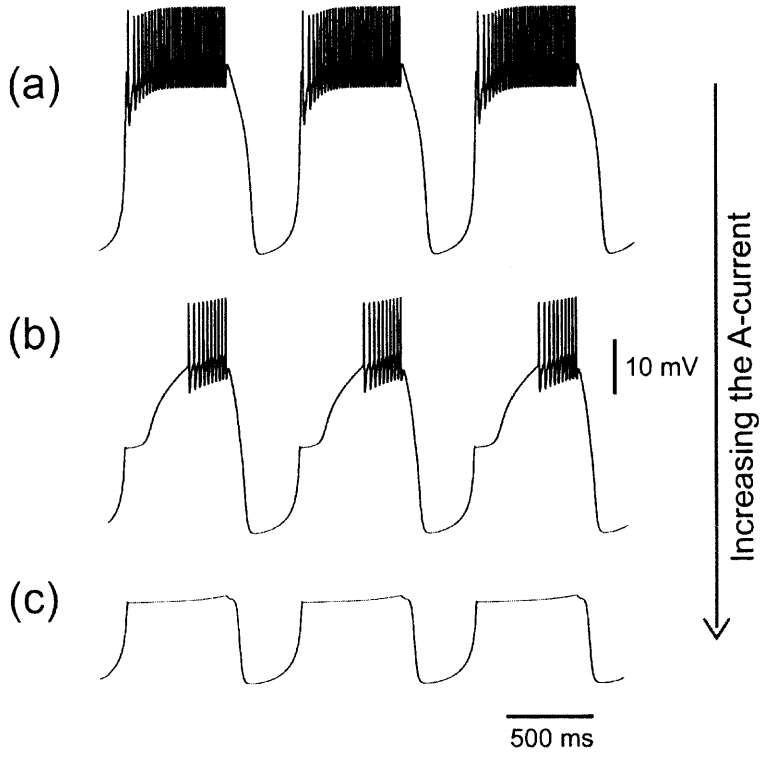

Figure 4.2 The Numerical Solutions of the Realistic PY Model. (a)-(c) show the membrane potential in Compartment S when the strength of the A-current is increasing. **(a)** When $g_A = 0$ in all the compartments, there is no delay before bursts. **(b)** When a moderate amount of A-current is evenly distributed in every compartment (g_A = 300 nS in Compartment S), there is a time delay before each burst. **(c)** When a strong A-current is evenly distributed in every compartment (g_A = 1,000 nS in Compartment S), the membrane potential cannot spike and therefore the activity phase becomes 1.

4.3.2 The Effect of the A-Current Distribution on the Activity Phase

In Chapter 2 and 3 it has been shown that the strength of the A-current plays an important role in modulating the time delay before bursts and therefore the activity phase of the follower neuron. The model which has been used in these two chapters is a single compartment isopotential model, therefore it does not provide any information about how the distribution of the A-current can affect the activity phase. With the help of the realistic model built in this chapter, it is possible to investigate if the distribution of the A-current at

each compartment can affect the activity phase of the follower PY neuron, given the amount of the A-current is constant.

This problem is examined based on a well-defined realistic PY model with a moderate A-current developed in the previous section. Five different protocols are applied to inject a certain amount of A-current (g_A = 500 nS) to this model:

Protocol 1. Add evenly to every compartment proportional to their surface areas

Protocol 2. Add to Compartment S only

Protocol 3. Add to Compartment P only

Protocol 4. Add to Compartment B only

Protocol 5. Add to Compartment D only

The activity phase at Compartment S is measured under each protocol (Figure 4.3(a)). It shows that Protocol 3 and 4 lead to more delayed activity phases, whereas Protocol 2 and 5 lead to relatively smaller phases than the phase under Protocol 1. Figure 4.3(b) shows the corresponding membrane potential in Compartment S under each protocol. The result indicates that the activity phase can be partially determined by the A-current distribution. When there is a fixed amount of A-current in the realistic PY model, the higher percentage located in the relatively small compartments, such as P or B, the greater the activity phase may be.

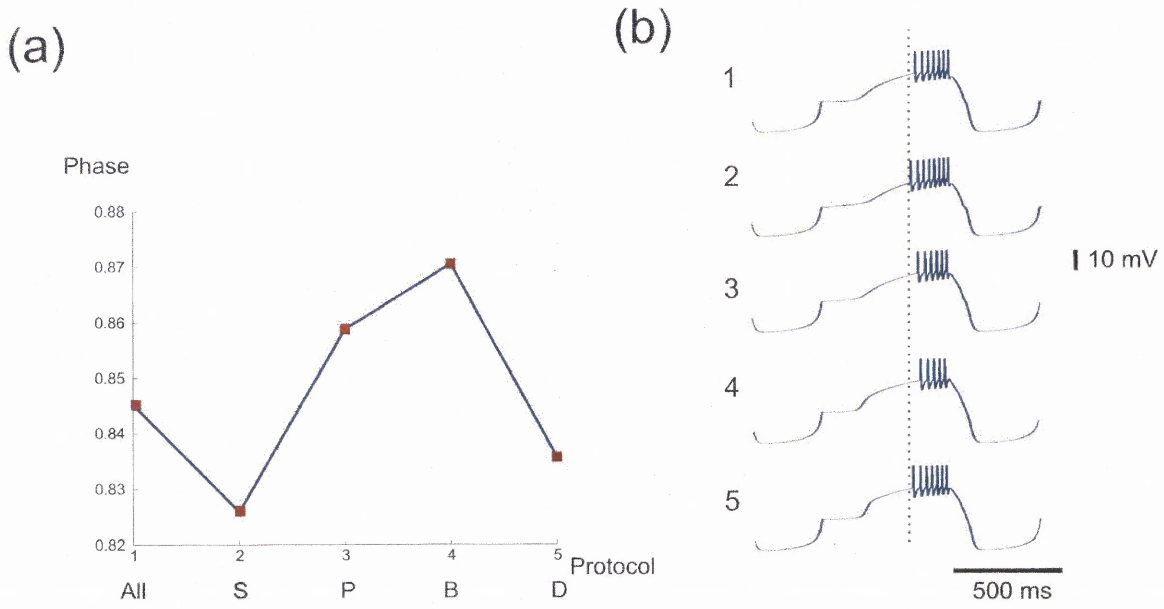

Figure 4.3 The Activity Phase in Compartment S of the Realistic PY Model under Five Different Protocols. (a) An additional A-current (g_A = 500 nS) is injected to a well-defined PY model under five protocols: 1. add evenly to every compartment based on its surface area; 2. add to S only; 3 add to P only; 4. add to B only; 5. add to D only. It shows that Protocol 3 and 4 provide relatively greater activity phases, and Protocol 2 and 5 provide relatively smaller activity phases, which indicates that a higher density A-current in a compartment may lead to a greater activity phase than the even distribution case. **(b)** The corresponding membrane potentials in Compartment S of the realistic PY model under the five protocols, respectively.

4.4 Summary

In Chapters 2 and 3 it is shown by modeling and experiments that the strength of the A-current, together with other intrinsic and synaptic properties, can affect the activity phase of the follower PY neuron. However, it is unknown whether the activity phase can be modulated by the morphology of the biological neurons and the distributions of the intrinsic and synaptic currents. This chapter provides the application of a Genetic Algorithm for developing a detailed model based on the biological shape and properties of

a follower PY neuron in the crustacean pyloric network. There are two benefits which can be obtained from this modeling work:

1. The spiking property is added to the model.

2. The effect of the A-current distribution in each compartment on the activity phase can be investigated.

By running the GA program in MATLAB and NETWORK, several candidate solutions are obtained, some of which show close simulations to the biological PY neuron. By changing the distribution of the A-current under five different protocols but keeping the total amount constant, it is shown that the distribution of the A-current also affects the activity phase of the PY neuron, given the total strength of the A-current is unchanged. In the computational simulation, a certain amount of additional A-current is injected into different compartments of a well-defined model PY neuron. When this A-current is injected into relatively large compartments such as S (for soma) or D (for dendritic tree), the delay of the activity phase is shorter than the phase delay while injecting the same amount of A-current evenly into all the compartments based on their surface areas. When the additional A-current is injected into relatively smaller compartments, such as P (for priaxion) or B (for branch), the activity phase becomes more delayed. The computational results show that the distribution of the A-current, or its density in every compartment, can lead to different activity phases, even though the total amount of the A-current keeps constant. The greater the density of the A-current in one (or more) compartment, the greater the phase delay will be.

This chapter only investigates the effect of the A-current distribution on the activity phase of the follower PY neuron. The same method can be applied to check whether the distribution of any other current can affect the activity phase. Also, related experiments can

be conducted to verify the modeling predictions. The GA program and the method of examining the current distribution shown in this chapter can be used to solve other complex or high-dimensional problems.

CHAPTER 5

OTHER FACTORS THAT MAY AFFECT THE ACTIVITY PHASE

5.1 Introduction

The effect of the A-current on the activity phase of the follower neuron has been explored in Chapters 2, 3 and 4. It has been shown that the A-current plays a significant role in determining the time delay to the bursts and therefore the activity phase. The analysis of the phase space shows that the A-current, together with other intrinsic properties, can lead to very different and complicated behaviors; the recursive equations provide fairly good prediction of the activity phase of the biological PY neurons; and the development of the realistic PY model simulates the biological PY neuron in a more detailed way with spiking property. It indicates that the distribution of the A-current at different parts of the PY neuron may also affect its activity phase.

This chapter shows that other factors, such as the existence of the h-current and the gap junction between two follower neurons, can also affect the activity phase of the follower PY neurons. The models in this chapter are developed from the three-variable model in Chapter 2, and the modeling results are compared with the experimental data.

5.2 The Effect of the h-Current on the Activity Phase

The h-current is a hyperpolarization activated current existing in many types of neurons. This current is activated by hyperpolarization beyond -50 to -70 mV, and depolarizes the cell slowly to its equilibrium voltage (Luthi and McCormick, 1998). It has been shown that the h-current plays roles in regulating the frequency of the network oscillations (Yue and

Huguenard, 2001), controlling the long term synaptic modulation (Harris-Warrick, 2002), and balancing the effect of the A-currernt (MacLean et al., 2003). Especially when the A-current increases, the h-current is enhanced due to the hyperpolarization and compensates for the function of the A-current.

This fact is explained by mathematical modeling based on the three-variable model we show in Chapter 2. A term and an equation are added into Equations (2.1) for expressing the mechanism of the h-current:

$$\begin{aligned}
\varepsilon\frac{dv}{dt} &= f(v,w) - g_A n_\infty(v)h(v-E_A) - g_h r(v-E_h) - I_{inh} \\
\frac{dw}{dt} &= \frac{w_\infty(v)-w}{\tau_w(v)} \\
\frac{dh}{dt} &= \frac{h_\infty(v)-h}{\tau_h(v)} \\
\frac{dr}{dt} &= \frac{r_\infty(v)-r}{\tau_r(v)}
\end{aligned} \tag{5.1}$$

where g_h and E_h represent the maximum conductance and the reverse potential of the h-current, r represents the activation fraction, and $r_\infty(v)$ and $\tau_r(v)$ represent the steady state value and the time constant of r respectively. Similar to Chapter 2, in this chapter it is assumed that the activation fraction of the A-current, $n_\infty(v)$, is a steep sigmoid, or the middle branch of the v-nullcline in the v-w phase plane is vertical (See Chapter 2 for details).

It has been shown in Chapter 2 that the stronger the A-current is, the more delayed the activity phase becomes given all the other parameters are fixed. When the A-current is strong enough, it may prevent the membrane potential from reaching the active state or spiking (Figure 2.1).

However, the presence of the h-current balances the effect of the A-current, as it is activated when the membrane potential is hyperpolarized. Therefore it can help the membrane potential to reach the active state or spiking state even with the presence of a strong A-current. Figure 5.1(a) shows the membrane potential of the follower PY neuron with (i) and without (ii) the h-current, when it contains a strong A-current.

This phenomenon can be explained by phase plane analysis in the v-w phase plane. Figure 5.1(b) shows the v and w nullclines in the v-w phase plane. Comparing the v-nullcine without the h-current, the presence of the h-current term causes an upward shift on the left and middle branches (LB and MB) of the v-nullcine when the membrane potential is moving on LB. Therefore, when the trajectory lands on MB after the inhibition, it is easier to encounter the lower knee (LK) and then jumps to the right branch (RB) which corresponds to the active state of the membrane potential. A detailed explanation of the dynamics on MB is shown in Chapters 2 and 3.

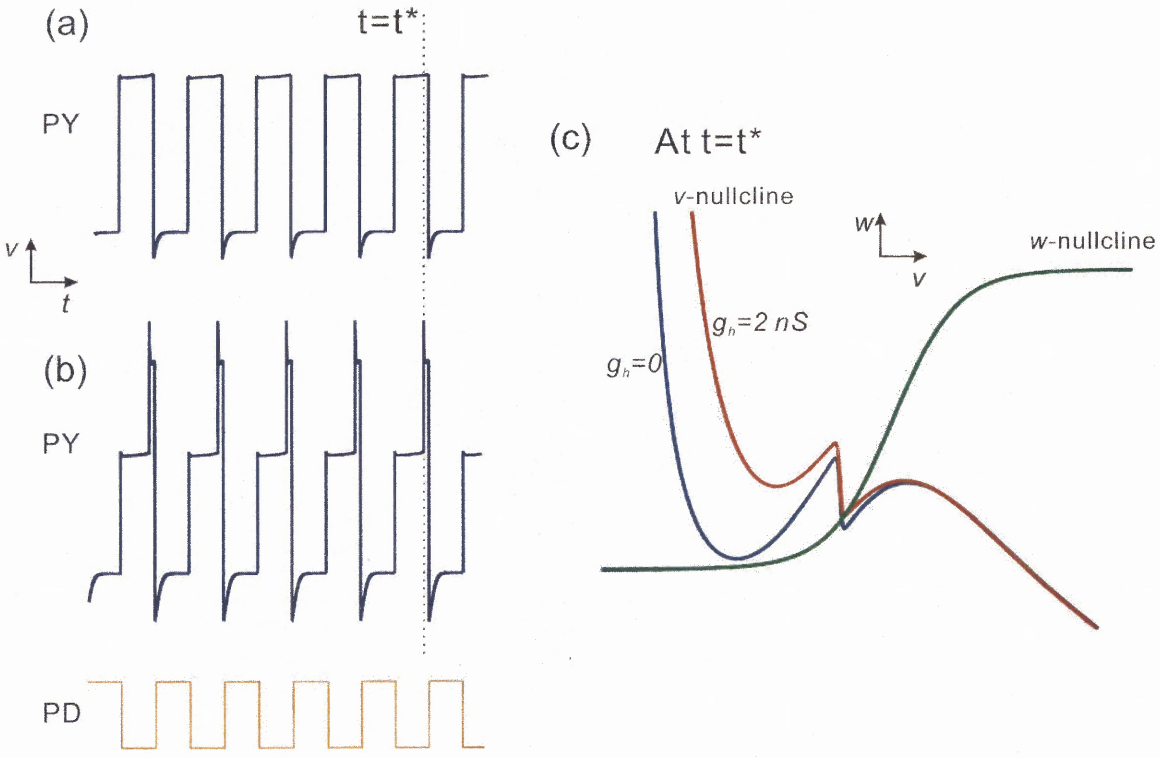

Figure 5.1 The Effect of the h-Current on the Activity Phase of the PY Neuron with a Strong A-Current. (a) The membrane potentials of PY without the h-current. The strong A-current prevents the membrane potential from reaching the active state. **(b)** With the presence of the h-current, the activity phase of PY is advanced and it can reach the active state. **(c)** The dynamics in the *v*-*w* phase plane with the presence of the h-current at time $t = t^*$. The h-current is activated at low voltage therefore it helps to moves up the left and the middle branches of the *v*-nullcline, which allows the trajectory to encounter the lower knee LK and then jump to the right branch corresponding to the active state of the membrane potential.

5.3 The Effect of the Gap-Junction between LP and PY on the Activity Phase

It has been shown that there is a rectifying gap junction between the two types of follower neurons LP and PY in the crustacean pyloric network (Mamiya et al., 2003). The LP neuron has a more advanced activity phase than the PY neurons as shown in Figure 1.1 of Chapter 1. It is possible that the LP neuron enhances the membrane potential of the PY

neuron through the gap junction therefore the PY neuron can reach the active state and spike even with the presence of a strong A-current.

In order to examine this possibility, an LP model is built by using the same equations (Equations (2.1)-(2.4)) as those for PY. The only difference is that g_A is smaller for the LP neuron. The two model neurons are then connected by adding the gap junction term to each model as shown below:

$$\begin{aligned} &\text{For LP and PY: } C_m \frac{dv}{dt} = f(v,w) - g_A n_\infty(v) h(v - E_A) - I_{syn} - I_{gap} \\ &\text{In LP: } \quad I_{gap} = g_{gap}(v_{LP} - v_{PY}) H(v_{LP} - v_{PY}) \\ &\text{In PY: } \quad I_{gap} = g_{gap}(v_{PY} - v_{LP}) H(v_{LP} - v_{PY}) \end{aligned} \tag{5.2}$$

where $H(x)$ is the heaviside function which equals 1 when $x>0$ and 0 when $x<0$. The rectifying gap junction from LP to PY means that when the membrane potential of LP is greater than the membrane potential of PY, the current is nonzero. Otherwise, it is zero due to the property of the heaviside function. In other words, it only exists when the membrane potential of LP is larger than PY.

Figure 5.2(a) and 5.2(b) show the membrane potentials of the LP and PY neurons without (a) and with (b) a rectifying gap junction between them. There is a moderate A-current in LP, and a strong A-current in PY. Therefore the PY neuron cannot reach the active state without the gap junction ((ii) in Fig 5.2a). However, when there is a gap junction between LP and PY, the activity phase of PY is advanced and it can reach the active state even with a strong A-current ((ii) in Fig 5.2b).

Figure 5.2(c) shows the dynamics for the PY neuron in the *v-w* phase plane. After the trajectory lands on the middle branch at point 1, it stays at the stable fixed point FP, and at the same time the lower knee (LK) of the middle branch moves up. Without the gap

junction from the LP neuron, the long middle branch will prevent LK to encounter the trajectory at FP during a single cycle. However, with the help of the gap junction, the *v*-nullcine is raised more (from [1] to [2] in Figure 5.2(c)), and therefore LK can reach the trajectory and allows it to jump to the right branch of the *v*-nullcline corresponding to the active state of the membrane potential in Figure 5.2(b).

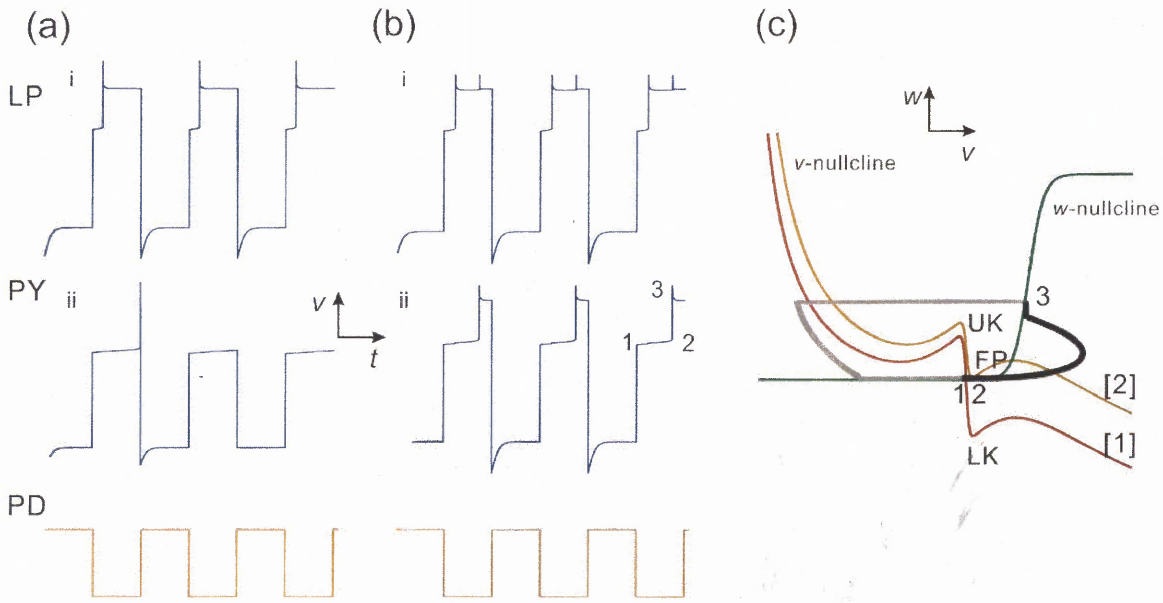

Figure 5.2 The Effect of the Gap Junction on the Activity Phase of the PY Neuron with a Strong A-Current. (a) The membrane potentials of LP and PY without a gap junction between them. LP contains a small amount of the A-current and PY contains a strong A-current therefore it cannot reach the active state. **(b)** With the presence of a gap junction between LP and PY, the activity phase of PY is advanced and it can reach the active state. **(c)** The dynamics in the *v*-*w* phase plane for PY. The gap junction helps to raise the *v*-nullcline from [1] to [2], and therefore allow the trajectory to jump to the right branch.

5.4 Summary

In the previous chapters it has been shown that the A-current plays an important role in modulating the activity phase of the follower PY neuron. Together with other intrinsic and synaptic properties, the strength and the distribution of the A-current can determine the behavior of the membrane potential and therefore the activity phase. It has also been shown that the dynamics of a single A-current can lead to complicated and somewhat unintuitive membrane potential behaviors (Chapter 3). In addition, the morphology of the follower neuron and the distribution of the A-current in each part of the neuron can also affect the activity phase, which is examined by developing a realistic model based on the shape and properties of the biological PY neuron (Chapter 4).

In this chapter, it is explained specifically that there are two other factors which can also play a role in modulating the activity phase of the follower PY neuron: One is the presence of the inward hyperpolarization activated current, or the h-current, and the other is the presence of a rectifying gap junction between the LP and PY neurons. It is shown that in each case, the effect of a strong A-current on the activity phase can be balanced, and any of these two factors may help the membrane potential to reach the active state even when the A-current is strong and the three-variable model neuron cannot reach the active state. The mechanism for each case is studied by using dynamical systems analysis in the *v*-*w* phase plane.

In summary, this chapter shows that even though the presence of the A-current can cause a phase delay before each burst, there are some intrinsic and synaptic properties, such as the h-current and the gap junction between the two types of follower neurons (LP and PY), which can balance the affect of the A-current and advance the activity phase. The

h-current is added into the three-variable model in Chapter 2 by adding a term and an ordinary differential equation into Equations (2.1) in Chapter 2 (Equations (5.1)), while the gap junction is added by adding another model neuron to simulate the follower LP neuron and a term into the equations for each model neuron to represent the gap junction between them (Equations (5.2)). In both cases in the v-w phase plane the middle branch of the v-nullcline is moved up a bit more when the trajectory is moving along it, due to the additional properties. Therefore the trajectory can encounter the lower knee LK and then jumps to the right branch (Figure 5.1(c) and 5.2(c)).

The techniques of mathematical modeling and dynamical systems analysis shown in this chapter can be applied to analyze the effect of other intrinsic or synaptic currents on the membrane potential behavior and the activity phase of the follower neuron.

CHAPTER 6

DISCUSSION

The transient potassium current or A-current has been shown to exist in various types of neurons (Huguenard et al., 1991; Herrington and Lingle, 1994; Wustenberg et al., 2004) and is known to be important in setting the timing of action potential(Gerber and Jakobsson, 1993), especially following inhibitory input (Harris-Warrick et al., 1995a), contributing to the generation of a coordinated motor pattern (Hess and El Manira, 2001), and acting as a bursting trigger in the absence of a slow variable (Tabak et al., 2007; Toporikova et al., 2007). In a network consisting of bursting neurons, the A-current often acts to delay the onset of the burst, thus setting the activity phase of different follower neurons within the network (Harris-Warrick et al., 1995a).

In a previous study Bose et al. (2004) have examined the interaction between the A-current and the short-term synaptic depression which promotes the phase maintenance in a follower neuron when the frequency of the periodic input is varied. Since this previous study was focused on investigating the effect of synaptic depression, only a single case associated with the mechanism of the A-current was considered. The research in this dissertation is mainly focused on understanding how the parameters associated with the A-current and other intrinsic and synaptic properties lead to different activity phases of a follower neuron. Therefore, more cases are considered and a complete analysis is achieved for all the possible parameter combinations.

There are four stages in this research. In the first stage, a three-variable model is built in order to explore the effect of the A-current on the behavior of a follower neuron and

to predict the activity phase of the biological PY neuron in the crustacean pyloric network. Dynamical systems analysis is applied to determine the fate of the trajectory of the follower neuron following inhibition in a single cycle. A set of recursive equations are then derived to describe the steady state activity phase of this neuron in response to a periodic input. The activity phase predicted by these equations matched the activity phase of follower PY neurons in the crustacean pyloric network when the cycle period was varied through different experimental protocols.

In the second stage, a systematic and complete classification is achieved using the geometric phase plane analysis. Two categories and eight cases are obtained based on the shapes and positions of the nullclines in a slow manifold – the v-w phase plane. In each case, the time constants of the two slow variables w and h are compared and all the possible trajectories are given as subcases. It is shown that even a simple three-variable model can lead to very complicated results. The fate of the trajectory is determined by a combination of parameters, and different sets of parameters can result in the same membrane potential behavior. Recursive equations are derived for tracking both variables w and h over cycles, and steady state values are expressed analytically. The weak inhibition case is also considered which can lead to some unintuitive solutions when the A-current is relatively strong. The behavior of the follower neuron can be predicted by using the equations representing the steady state values of h and w.

In the third stage, a five-compartment computational model is developed based on the biological shape and properties of the PY neuron in order to simulate the spiking property and to explore the effect of the current distribution on the activity phase. The model is built by applying a Genetic Algorithm in MATLAB and NETWORK, which

provides a heuristic method to compute the possible sets of parameters for all the intrinsic and synaptic currents for achieving the ideal membrane potential behavior. By changing the density of the A-current in each compartment under five different protocols, it is shown that the morphology of the follower neuron and the distribution of the A-current do have an effect on the activity phase. In fact the higher the A-current density is in one compartment, the greater the activity phase becomes.

In the fourth stage, the effects of the hyperpolarization activated current (h-current) and the gap junction between the LP and PY neurons on the activity phase of the follower PY neuron with a strong A-current are considered. Terms and differential equation representing the presence of the h-current and the gap junction are added into the three-variable model built in the first stage respectively, and phase plane analysis is applied for understanding the dynamics of the follower PY neuron. In each case because of the effect of the additional term, the middle branch of the v-nullcline in the v-w phase plane is moved up during the time the trajectory is moving along it, therefore the trajectory can encounter the lower knee of the middle branch and then jump to the right branch even if the A-current is strong and the middle branch is relatively long.

The above four stages provide a comprehensive study of the effect of the A-current, together with other intrinsic and synaptic properties, on the activity phase of the follower PY neuron. With the help of the mathematical and computational models, both the kinetics and the distributions of the A-current and other currents are explored and the activity phase of the biological follower PY neuron can be predicted using a set of recursive equations and the steady state expressions for the bursting phase and the slow variables. The specific achievements from this study are summarized by answering the following questions:

How does the A-current affect the behavior of the neuron following inhibition?

A typical response of a follower neuron in an inhibitory network is to rebound to an active state following the inhibition, but the transition to the active state may be delayed by the amount and kinetics of the A-current. For example, in the crustacean pyloric network, the follower LP and PY neurons show different burst phases, which are partially determined by the different amount and specific properties of the A-current (Tierney and Harris-Warrick, 1992). It has been suggested that the variation in the phase of different PY neurons may be determined by the different levels of A-current expressed in these neurons (Hooper, 1998). In fact, experiments show that different PY neurons in the same preparation burst in different phases. Furthermore, their burst phases can be modulated by injecting an artificial A-current (Figures 2.1, 2.2). Two important questions regarding the phase of the follower neurons can be asked first. 1. Following inhibition, how do the parameters of the A-current and other intrinsic properties determine the time delay before the burst (active state)? 2. During the rhythmic activity, how do different network parameters, including the cycle period, duration of inhibition and the strength and kinetics of the A-current interact to determine the activity phase of the follower neuron?

These two questions are addressed by using a minimal three-variable model and geometric phase plane analysis. The geometric analysis of the model is focused on the phase plane of the two slow variables w and h, which represent the activation variable of the potassium current and the A-current inactivation respectively, to determine the post-inhibition time delay. Depending on the parameters of the A-current, it is found that the structure of the phase plane (Figure 2.3) can be used to determine the possible behaviors of the trajectory following inhibition; in particular, whether the trajectory can

jump to the active state or return to the inactive state. It is then shown that the time constants for the two slow variables (Equations (2.1)) play an important role in determining the evolution of the trajectory and the time delay before the burst (Figure 2.4). The phase-plane analysis also demonstrates that distinct combinations of model parameters can give rise to similar time delays and that, in each case, the parameters that control the transition to the active state could be different.

The steady state activity phase in response to a periodic inhibitory input cannot be determined solely by the intrinsic properties of the follower neuron. This phase depends on the post-inhibition time delay of the follower neuron and also on the strength and duration of the inhibition and on the period of the rhythmic input. The duration and period of the inhibitory input are described in the model by the active and inactive durations, T_{act} and T_{in}, of the pacemaker neurons. Several sets of recursive equations that describe the steady state maximum value for the slow variables and the steady state time delay caused by the A-current are derived. These factors in turn determine the steady state activity phase of the follower neuron. Similar recursive models, based on steady state assumptions, have been used to analyze the anti-bursting phase of a two-cell inhibitory network which is affected by both the intrinsic properties and the dynamics of the synapses (Matveev et al., 2007) and to investigate how the firing rate of the pre-synaptic neurons and the synaptic plasticity affect the firing activity of the post-synaptic neuron in a multi-input and single-output network (Rubin, 2001).

What can we learn from the complete classification?

The A-current has been shown to play an important role in modulating the bursting phase of the neurons following periodic inhibition (Harris-Warrick et al., 1995a; Harris-Warrick et al., 1995b). The first stage of the work is to predict the activity phase of the biological PY neuron by analyzing the phase planes and deriving a set of recursive equations (Equations (2.16)-(2.19)) based on a three-variable model. Under the assumption that the middle branch is vertical, two cases are obtained and the behavior of the trajectory in each case is analyzed depending on various time constants (Chapter 2).

After this study, a complete characterization of the potential behaviors of the neuron following inhibitory inputs based on the geometric structure of the nullclines in two phase planes is shown (Chapter 3). Based on the parameters of the model, the post-inhibition behavior of the follower neuron can be classified into two categories that include eight cases, in each of which a geometric approach is used to determine the dynamics of the follower neuron. In parallel, the numerical solution of the model is used to verify the predictions of the mathematical analysis for the steady state values of the slow variables w and h and the activity phase φ. The same analysis and computation are also done for the weak inhibition case, and the unintuitive solutions can be predicted by tracing the values of the slow variables over cycles based on the recursive equations.

This technique allows scientists to systematically explore the multitude of potential behaviors of the follower neuron's trajectory and therefore predict both its transient and stationary activity in response to rhythmic synaptic inputs. Surprisingly, even a small number of variables and parameters can give rise to a rich set of behaviors of the follower

neuron. Yet, the systematic method can be generalized to understand factors that determine the oscillatory activity of follower neurons that involve a large number of parameters.

How the distribution of the A-current affects the activity phase?

Research indicates that there are phase differences between the follower LP and PY neurons in the crustacean pyloric system (Harris-Warrick et al., 1995a; Harris-Warrick et al., 1995b). Moreover, the experiment in Chapter 2 (Figure 2.1(a)) shows that even the same type neurons (PY) can have fairly different activity phase. It has been shown that the strength of the A-current can partially modulate the activity phases of the follower PY neurons (Harris-Warrick et al., 1995a). However, there is no evidence that the distribution of the A-current in different parts of the PY neuron can affect the activity phase.

In order to examine this possibility, a five-compartment model is built and a Genetic Algorithm is applied to compute the possible sets of parameters. After the model is well-defined, an additional amount of A-current is injected into the model neuron under five different protocols. The first protocol requires the A-current to be injected into all the compartments evenly based on their surface areas, while the second to the fifth protocols allow the A-current to be injected only into one of the compartments, i.e. Compartment S (for soma), P (for priaxion), B (for branch) or D (for dendritic tree) in sequence. The total amount of the A-current in all the five protocols is kept constant. Figure 4.3 shows the activity phase under each of the five protocols. The computational results imply that the density of the A-current in each compartment can affect the activity phase of the follower neuron even if the total amount keeps constant. The greater the density is in one compartment, the more delay the activity phase becomes. This modeling result can be

verified by conducting corresponding experiments with the biological PY neuron(s). This method can be used to investigate the effect of other current distribution(s) on the activity phase.

What do our results imply for the biological system?

The activity phases of CPG neurons are often determined by the frequency of network oscillations. In some cases, such as fish swimming, strict phase maintenance is required to produce a meaningful motor output (Grillner, 2006). In other cases, the activity phase of different neurons, and therefore the muscles that they control, increases or decreases as a function of network frequency (Hooper, 1997b). In the crustacean pyloric network, different neurons show different dependencies on the network frequency (Hooper, 1997a, b) and the mechanisms underlying these dependencies are largely unknown. In this study several sets of recursive equations are derived to show how the phase of a follower neuron with A-current is a function of the network frequency. In the model, this frequency is determined by the period of the pacemaker input. Because there is a dominance of inhibitory connections in CPG networks (Friesen, 1994; Marder and Bucher, 2001; Marder et al., 2005) and the potassium A-current is a common current present in most neurons, it is expected that the analysis in this dissertation could be relevant for determining the activity phase of neurons in a variety of CPG networks.

The results indicate that the activity phase of a follower neuron with A-current is not only a function of the period (P) of the input it receives but also a function of how P is changed. For example, if P is doubled, the phase of the follower neuron can become larger or smaller, depending on whether the duration of the synaptic input is increased or not.

This is because the extent to which the A-current recovers from inactivation depends both on P (= T_{act} + T_{in}) and on the duration for which the neuron remains inhibited (T_{act}). Three protocols are applied for changing P. It is shown that if P is changed but T_{act} or the duty cycle (T_{act} / P) is fixed, the phase of the follower neuron decreases as P increases. Both these mechanisms of changing period occur in CPG networks, for example when the swing phase of locomotion remains constant despite a ten-fold variation in the cycle frequency (Grillner, 2006). However, if P is changed by keeping T_{in} fixed, the phase of the follower neuron increases as P is increased. The theoretical predictions were then verified through a set of experiments conducted in follower PY neurons showing a close match between experiment and theory. Thus, the analysis in this dissertation provides a basic explanation for how the changes in phase depend not only on P but on how P is changed.

Rhythmic biological networks in general and the crustacean pyloric network in particular may have many follower neurons that both receive periodic driving input and interact with one another. In the crab pyloric network, for instance, there are three to five PY neurons and other types of follower neurons which interact with the PY neurons through chemical and electrical synapses. Moreover, the presence of neuromodulators results in intrinsic or synaptic modifications and therefore changes the activity phase of the follower neurons. For example, dopamine can reduce the strength of the A-current therefore prolonging the duration of bursting (Harris-Warrick et al., 1995a). The modeling results provide a first-order approximation for understanding the activity of the individual follower neurons but do not account for the interaction among such neurons. Similar techniques can be used to account for inputs from other network neurons in order to determine the activity phase of these neurons and the long-term fate of their trajectories. As

the number of neurons involved and thus the complexity of the network is increased, the simplifying techniques utilized in this study may be of critical importance for understanding the underlying dynamics.

Conclusions

The transient A-current, interacting with other intrinsic and synaptic properties, plays an important role in modulating the activity phase of the follower neurons. A three-variable model is built for exploring the current kinetics that determine the activity time of a neuron with A-current following periodic inhibitory inputs. By solving the model system analytically, the activity phase of the biological follower PY neurons can be predicted by recursive equations. The results indicate that, even with a very simple model neuron, the interaction of the A-current parameters and other intrinsic parameters can be quite complex and lead to distinct model behaviors. Although the role of other factors such as synaptic dynamics and the interaction with other network neurons that can affect the role of the A-current in determining the activity phase remains to be explored, the basic geometric tools that could be used for such analysis in more complicated settings have been provided. Moreover, not only the kinetics of the intrinsic currents, but also the morphology of the follower neuron and the A-current distribution can play a role in modulating the activity phase of the follower neuron. This fact is examined by building a five-compartment computational model and allocating a constant amount of A-current in each compartment under five different protocols. The analysis and computation in this dissertation demonstrate that depending on the model configurations corresponding to different states of the biological neuron, different parameters can control the post-inhibition activity phase.

This indicates that extrinsic factors such as neuromodulators that modify the activity phase of neurons may be targeted to change the appropriate parameter(s) depending on the state of the follower neuron.

REFERENCES

Abbott LF, Marder E, Hooper SL (1991) Oscillating Networks: Control of burst duration by electrically coupled neurons. Neural Comput 3:487-497.

Bell J, Craciun G (2005) A distributed parameter identification problem in neuronal cable theory models. Math Biosci 194:1-19.

Bidaut M (1980) Pharmacological dissection of pyloric network of the lobster stomatogastric ganglion using picrotoxin. J Neurophysiol 44:1089-1101.

Bleeck S, Patterson RD, Winter IM (2003) Using genetic algorithms to find the most effective stimulus for sensory neurons. J Neurosci Methods 125:73-82.

Bose A, Manor Y, Nadim F (2004) The activity phase of postsynaptic neurons in a simplified rhythmic network. J Comput Neurosci 17:245-261.

Brizzi L, Meunier C, Zytnicki D, Donnet M, Hansel D, D'Incamps BL, Van Vreeswijk C (2004) How shunting inhibition affects the discharge of lumbar motoneurones: a dynamic clamp study in anaesthetized cats. J Physiol 558:671-683.

Bucher D, Prinz AA, Marder E (2005) Animal-to-animal variability in motor pattern production in adults and during growth. J Neurosci 25:1611-1619.

Buchholtz F, Golowasch J, Epstein IR, Marder E (1992) Mathematical model of an identified stomatogastric ganglion neuron. J Neurophysiol 67:332-340.

Chueshov I (2002) Monotone random systems : theory and applications. Berlin ; New York: Springer-Verlag.

Connor JA, Stevens CF (1971) Prediction of repetitive firing behaviour from voltage clamp data on an isolated neurone soma. J Physiol 213:31-53.

Debanne D, Guerineau NC, Gahwiler BH, Thompson SM (1997) Action-potential propagation gated by an axonal I(A)-like K+ conductance in hippocampus. Nature 389:286-289.

Ermentrout GB, Kopell N (1998) Fine structure of neural spiking and synchronization in the presence of conduction delays. Proc Natl Acad Sci U S A 95:1259-1264.

Friesen WO (1994) Reciprocal inhibition: a mechanism underlying oscillatory animal movements. Neurosci Biobehav Rev 18:547-553.

Gerber B, Jakobsson E (1993) Functional significance of the A-current. Biol Cybern 70:109-114.

Golowasch J, Marder E (1992) Ionic currents of the lateral pyloric neuron of the stomatogastric ganglion of the crab. J Neurophysiol 67:318-331.

Golowasch J, Casey M, Abbott LF, Marder E (1999) Network stability from activity-dependent regulation of neuronal conductances. Neural Comput 11:1079-1096.

Grillner S (2006) Biological pattern generation: the cellular and computational logic of networks in motion. Neuron 52:751-766.

Harris-Warrick RM (2002) Voltage-sensitive ion channels in rhythmic motor systems. Curr Opin Neurobiol 12:646-651.

Harris-Warrick RM, Coniglio LM, Barazangi N, Guckenheimer J, Gueron S (1995a) Dopamine modulation of transient potassium current evokes phase shifts in a central pattern generator network. J Neurosci 15:342-358.

Harris-Warrick RM, Coniglio LM, Levini RM, Gueron S, Guckenheimer J (1995b) Dopamine modulation of two subthreshold currents produces phase shifts in activity of an identified motoneuron. J Neurophysiol 74:1404-1420.

Herrington J, Lingle CJ (1994) Multiple components of voltage-dependent potassium current in normal rat anterior pituitary cells. J Neurophysiol 72:719-729.

Hess D, El Manira A (2001) Characterization of a high-voltage-activated IA current with a role in spike timing and locomotor pattern generation. Proc Natl Acad Sci U S A 98:5276-5281.

Hodge A, Edwards R, Paul DH, van den Driessche P (2006) Neuronal network models of phase separation between limb CPGs of digging sand crabs. Biol Cybern 95:55-68.

Hodgkin AL, Huxley AF (1952) The components of membrane conductance in the giant axon of Loligo. J Physiol 116:473-496.

Hooper SL (1997a) The pyloric pattern of the lobster (Panulirus interruptus) stomatogastric ganglion comprises two phase-maintaining subsets. J Comput Neurosci 4:207-219.

Hooper SL (1997b) Phase maintenance in the pyloric pattern of the lobster (Panulirus interruptus) stomatogastric ganglion. J Comput Neurosci 4:191-205.

Hooper SL (1998) Transduction of temporal patterns by single neurons. Nat Neurosci 1:720-726.

Hormuzdi SG, Filippov MA, Mitropoulou G, Monyer H, Bruzzone R (2004) Electrical synapses: a dynamic signaling system that shapes the activity of neuronal networks. Biochim Biophys Acta 1662:113-137.

Huguenard JR, Coulter DA, Prince DA (1991) A fast transient potassium current in thalamic relay neurons: kinetics of activation and inactivation. J Neurophysiol 66:1304-1315.

Jaeger D, Bower JM (1999) Synaptic control of spiking in cerebellar Purkinje cells: dynamic current clamp based on model conductances. J Neurosci 19:6090-6101.

Johnson SM, Smith JC, Funk GD, Feldman JL (1994) Pacemaker behavior of respiratory neurons in medullary slices from neonatal rat. J Neurophysiol 72:2598-2608.

Llinas R, Sugimori M, Simon SM (1982) Transmission by presynaptic spike-like depolarization in the squid giant synapse. Proc Natl Acad Sci U S A 79:2415-2419.

Luthi A, McCormick DA (1998) H-current: properties of a neuronal and network pacemaker. Neuron 21:9-12.

MacLean JN, Zhang Y, Johnson BR, Harris-Warrick RM (2003) Activity-independent homeostasis in rhythmically active neurons. Neuron 37:109-120.

MacLean JN, Zhang Y, Goeritz ML, Casey R, Oliva R, Guckenheimer J, Harris-Warrick RM (2005) Activity-independent coregulation of IA and Ih in rhythmically active neurons. J Neurophysiol 94:3601-3617.

Mamiya A, Manor Y, Nadim F (2003) Short-term dynamics of a mixed chemical and electrical synapse in a rhythmic network. J Neurosci 23:9557-9564.

Marder E, Paupardin-Tritsch D (1978) The pharmacological properties of some crustacean neuronal acetylcholine, gamma-aminobutyric acid, and L-glutamate responses. J Physiol 280:213-236.

Marder E, Eisen JS (1984) Transmitter identification of pyloric neurons: electrically coupled neurons use different transmitters. J Neurophysiol 51:1345-1361.

Marder E, Calabrese RL (1996) Principles of rhythmic motor pattern generation. Physiol Rev 76:687-717.

Marder E, Bucher D (2001) Central pattern generators and the control of rhythmic movements. Curr Biol 11:R986-996.

Marder E, Bucher D (2007) Understanding circuit dynamics using the stomatogastric nervous system of lobsters and crabs. Annu Rev Physiol 69:291-316.

Marder E, Bucher D, Schulz DJ, Taylor AL (2005) Invertebrate central pattern generation moves along. Curr Biol 15:R685-699.

Matveev V, Bose A, Nadim F (2007) Capturing the bursting dynamics of a two-cell inhibitory network using a one-dimensional map. J Comput Neurosci 23:169-187.

McCormick DA, Bal T (1997) Sleep and arousal: thalamocortical mechanisms. Annu Rev Neurosci 20:185-215.

Meyrand P, Weimann JM, Marder E (1992) Multiple axonal spike initiation zones in a motor neuron: serotonin activation. J Neurosci 12:2803-2812.

Mishchenko EF, Rosov NK (1980) Differential equations with a small parameter and relaxation oscillations. New York: Plenum Press.

Moore RY (1999) A clock for the ages. Science 284:2102-2103.

Morris C, Lecar H (1981) Voltage oscillations in the barnacle giant muscle fiber. Biophys J 35:193-213.

Mouser C, Nadim F, Bose A (2008) Maintaining phase of the crustacean tri-phasic pyloric rhythm. J Math Biol 57:161-181.

Nowak LG, Azouz R, Sanchez-Vives MV, Gray CM, McCormick DA (2003) Electrophysiological classes of cat primary visual cortical neurons in vivo as revealed by quantitative analyses. J Neurophysiol 89:1541-1566.

Nusbaum MP, Beenhakker MP (2002) A small-systems approach to motor pattern generation. Nature 417:343-350.

Pearson JD (1993) The control of production and release of haemostatic factors in the endothelial cell. Baillieres Clin Haematol 6:629-651.

Perko L (2001) Differential equations and dynamical systems, 3rd Edition. New York: Springer.

Prinz AA, Abbott LF, Marder E (2004) The dynamic clamp comes of age. Trends Neurosci 27:218-224.

Rabbah P, Nadim F (2005) Synaptic dynamics do not determine proper phase of activity in a central pattern generator. J Neurosci 25:11269-11278.

Rabbah P, Nadim F (2007) Distinct synaptic dynamics of heterogeneous pacemaker neurons in an oscillatory network. J Neurophysiol 97:2239-2253.

Rabbah P, Golowasch J, Nadim F (2005) Effect of electrical coupling on ionic current and synaptic potential measurements. J Neurophysiol 94:519-530.

Rinzel J, Ermentrout GB (1998) Analysis of neural excitability and oscillations. In: Methods in Neuronal Modeling: From Ions to Networks (Koch C, Segev I, eds), pp 251-291. Cambridge, MA: MIT Press.

Rubin JE (2001) Steady states in an iterative model for multiplicative spike-timing-dependent plasticity. Network 12:131-140.

Selverston AI (2005) A neural infrastructure for rhythmic motor patterns. Cell Mol Neurobiol 25:223-244.

Soto-Trevino C, Rabbah P, Marder E, Nadim F (2005) Computational model of electrically coupled, intrinsically distinct pacemaker neurons. J Neurophysiol 94:590-604.

Swensen AM, Marder E (2000) Multiple peptides converge to activate the same voltage-dependent current in a central pattern-generating circuit. J Neurosci 20:6752-6759.

Tabak J, Toporikova N, Freeman ME, Bertram R (2007) Low dose of dopamine may stimulate prolactin secretion by increasing fast potassium currents. J Comput Neurosci 22:211-222.

Tierney AJ, Harris-Warrick RM (1992) Physiological role of the transient potassium current in the pyloric circuit of the lobster stomatogastric ganglion. J Neurophysiol 67:599-609.

Timofeev I, Grenier F, Bazhenov M, Sejnowski TJ, Steriade M (2000) Origin of slow cortical oscillations in deafferented cortical slabs. Cereb Cortex 10:1185-1199.

Tobin AE, Van Hooser SD, Calabrese RL (2006) Creation and reduction of a morphologically detailed model of a leech heart interneuron. J Neurophysiol 96:2107-2120.

Toporikova N, Tabak J, Freeman ME, Bertram R (2007) A-Type K(+) Current Can Act as a Trigger for Bursting in the Absence of a Slow Variable. Neural Comput.

van Batenburg FH, Gultyaev AP, Pleij CW (1995) An APL-programmed genetic algorithm for the prediction of RNA secondary structure. J Theor Biol 174:269-280.

Verhulst F (2005) Methods and applications of singular perturbations : boundary layers and multiple timescale dynamics. New York: Springer Science+Business Media.

Walters JR, Hu D, Itoga CA, Parr-Brownlie LC, Bergstrom DA (2007) Phase relationships support a role for coordinated activity in the indirect pathway in organizing slow oscillations in basal ganglia output after loss of dopamine. Neuroscience 144:762-776.

Wilders R (2006) Dynamic clamp: a powerful tool in cardiac electrophysiology. J Physiol 576:349-359.

Willett P (1995) Genetic algorithms in molecular recognition and design. Trends Biotechnol 13:516-521.

Wustenberg DG, Boytcheva M, Grunewald B, Byrne JH, Menzel R, Baxter DA (2004) Current- and voltage-clamp recordings and computer simulations of Kenyon cells in the honeybee. J Neurophysiol 92:2589-2603.

Yue BW, Huguenard JR (2001) The role of H-current in regulating strength and frequency of thalamic network oscillations. Thalamus Relat Syst 1:95-103.

Zhang Y, Nadim F (2008) A detailed mathematical analysis of the interaction between the A-current and other intrinsic properties in setting the phase of a follower neuron in an inhibitory network. In preparation.